Development of Light-Responsive Polymeric Membranes for Controlled Caffeine Delivery Based on Photochromic Spiro-Compounds

Inauguraldissertation

zur

Erlangung der Würde eines Doktors der Philosophie

vorgelegt der

Philosophisch-Naturwissenschaftlichen Fakultät

der Universität Basel

von

Lukas Baumann

aus Wattwil SG, Schweiz

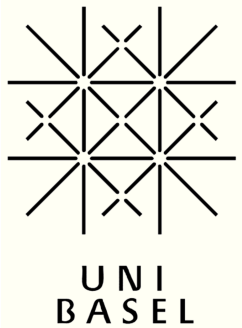

Basel 2013

Genehmigt von der Philosophisch-Naturwissenschaftlichen Fakultät

auf Antrag von

Prof. Dr. Wolfgang Meier

und

Prof. Dr. Marcus Textor

Basel, den 26. Februar 2013

Prof. Dr. Jörg Schibler
Dekan

creative commons

Namensnennung-Keine kommerzielle Nutzung-Keine Bearbeitung 2.5 Schweiz

---

Sie dürfen:

das Werk vervielfältigen, verbreiten und öffentlich zugänglich machen

Zu den folgenden Bedingungen:

Namensnennung. Sie müssen den Namen des Autors/Rechteinhabers in der von ihm festgelegten Weise nennen (wodurch aber nicht der Eindruck entstehen darf, Sie oder die Nutzung des Werkes durch Sie würden entlohnt).

Keine kommerzielle Nutzung. Dieses Werk darf nicht für kommerzielle Zwecke verwendet werden.

Keine Bearbeitung. Dieses Werk darf nicht bearbeitet oder in anderer Weise verändert werden.

- Im Falle einer Verbreitung müssen Sie anderen die Lizenzbedingungen, unter welche dieses Werk fällt, mitteilen. Am Einfachsten ist es, einen Link auf diese Seite einzubinden.
- Jede der vorgenannten Bedingungen kann aufgehoben werden, sofern Sie die Einwilligung des Rechteinhabers dazu erhalten.
- Diese Lizenz lässt die Urheberpersönlichkeitsrechte unberührt.

Die gesetzlichen Schranken des Urheberrechts bleiben hiervon unberührt.

Die Commons Deed ist eine Zusammenfassung des Lizenzvertrags in allgemeinverständlicher Sprache: http://creativecommons.org/licenses/by-nc-nd/2.5/ch/legalcode.de

Haftungsausschluss:
Die Commons Deed ist kein Lizenzvertrag. Sie ist lediglich ein Referenztext, der den zugrundeliegenden Lizenzvertrag übersichtlich und in allgemeinverständlicher Sprache wiedergibt. Die Deed selbst entfaltet keine juristische Wirkung und erscheint im eigentlichen Lizenzvertrag nicht. Creative Commons ist keine Rechtsanwaltsgesellschaft und leistet keine Rechtsberatung. Die Weitergabe und Verlinkung des Commons Deeds führt zu keinem Mandatsverhältnis.

Quelle: http://creativecommons.org/licenses/by-nc-nd/2.5/ch/ Datum: 3.4.2009

„Aller Anfang ist schwer!
Das mag in einem gewissen Sinne wahr sein;
allgemeiner aber kann man sagen:
aller Anfang ist leicht,
und die letzten Stufen werden am schwersten und seltensten erstiegen.“

Johann Wolfgang von Goethe, Wilhelm Meisters Wanderjahre – Band 1

ABSTRACT

Different approaches to obtain light-responsive membranes with the ability to switch their caffeine permeability resistance were developed in a copolymerization and in a postmodification process.
Synthesis of six photochromic methacrylic and acrylic spiropyrans and spirooxazines was successfully achieved. Copolymerization of these monomeric spiro-compounds resulted in photochromic materials. Additionally, a spiropyran with carboxylic acid functionality was synthesized. This enabled to postmodify non-photochromic polymeric materials with alcohols or amines on their surface to obtain photochromic materials.
The first developed approach was to coat porous polymeric membranes with photochromic materials. Covalently linked coatings were achieved either by surface induced atom transfer random polymerization (ATRP) or by plasma activation of the membrane surface followed by random free radical polymerization. Copolymerization of spiro-compounds during the coating process as well as postmodification of preformed non-photochromic coatings with spiropyran resulted in photochromic membranes. UV-irradiation of such membranes resulted in a strong coloration of the membrane, in a reduction of surface tension and in a decreased caffeine permeability resistance.
Plasma activation resulted in thin coatings with thicknesses below 10 nm. Nevertheless it was possible to produce a membrane that reduced its caffeine permeability resistance of about 97% when the membrane was irradiated with UV-light compared to measurements at daylight.
Thicknesses of ATRP-coatings were found to be depending on the polymerization time and the monomer concentration during the polymerization process. If too much coating was on the membrane, no caffeine permeability was any longer detectable. If there was not enough coating on the membrane, the caffeine permeability resistance was not switching. Therefore, an intermediate coating thickness turned out to be important for the production of useful photochromic membranes. Membranes produced with an ATRP-process lowered in the best case their permeability resistance of about 65% under UV-irradiation compared to measurements at daylight.
Production of nonporous photochromic membranes was achieved by producing amphiphilic conetworks containing spiropyrans. UV-irradiation of such photochromic amphiphilic conetworks resulted in a red coloration and in a decreased caffeine permeability resistance. Changing the composition of the amphiphilic conetwork allowed tuning the basic caffeine permeability resistance. Copolymerization of spiropyran during the production of the amphiphilic conetwork resulted in a membrane that lowered its caffeine permeability resistance under UV-irradiation of around 43% compared to measurements at daylight.
Combination of porous membranes with amphiphilic conetworks was achieved in a grafting through process. The surface of a porous membrane was coated with acrylic units and the amphiphilic network was produced on that surface. This covalently linked amphiphilic conetwork resulted in an inversed permeability switch. The caffeine permeability resistance was about eight times higher under UV-irradiation than at daylight.
Stability measurements under UV-irradiation showed that postmodified membranes had in general lower fading rates than copolymerized membranes.

CONTENT

ACKNOWLEDGEMENT

I am very grateful to:

- Lukas Scherer for supervising my PhD-studies at EMPA and for all the fruitful discussions and inputs. I appreciated the good collaboration and the stimulating ambience within the medical textile group at EMPA.
- René Rossi who allowed me to work in his laboratory. I enjoyed the open minded and interdisciplinary atmosphere in the laboratory for protection and physiology.
- my doctor-father Wolfgang Meier for mentoring and supporting me during my PhD-studies.
- Marcus Textor who agreed to be second examiner for my PhD-thesis.
- Smahan Toughrai for all her help regarding various things at University of Basel, e.g. elemental analysis, AFM measurement or discussion about surface-induced ATRP.
- Justyna Kowal for supporting me with ellipsometric measurements.
- Martin Rother and Nico Bruns. They provided a lot of knowledge about the production and analysis of amphiphilic conetworks.
- Sabrina Küpfer who performed a lot of experiments with photochromic amphiphilic conetworks within the scope of her master's thesis.
- Susanne Widmer for all her experiments conducted with photochromic mesoporous silicates within her master's thesis (Results not shown in this thesis) and for proofreading Chapter 2.
- Barbara Hanselmann, Urs Schütz and Dirk Hegemann for all their help regarding plasma processes.
- Karl Kehl and Sofia Al Gorani-Szigeti for performing time consuming permeability measurements.
- Aybige Aygen who performed several synthetic steps during her internship at EMPA.
- Daniel Rentsch for performing the NMR-measurements.
- Patrick Rupper for performing the XPS-measurements.
- Laetitia Bernard for performing the ToF-SIMS analysis.
- Aliaksei Vetushka and Patrik Schmutz for their support regarding AFM-measurements at EMPA.
- Dominik Marti and Martin Frenz for the collaboration regarding the two photon analysis.
- Gelu-Marius Rotaru for his support regarding the tribology measurements. (Results not shown in this thesis)
- our partners from University Hospital Zurich – Martin Wolf and Damien de Courten – for the interesting discussions and the non-bureaucratic collaboration.
- Thomas Baumann for proofreading the whole manuscript of this thesis.
- Max Aeberhard, Elisabeth Michel, Urs Bünter and Benno Wüst for their helpfulness in various concerns.

The financial support of NRP 62 – smart materials – is acknowledged.

Last but not least I am very grateful to all the people who supported me in my non-scientific life during the last three years.

ABBREVIATIONS

Δc	difference in concentration
Δm	difference in weight
ΔT	difference in temperature
A	area
AcCl	acetyl chloride
AcOH	acetic acid
act	activation
AEMA	2-aminoethyl methacrylate
AFM	atomic force microscopy
AMPS	2-acrylamido-2-methylpropane sulfonic acid
ARGET	activators regenerated by electron transfer
AscA	ascorbic acid
At.%	atomic percentage
ATR	attenuated total reflectance
ATRP	atom-transfer radical-polymerization
BABE	Bandbeschichtungsanlage
bipy	2,2'-bipyridine
c	concentration
CA	contact angle
caff	Caffeine
$CDCl_3$	Chloroform deuterated
CP	copolymerization
D	diffusion coefficient
d	thickness
deact	deactivation
DCC	*N,N*'-dicyclohexylcarbodiimide
DCM	dichloromethane
DL	daylight
DMAP	4-dimethylaminopyridine
DMF	dimethylformamide
DMSO	dimethylsulfoxide
EA	elemental analysis
EDCI	1-ethyl-3-(3-dimethylaminopropyl)carbodiimide
ESI	electron spray ionization
Et_2O	diethyl ether
EtOAc	ethyl acetate
EtOH	ethanol
F	flux
FDA	food and drug administration

HCl	hydrochloric acid
HEA	2-hydroxyethyl acrylate
HEMA	2-hydroxyethyl methacrylate
HMBC	heteronuclear multiple-bond correlation spectroscopy
HSQC	heteronuclear single-quantum correlation spectroscopy
Hx	hexane
Init.	initiator
IR	infrared
k	speed of reaction
LR	low resolution
M	monomer
MAA	methacrylic acid
MC	merocyanine
MeCN	acetonitrile
MEK	methylethylketone (2-butanone)
Mem	membrane
MeOH	methanol
MMA	methyl methacrylate
MS	mass spectroscopy
mu	mass units
N	number of molecules
NMR	nuclear magnetic resonance spectroscopy
NOESY	nuclear overhauser effect spectroscopy
Oct	octanoic acid
orig.	original
p	poly
PC	polycarbonate
PDI	polydispersity index
PDMS	poly(dimethylsiloxane)
PDMS*	bitelechelic poly(dimethylsiloxane)
PES	polyester
PESF	polyethersulfone
PhCl	chlorobenzene
Pip	piperidine
PM	postmodification
PLC	preparative layer chromatography
Pol	polymerization
PVDF	polyvinylidene fluoride
R	permeability resistance
R (%)	reflection in %
RAFT	reversible addition−fragmentation chain-transfer polymerization
RF	radio frequency
RT	room temperature

Rxn	reaction
S	swelling
SEM	scanning electron microscopy
SO	spirooxazine
SP	spiropyran
T	temperature
t	time
T (%)	transmission in %
TBME	*tert*-butyl methyl ether
TE	track etched
TEM	transmission electron microscopy
TEWL	transepidermal water loss
THF	tetrahydrofuran
TLC	thin layer chromatography
TMS	trimethylsilyl
Tof-SIMS	time of flight secondary ions mass spectroscopy
Tol	toluene
UV	ultraviolet
V	volume
Vis	visible
vol.	volume
wt.	weight
X	halide
XPS	x-ray photoelectron spectroscopy

1. INTRODUCTION

1.1. MOTIVATION

Preterm neonates show an increased risk of apnea due to the fact that their respiratory systems are not fully developed yet.[1, 2] Schmidt *et al.* applied 5.0 mg caffeine per kilogram bodyweight per day to preterm neonates to prevent apnea and increased that dose to 10.0 mg caffeine per kilogram bodyweight per day if apnea persisted.[3] This caffeine treatment resulted in an increased rate of survival without disability of preterm neonates because of lowered occurrence of apnea.[3]

Today caffeine is applied orally or via infusion. Oral application of a drug results usually in a big deviation of drug-concentration in the body over time. This deviation includes the risk of an overdose shortly after application or an under-supply at a later stage (Figure 1.1). Application via infusion allows better control of the drug-concentration in the body but always involves a high risk of infections. For preterm neonates, an infection represents a life-threatening situation and has to be avoided as far as possible.[4, 5] The ultimate objective of drug therapy is therefore a noninvasive device which senses the patient's drug requirement and then delivers the right dose of the active agent at the right rate.[6] Transdermal drug delivery is the most prominent approach for noninvasive therapies. Caffeine is known for its ability to penetrate skin quite easily.[7, 8] Therefore, it is a good candidate for a transdermal delivery approach.

The caffeine-concentration in the body after transdermal drug delivery is not only influenced by the rate of caffeine delivery, but also by the resistance of the skin towards caffeine. The skin of preterm neonates represents only a minimal hindrance for caffeine directly after birth due to the undeveloped stratum corneum especially of preterm neonates. This eases the transdermal caffeine delivery. Since the skin properties of neonates change rather rapidly and the resistance towards caffeine increases over time, it is not suitable to develop a transdermal caffeine delivery system with a fixed delivery rate.[9, 10] There is also a major deviation in skin resistance comparing the skin of different patients.[11] A device adapting its caffeine-delivery rate triggered by an external stimulus represents a suitable solution for the problem with different and changing skin resistances.[12, 13] Changing the delivery rate of the setup allows compensating for the change in skin resistance. The easiest design of an adaptive device is a system with a high and a low delivery rate. Such a tow-level device has a high potential for application in a transdermal drug-delivery setup. Connecting a two-level delivery system to an appropriate sensor allows controlling the caffeine delivery to a high degree. The delivery system could be kept at its high delivery rate (F_{high}) until the sensor detects a defined maximal caffeine-concentration (c_{max}). Then the system has to be switched to its low delivery rate (F_{low}) until a minimal caffeine-concentration (c_{min}) is reached. Switching the delivery rate back and forth allows keeping caffeine-concentration in the body within a defined range (Figure 1.1).

For the development of a drug delivery system, it is important that all the used components are biocompatible. For a transdermal drug-delivery setup it is further important to choose flexible and mechanically stable materials that allow a tight contact with the skin without limiting the agility of the person and without getting damaged upon movements of the patient. Good candidates that

fulfill all these requirements are polycarbonate (PC) and polyester (PES) membranes and polydimethylsiloxane (PDMS) based amphiphilic conetworks. [14-16]

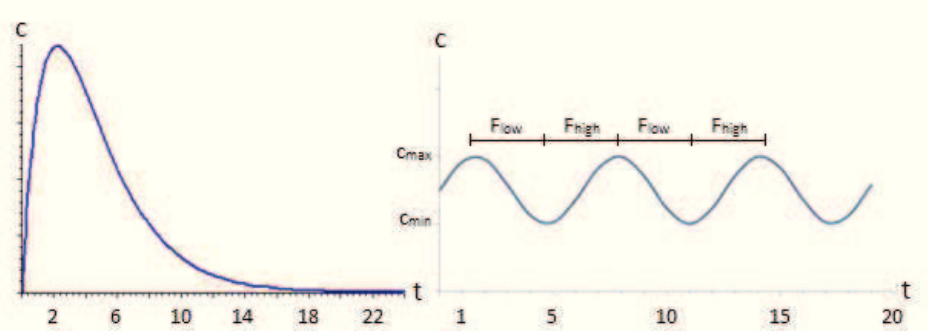

Figure 1.1 Caffeine concentration over time after oral application once a day (left) and while adaptive transdermal application (right).

Triggered and reversible changes of material properties can be achieved by integrating molecular switches into corresponding materials. Molecular switches as well as adaptive materials have been reported intensively.[17-19] Temperature[20], pH[21], chemical stimuli[22] and light[23] are known to be suitable triggers for adaptive materials. Chemical stimuli and pH-changes are not suitable for applications on human skin due to missing biocompatibility. Temperature shows a good biocompatibility within a certain range. However, applying and removing heat is a slow process resulting in slowly reacting materials. Therefore, the focus of this investigation was set on light-responsive materials. Light can be applied rapidly, remotely and reversibly at the outer face of the body. Additionally, light is a clean stimulus that easily can be focused on small and defined areas of the body.
The aim of the project was to integrate a light-responsive molecule into a biocompatible membrane in such a manner that the caffeine permeability of the membrane can be switched from one into another state triggered by light.

1.2. DIFFUSION AND PERMEABILITY RESISTANCE OF MEMBRANES[24]

Material flux (F) through a membrane can be determined by measuring the amount of material per time per area that passes through the membrane. Driving force for the net-diffusion of material through a membrane is a concentration difference from one side to the other side of the membrane. Dividing this concentration difference (Δc) by the measured flux (F), results in the permeability resistance (R) of the membrane towards the measured material.

$$R = \frac{\Delta c}{F} \tag{1}$$

This formula is derived from Fick's law of diffusion:

$$F = -\mathrm{D}\frac{\delta c}{\delta \mathrm{x}} \tag{2}$$

were D represents the diffusion coefficient, c stands for the concentration and x is representing the position within the sample. Assuming that no concentration gradients occur within the time span of the measurement and the concentration difference from one side to the other side of the membrane stays constant, the differential equation (2) can be transformed into the linear equation (3).

$$F = -\mathrm{D} * \Delta \mathrm{c} \tag{3}$$

Comparing (1) and (3) shows that the permeability resistance R is reciprocally proportional to -D. Diffusion values for molecules found in literature are usually measured for free diffusion. Since diffusion through a porous medium is of interest in the present case, it is not possible to calculate R from literature values of D. But measuring R allows calculating the coefficient of the hindered diffusion through the measured membrane.

If the material flux through a membrane has to be altered at a constant concentration difference, the resistance of the membrane has to be changed. As shown before, the resistance of the membrane depends on the apparent diffusion coefficient. By changing for example the electrostatic interactions of the molecule or the solvent with the membrane material, the apparent diffusion coefficient can be altered.

In case of diffusion through porous membranes, not the whole macroscopic area of the membrane is accessible for diffusion. Only open pores are relevant for diffusion.

The area relevant for diffusion in equations (1) and (2) was assumed to be the macroscopic area of the membrane. This constant value was included in the flux (F) representing the amount of material (n) per area (A) per time (t) that diffuses through a membrane:

$$F = \frac{\mathrm{n}}{\mathrm{A} * \mathrm{t}} \tag{4}$$

Combining equation (4) with equation (3) results in the following equation:

$$\frac{n}{t} = -D * A * \Delta c \tag{5}$$

Equation (5) shows that it is also possible to influence the flux through a membrane by changing the accessible diffusion area.

In practical approaches it is often unclear whether a change in material flux through a membrane is caused by a changed pore size, an altered diffusion coefficient or changes of both parameters at the same time. Therefore, using permeability resistance (R) from equation (1) as characteristic for membranes turned out to be practicable. Equation (1) can be applied for nonporous as well as porous systems. Therefore, working with permeability resistance (R) allows comparing all types of membranes. Switching potential of photochromic membranes can also be reported by comparing permeability resistances of photochromic membranes at daylight and under UV-irradiation.

1.3. PHOTOCHROMIC MOLECULES AND MATERIALS

Photochromism is defined as a reversible photo-transformation of a chemical species between two forms having different absorption spectra.[25] Not many light-responsive molecules undergo reversible photochemistry. Therefore, photochromic structures are of great interest for the development of light-responsive materials. Today, photochromic compounds are used for example in sunglasses,[26] data-storage systems,[27] sensors[28] and for responsive surfaces.[29] Photochromic switches were also incorporated into peptides to influence biochemical processes triggered by light.[30, 31] In Australia the incorporation of photochromic molecules into banknotes for protection against forgery was discussed.[32] The most commonly used photochromic molecules are azobenzenes, dithienylethenes, spiropyrans and spirooxazines (Figure 1.2).[33, 34] These photochromic molecules undergo a reversible structural rearrangement causing a strong coloration of the molecules when irradiated with UV-light.[35, 36]

The absorption spectra of these photochromic molecules strongly depend on the substituents that are conjugated with the π-electron-system. Auxochromic substituents (in the case of spiropyran usually electron donating groups) for example cause a bathochromic shift in absorption.[33, 34]

Since a change in polarity is much more likely to have an impact on the permeability resistance of a membrane than only a changed light absorption, spiropyran (SP) and spirooxazine (SO) with their highly polar merocyanine (MC) states are the most promising candidates for the development of a photochromic membrane with adaptable caffeine permeability. Additionally, it is known from literature that spiropyran in solution at concentrations below 10^{-6} M does not cause cell toxicity.[37] Therefore, chances are high that spiropyran bound to a solid polymer does not induce any cell toxicity.

UV-irradiation of spiropyran or spirooxazine induces a heterolytic ring-opening reaction leading to a polar and colored MC-state. Illuminating the MC-structure with visible light triggers the ring-closing reaction back into its initial SP-state (Figure 1.3).

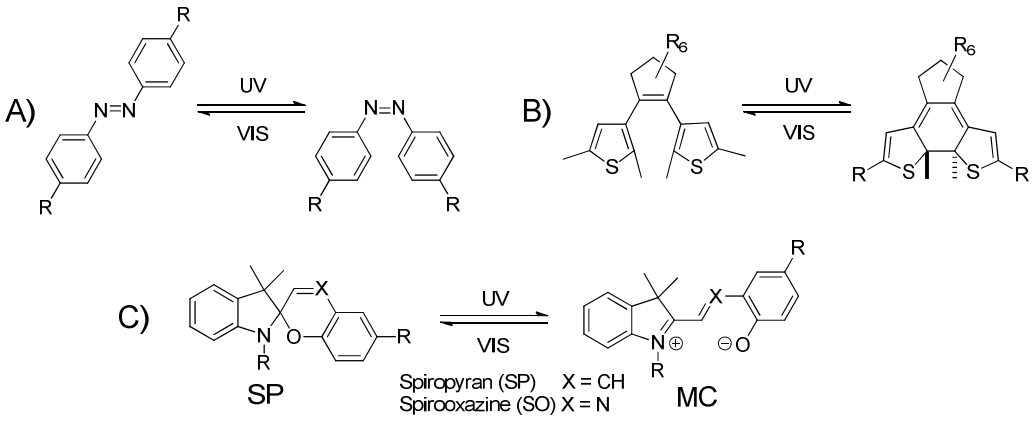

Figure 1.2 Main photochromic families: A) trans-cis isomerization of azobenzene B) pericyclic ring-closing and opening reaction of dithienylethene C) heterolytic ring-opening and -closing reaction of spiropyran and spirooxazine.

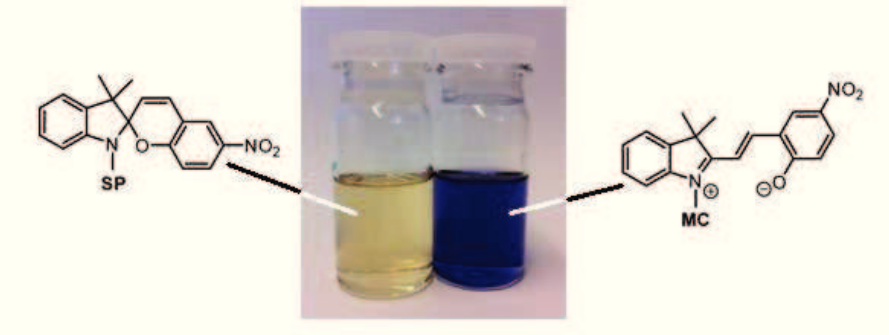

Figure 1.3 Spiropyran dissolved in ethyl acetate at daylight (left) and after UV-irradiation (right).

There are two approaches that allow benefiting from the light-induced polarity change of spiropyran and spirooxazine in order to achieve a membrane with changeable permeability. One approach is to change the solubility of a polymer that is grafted onto a porous membrane.[38] For the drug delivery setup, it is assumed that a polar solvent (e.g. water) is used. If the spiropyran in the polymer is in its SP-state, the polarity of the polymer is low. Therefore the solubility of the polymer is low and the polymer-strands are collapsed. This results in a membrane with open pores and a high caffeine permeability (Figure 1.4 a)). If the spiropyran in the grafted polymer is switched into its MC-state, the polymer becomes soluble and swells. The pores are now blocked resulting in a membrane with low caffeine permeability due to only a small area accessible for diffusion (Figure 1.4 b)).[39, 40] The second approach benefits directly from the changeable polarity of spiropyran. If a surface is coated with spiropyran, its surface tension depends on the actual state of the spiropyran. If spiropyran is in its nonpolar SP-state, the coated surface is rather hydrophobic, resulting in a low permeability for aqueous solutions (Figure 1.4 c)). If spiropyran is switched into its MC-state, the surface becomes more hydrophilic and the permeability rate of aqueous solution is expected to increase (Figure 1.4 d)).[41]

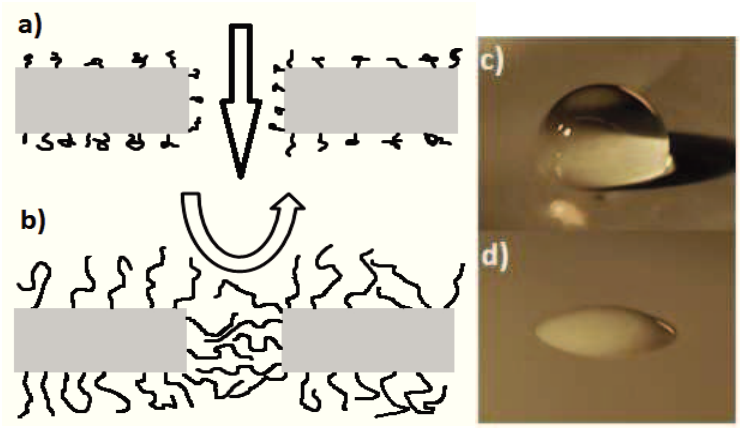

Figure 1.4 Influencing the permeability of a membrane by benefiting from spiropyran's polarity change: **a)** + **b)** changing the solubility of a polymer resulting in a steric hindrance in pores; **c)** + **d)** changing the surface tension of a membrane resulting in an electrostatic control over the permeability rate of a membrane.

1.4. POLYMERIC COATINGS ON POROUS POLYMERIC MEMBRANES

Surface is the place where interaction of a material with its surrounding takes place. To tune the property of a material, it is essential to modify its surface in a predictable way.[42-45]

Coatings are widely used to change the surface-properties of materials without changing their bulk properties. One possibility to coat a porous polymeric membrane is to deposit surface-active materials.[44, 46] Dip-coating, spin-coating and Langmuir-Blodgett processes are commonly used to apply such coatings.[47, 48] Spin-coating is a powerful approach to coat flat surfaces. If it is applied to porous substrates, the porous material might get entirely covered what could result in blocked pores.[49] In some cases, the physisorbed materials lack long-term stability, especially when exposed to mechanical forces as for example friction.[50]

A coating can also be covalently linked to a surface in order to improve its mechanical stability. Polymers are often used to create such chemisorbed coatings. Covalent linkage of polymers can be achieved by *grafting* preformed polymers *to* a surface[51], by *grafting* a growing polymer *through* a suitable surface[52] or by growing polymers from an activated surface (*grafting from*) (Figure 1.5).[13, 45, 50, 53-55]

Grafting-to-approaches sometimes show limitations regarding coverage homogeneity of the surfaces due to steric repulsion of the preformed polymers.[56] Today, *grafting from* is one of the most promising approaches for surface modifications. There are several ways to achieve surface activation to induce polymerization, including plasma discharge methods[57-61], UV-irradiation[62, 63], ozone treatment[64], γ-ray irradiation[54] and chemical activation. Random free radical polymerization directly after surface activation is the simplest approach to achieve a grafted polymeric coating. After activation, the sample has only to be treated with a monomer solution. Drawback of this approach is the lack of control over the polymerization process. The size of the grafted polymers cannot be predicted and a large polydispersity index (PDI) is usually obtained for such processes.[65, 66]

Living polymerization methods offer more control over the polymerization process. The size of the grafted polymers can be adjusted by changing the reaction time.[67] Living polymerization processes commonly used for grafting processes of (meth)acrylates on surfaces are atom transfer radical polymerization (ATRP) and reversible addition−fragmentation chain-transfer polymerization (RAFT) (Figure 1.6).[68] Drawback of the RAFT-mechanism is the fact that polymers do not only grow on the surface but also in solution. Therefore the viscosity of the monomer solution changes over time, influencing the polymerization process. Additionally it can be difficult to remove non-covalently bound polymers.

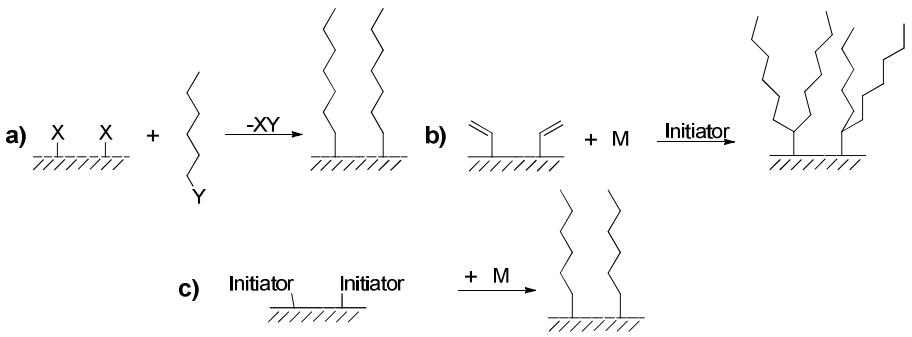

Figure 1.5 Methods to graft polymers on a surface: **a)** grafting to; **b)** grafting through; **c)** grafting from.

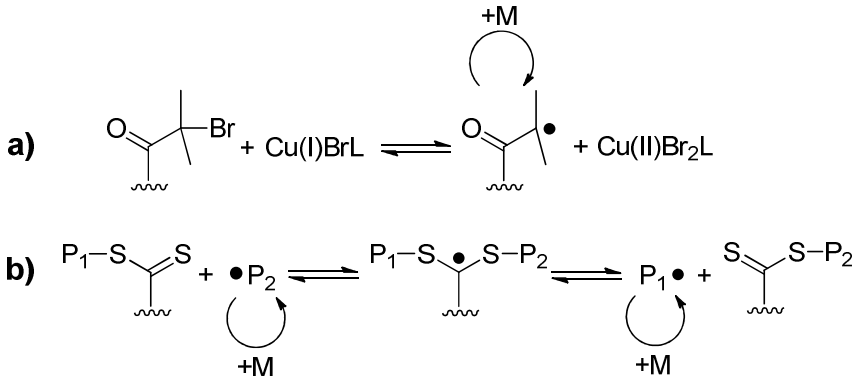

Figure 1.6 Living polymerization mechanism: **a)** atom transfer radical polymerization (ATRP); **b)** reversible addition-fragmentation chain-transfer polymerization (RAFT).

Grafted polymer coatings have been shown to create gating membranes. Most prominently reported is the change in steric hindrance of thermo-responsive coatings. At low temperature, the polymers are swollen and the pores are closed. When the temperature is increased, polymers collapse and the pores are opened (similar to Figure 1.4 a) + b)).[39]

Achieving a steric hindrance can be demanding if the ratio of pore diameter to molecular radius is large. In such a case, the pores have to be covered entirely for the swollen state of the polymer. Thus, a thick coating is needed for the successful gating of a membrane by steric interaction. The layer should not be too large either, since otherwise no permeability change would be observed. To tune the thickness of grafted layers is generally very demanding.

An alternative approach which has been reported in literature is to change the hydrophilicity of a membrane by an external trigger.[41] To influence the surface tension of a membrane, already a very thin coating is sufficient. Changing the hydrophilicity of a membrane influences the wetting behavior of the pores. If the pore surface is hydrophilic, aqueous solutions pass through easily. If the pore surface is changed to a hydrophobic state, less aqueous solution is able to pass through (similar to Figure 1.4 c) + d)).[41]

Up to now, only very little reports on spiropyran containing coatings regulating the permeability of porous membranes can be found in literature.[69] No reports about spirooxazine containing coatings regulating the permeability of a porous membrane have been reported in literature. The applicability of spiropyran-based photochromic coatings was only shown for solvent mixtures[40, 70] or water[71] in filtration applications. Changed steric hindrance due to changed polymer solubility[70] as well as changed wetting behavior[41] of spiropyran based photochromic membranes were reported. Additionally the general wettability[41] and antifouling properties[62] of spiropyran-coated porous membranes were investigated. No report on drug delivery applications or on general diffusion of aqueous solutes through such membranes has been found in literature.

Since changing steric hindrance as well as changing the surface tension is possible by using spiropyran coatings, it is assumed that the thickness of the coating has a major impact on the predominant mechanism. If the coating is much thinner than the pore radius, changes in hydrophilicity are expected to be most important. If the coating is thick enough to close the pores in its swollen state, steric interactions are likely to become predominant. Therefore, control over the

polymerization process and over the coating thickness could be essential for the control over the permeability of coated membranes.

1.5. NON-POROUS PHOTOCHROMIC MEMBRANES

Aqueous solutions are not only able to pass through porous membranes but also through nonporous materials if these materials are hydrophilic and capable of swelling. Hydrogels and amphiphilic conetworks for example are well known materials with such properties.[52, 72] Nonporous materials usually have much higher permeability resistances compared to porous materials since the aqueous solution has to pass through the polymeric matrix. The advantage of some nonporous material is the fact that they can be produced easily.[52] Only a bulk material has to be created and no pore-crating mechanism is needed. Homemade preparation of a membrane generates additional degrees of freedom. If a nonporous membrane is formed, changing the thickness for example allows setting the basic permeability resistance of the membrane.[73, 74]

Photochromic hydrogels are known in literature for different approaches.[75, 76] No report of photochromic amphiphilic conetworks for controlled drug delivery was found in literature.

If a nonporous spiropyran-containing material with a moderate hydrophilicity is produced, it is possible to switch that material into a highly hydrophilic state by switching spiropyran into its MC-state. The material is expected to swell more and the polymeric matrix gets less tight.[72] The increased hydrophilicity together with the lowered matrix density is expected to result in an increased permeability of aqueous solution, thus allowing light-induced control over the permeability of a nonporous material.

In the case of amphiphilic conetworks, it is also possible that switching spiropyran from one into its other state has an impact on the distribution of the hydrophilic and the hydrophobic domains.

1.6. TRANSDERMAL DRUG DELIVERY SYSTEMS

The ultimate objective of drug therapy is a noninvasive device which measures the patient's drug requirement and then delivers the right dose of the active agent at the right rate. Passive transdermal delivery meets the non-invasive criterion and is able to provide drug input over extended periods of time at controlled rates. But most patches provide only zero-order delivery and cannot offer a monitoring capability.[6]

Drug delivery through skin seems to be reasonable due to the big area of skin and the easy access to it. But it should also be considered that the main function of skin is to protect the body from external insults. The *stratum corneum* is the outermost layer of the skin. This part of the *epidermis* consists of dead, flattened keratinocytes and is between 10 and several 100 μm thick, depending on the part of the body and the age of the person.[11] The *stratum corneum* builds the main barrier for external insults or applied drugs.[6, 11]

Patches for transdermal drug delivery (first generation) usually consist of four layers (Figure 1.7): an impermeable backing membrane (**1**), a drug reservoir (**2**), a semi-permeable membrane that may serve as a rate limiting barrier (**3**) and an adhesive layer (**4**).[77]

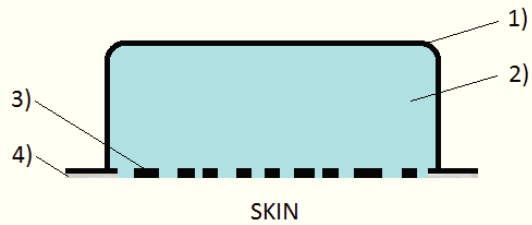

Figure 1.7 Patch for transdermal drug delivery: **1)** impermeable backing membrane; **2)** drug reservoir; **3)** semi-permeable membrane; **4)** adhesive layer.

It is also possible to incorporate the drugs into a polymer matrix. Adjusting the delivery rate of the polymeric matrix allows avoiding the semipermeable membrane. Including the drugs into an adhesive polymer would even allow eliminating this layer ending up in a two-layer system.[77]
The first transdermal drug delivery system (Trandserm-SCOP) was approved by the food and drug administration (FDA) in 1979.[78] Since then, a lot of development has taken place.
First generation transdermal delivery systems are widely used in clinical applications nowadays with a steady increase. These setups are quite simple but also limited to small, lipophilic, low-dose drugs. Second generation delivery systems using chemical enhancers[79], ultrasound[80] or iontophoresis[6] to lower the skin resistance towards the drug resulted also in some clinical product, suitable for less hydrophobic drugs.[77] Third generation setups target their effects to *stratum corneum* by using for example micro-needles or thermal ablation. This approach would allow delivering macromolecules and vaccines through skin.[77]
Preterm neonates however, do not have any *stratum corneum* directly after birth. Therefore, their skin is highly permeable what eases the transdermal drug delivery.[81] No chemical enhancers or micro needles are needed and a first-generation drug-delivery setup is suitable within the limitations mentioned in Chapter 1.1. The aim of this work was the development of a light-responsive membrane with a switchable caffeine permeability resistance as a centerpiece of an adaptive first generation drug delivery setup.

1.7. REFERENCES

1. G. Polgar and T. R. Weng, *The American review of respiratory disease*, 1979, **120**, 625-695.
2. W. J. R. Daily, M. Klaus, H. Belton and P. Meyer, *Pediatrics*, 1969, **43**, 510-518.
3. B. Schmidt, P. J. Anderson, L. W. Doyle and et al., *JAMA: The Journal of the American Medical Association*, 2012, **307**, 275-282.
4. B. J. Stoll, N. Hansen, A. A. Fanaroff, L. L. Wright, W. A. Carlo, R. A. Ehrenkranz, J. A. Lemons, E. F. Donovan, A. R. Stark, J. E. Tyson, W. Oh, C. R. Bauer, S. B. Korones, S. Shankaran, A. R. Laptook, D. K. Stevenson, L.-A. Papile and W. K. Poole, *New England Journal of Medicine*, 2002, **347**, 240-247.
5. A. K. M. Zaidi, W. C. Huskins, D. Thaver, Z. A. Bhutta, Z. Abbas and D. A. Goldmann, *The Lancet*, 2005, **365**, 1175-1188.
6. R. Guy, in *Drug Delivery*, ed. M. Schäfer-Korting, Springer Berlin Heidelberg, 2010, pp. 399-410.
7. M. J. Bartek, J. A. Labudde and H. I. Maibach, *J Investig Dermatol*, 1972, **58**, 114-123.
8. I. P. Dick and R. C. Scott, *Journal of Pharmacy and Pharmacology*, 1992, **44**, 640-645.
9. N. Barker, J. Hadgraft and N. Rutter, *J Investig Dermatol*, 1987, **88**, 409-411.
10. R. L. Nachman and N. B. Esterly, *The Journal of Pediatrics*, 1971, **79**, 628-632.
11. M. F. Wilkosz and R. H. Bogner, *US pharmacist*, 2003, **28**.
12. M. Gagliardi, D. Silvestri and C. Cristallini, *Drug Delivery*, 2010, **17**, 452-465.
13. R. Bengt, *International Journal of Adhesion and Adhesives*, 1999, **19**, 337-343.
14. D. C. Schohn, H. A. Jahn, M. Eber and G. Hauptmann, *Blood Purification*, 1986, **4**, 102-111.
15. M. H. R. Magno, J. Kim, A. Srinivasan, S. McBride, D. Bolikal, A. Darr, J. O. Hollinger and J. Kohn, *Journal of Materials Chemistry*, 2010, **20**, 8885-8893.
16. G. Erdodi and J. P. Kennedy, *Progress in Polymer Science*, 2006, **31**, 1-18.
17. B. S. Lukyanov and M. B. Lukyanova, *Chem Heterocycl Compd*, 2005, **41**, 281-311.
18. E. Ruel-Gariépy and J.-C. Leroux, *European Journal of Pharmaceutics and Biopharmaceutics*, 2004, **58**, 409-426.
19. V. Giurgiutiu, *Journal of Intelligent Material Systems and Structures*, 2000, **11**, 525-544.
20. L. E. Bromberg and E. S. Ron, *Advanced Drug Delivery Reviews*, 1998, **31**, 197-221.
21. D. M. Lynn, M. M. Amiji and R. Langer, *Angewandte Chemie International Edition*, 2001, **40**, 1707-1710.
22. Y. Lu and J. Liu, *Accounts of Chemical Research*, 2007, **40**, 315-323.
23. I. Roy and M. N. Gupta, *Chemistry & Biology*, 2003, **10**, 1161-1171.
24. E. L. Cussler, *Diffusion - Mass Transfer in Fluid Systems*, Cambridge University Press, Cambridge, 2009.
25. M. Irie, *Chemical Reviews*, 2000, **100**, 1683-1684.
26. B. Osterby, R. D. McKelvey and L. Hill, *Journal of Chemical Education*, 1991, **68**, 424.
27. A. Y. Bobrovsky, N. I. Boiko and V. P. Shibaev, *Liquid Crystals*, 2000, **27**, 57-62.
28. N. Shao, Y. Zhang, S. Cheung, R. Yang, W. Chan, T. Mo, K. Li and F. Liu, *Analytical Chemistry*, 2005, **77**, 7294-7303.
29. A. Athanassiou, M. I. Lygeraki, D. Pisignano, K. Lakiotaki, M. Varda, E. Mele, C. Fotakis, R. Cingolani and S. H. Anastasiadis, *Langmuir*, 2006, **22**, 2329-2333.
30. T. Stafforst and D. Hilvert, *Chemical Communications*, 2009, **45**, 287-288.
31. P. H. Vandewyer and G. Smets, *Journal of Polymer Science Part A-1: Polymer Chemistry*, 1970, **8**, 2361-2374.
32. E. L. Prime and D. H. Solomon, *Angewandte Chemie International Edition*, 2010, **49**, 3726-3736.
33. G. H. Brown, R. Livingston and R. C. Bertelson, *Potochromism*, Wiley-Interscience, New York, 1971.
34. H. Dürr, H. Bouas-Laurent, R. Guglielmetti and N. Y. C. Chu, *Photochromism – molecules and systems*, Elsevier, Amsterdam, 1990.
35. C. B. McArdle, J. C. Crano, W. S. Kwak, C. N. Welch and M. Irie, *Applied Photochromic Polymer Systems*, Blackie & Son Ltd, Glasgow, 1992.
36. J. C. Crano and R. J. Guglielmetti, *Main Photochromic Families*, Plenum Press, New York, 1999.
37. D. Movia, A. Prina-Mello, Y. Volkov and S. Giordani, *Chemical Research in Toxicology*, 2010, **23**, 1459-1466.
38. Y. Ito, S. Kotera, M. Inaba, K. Kono and Y. Imanishi, *Polymer*, 1990, **31**, 2157-2161.
39. Y. Li, L.-Y. Chu, J.-H. Zhu, H.-D. Wang, S.-L. Xia and W.-M. Chen, *Industrial & Engineering Chemistry Research*, 2004, **43**, 2643-2649.
40. Y. S. Park, Y. Ito and Y. Imanishi, *Macromolecules*, 1998, **31**, 2606-2610.
41. I. Vlassiouk, C.-D. Park, S. A. Vail, D. Gust and S. Smirnov, *Nano Letters*, 2006, **6**, 1013-1017.
42. K. Kato, E. Uchida, E.-T. Kang, Y. Uyama and Y. Ikada, *Progress in Polymer Science*, 2003, **28**, 209-259.
43. T. Cai, M. Li, K.-G. Neoh and E.-T. Kang, *Journal of Materials Chemistry*, 2012, **22**, 16248-16258.

44. Z. Xu, L. Wan and X. Huang, Springer Berlin Heidelberg, 2009, pp. 80-149.
45. A. Friebe and M. Ulbricht, *Langmuir*, 2007, **23**, 10316-10322.
46. M. Ozdemir, C. U. Yurteri and H. Sadikoglu, *Critical Reviews in Food Science and Nutrition*, 1999, **39**, 457-477.
47. I. R. Peterson, *Journal of Physics D: Applied Physics*, 1990, **23**, 379.
48. P. Jiang and M. J. McFarland, *Journal of the American Chemical Society*, 2004, **126**, 13778-13786.
49. B. Tieke, *Advanced Materials*, 1991, **3**, 532-541.
50. J. Deng, L. Wang, L. Liu and W. Yang, *Progress in Polymer Science*, 2009, **34**, 156-193.
51. Z. Jia, S. Du and G. Tian, *Journal of Macromolecular Science, Part A*, 2007, **44**, 299-304.
52. N. Bruns, J. Scherble, L. Hartmann, R. Thomann, B. Iván, R. Mülhaupt and J. C. Tiller, *Macromolecules*, 2005, **38**, 2431-2438.
53. K. C. Khulbe, C. Feng and T. Matsuura, *Journal of Applied Polymer Science*, **115**, 855-895.
54. Z. Lin, T. W. Xu and L. Zhang, *Radiation Physics and Chemistry*, 2006, **75**, 532-540.
55. C. Geismann and M. Ulbricht, *Macromolecular Chemistry and Physics*, 2005, **206**, 268-281.
56. B. Zhao and W. J. Brittain, *Progress in Polymer Science*, 2000, **25**, 677-710.
57. L. Y. Chu, T. Niitsuma, T. Yamaguchi and S. Nakao, *Aiche Journal*, 2003, **49**, 896-909.
58. T. Hirotsu and S. Nakajima, *Journal of Applied Polymer Science*, 1988, **36**, 177-189.
59. S. Y. Kim, T. Kanamori and T. Shinbo, *Journal of Applied Polymer Science*, 2002, **84**, 1168-1177.
60. D. S. Wavhal and E. R. Fisher, *Langmuir*, 2003, **19**, 79-85.
61. R. Xie, L.-Y. Chu, W.-M. Chen, W. Xiao, H.-D. Wang and J.-B. Qu, *Journal of Membrane Science*, 2005, **258**, 157-166.
62. A. Nayak, H. W. Liu and G. Belfort, *Angewandte Chemie-International Edition*, 2006, **45**, 4094-4098.
63. G. G. Wu, Y. P. Li, M. Han and X. X. Liu, *Journal of Membrane Science*, 2006, **283**, 13-20.
64. L. Ying, W. H. Yu, E. T. Kang and K. G. Neoh, *Langmuir*, 2004, **20**, 6032-6040.
65. J. He, H. Zhang, J. Chen and Y. Yang, *Macromolecules*, 1997, **30**, 8010-8018.
66. M. Al-Harthi, J. B. P. Soares and L. C. Simon, *Macromolecular Materials and Engineering*, 2006, **291**, 993-1003.
67. K. Matyjaszewski, *Progress in Polymer Science*, 2005, **30**, 858-875.
68. S. Edmondson, V. L. Osborne and W. T. S. Huck, *Chemical Society Reviews*, 2004, **33**, 14-22.
69. D. Wandera, S. R. Wickramasinghe and S. M. Husson, *Journal of Membrane Science*, 2010, **357**, 6-35.
70. D. J. Chung, Y. Ito and Y. Imanishi, *Journal of Applied Polymer Science*, 1994, **51**, 2027-2033.
71. K. Sumaru, K. Ohi, T. Takagi, T. Kanamori and T. Shinbo, *Langmuir*, 2006, **22**, 4353-4356.
72. M.-S. Kang and V. K. Gupta, *The Journal of Physical Chemistry B*, 2002, **106**, 4127-4132.
73. S. Paula, A. G. Volkov, A. N. Van Hoek, T. H. Haines and D. W. Deamer, *Biophysical Journal*, 1996, **70**, 339-348.
74. J. G. Wijmans and R. W. Baker, *Journal of Membrane Science*, 1995, **107**, 1-21.
75. K. Matsubara, M. Watanabe and Y. Takeoka, *Angewandte Chemie International Edition*, 2007, **46**, 1688-1692.
76. S. Wang, M.-S. Choi and S.-H. Kim, *Dyes and Pigments*, 2008, **78**, 8-14.
77. M. R. Prausnitz and R. Langer, *Nat Biotech*, 2008, **26**, 1261-1268.
78. V. Prabhakar, A. Shivendra, S. Ritika and S. Sharma, *International Research Journal of Pharmacy*, 2012, **3**, 4.
79. E. Touitou, H. E. Junginger, N. D. Weiner, T. Nagai and M. Mezei, *Journal of Pharmaceutical Sciences*, 1994, **83**, 1189-1203.
80. S. Mitragotri, D. A. Edwards, D. Blankschtein and R. Langer, *Journal of Pharmaceutical Sciences*, 1995, **84**, 697-706.
81. D. A. Barrett and N. Rutter, *Critical reviews in therapeutic drug carrier systems*, 1994, **11**, 1-30.

2. SYNTHESIS OF SPIROCOMPOUNDS

2.1. INTRODUCTION

Spiropyrans (SP) and spirooxazines (SO) are well-known photochromic molecular switches.[1-4] Since 1952, when photochromism of spiropyran first was reported by Hirshberg and Fischer[5], a lot of investigations have been made in the field of photochromic spiro-compounds. Chemical as well as physical properties of spiropyrans and spirooxazines have been studied carefully.[1, 2] A reversible, photo-induced electrocyclic ring-opening reaction takes place whenever a spiropyran or a spirooxazine is exposed to UV-light with appropriate wavelength. The heterolytic ring-opening reaction transforms uncolored, nonpolar spiropyran or spirooxazine into the corresponding colored and polar merocyanine-state (MC). Illuminating merocyanine with visible light (e.g. 650 nm) converts it back into its initial SP-state. Alternatively, transformation from the energetically higher MC-state into its energetically more stable SP-state can also be thermally induced (Figure 2.1).[1-3]

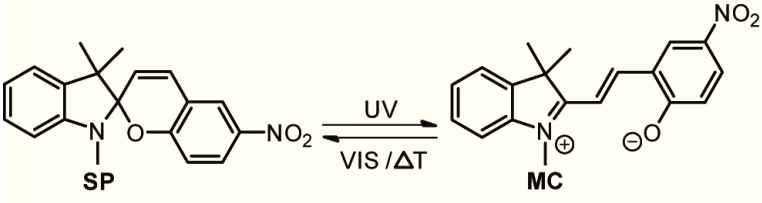

Figure 2.1 Spiropyran in its SP (closed, nonpolar) and its MC (open, polar) state.

In some rare cases, the MC-state is energetically more stable than the corresponding SP-state. Therefore, such molecules are colored at ambient conditions and can be decolored by irradiation with visible light. This phenomenon is called inverse photochromism.[6-8] Heating these samples would accordingly induce ring-opening instead of ring-closing reaction.

Usually, spiropyrans and spirooxazines consist of an indoline- and a benzopyran- respectively an oxazine-part. They are linked by a spiro-carbon in the SP-state. This aligns the molecule into two orthogonal planes. After transformation into the MC-state, the molecule rearranges into a planar configuration leading to an extended conjugated π-electron-system. This rearrangement changes the absorption of the molecule which explains the appearing color (Figure 2.2).[9]

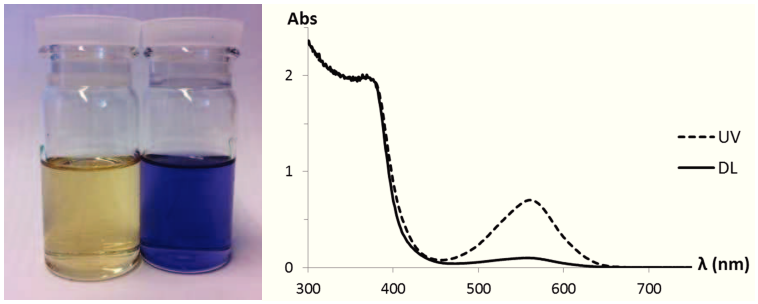

Figure 2.2 Left: Spiropyran in EtOAc at daylight (yellow) and after UV-irradiation (blue); right: corresponding UV-Vis spectra.

Merocyanine has two resonance structures (Figure 2.3). The zwitterionic structure is highly polar due to its localized charges. The corresponding quinoid structure is nonionic and therefore less polar.[10] The polarity of the surrounding and the substituents within the conjugated π-electron-system influence the character of the merocyanine. In polar surroundings, the charges are well stabilized and zwitterionic character can be observed for the merocyanine structure. Electron-withdrawing groups in ortho- or para-position to the oxygen anion and electron-donating groups in ortho- or para-position to the nitrogen cation also increase the zwitterionic character of the merocyanine.[10]

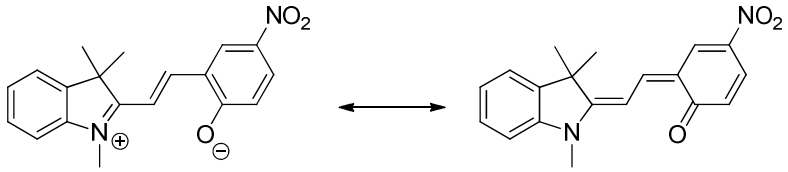

Figure 2.3 Zwitterionic (left) and quinoid (right) resonance structure of merocyanine.

At room temperature in the dark, merocyanine slowly undergoes a ring-closing reaction. The color disappears and the initial spiropyran can be recovered.[1] This thermal decoloration rate depends again on the polarity of the surrounding, the substituents in the π-electron-system and the temperature. To lower the decoloration-rate, the polar MC-state has to be stabilized. Electron-withdrawing groups in ortho- or para-position to the oxygen anion and electron-donating groups in ortho- or para-position to the nitrogen cation can significantly stabilize the zwitterionic merocyanine.[1, 2, 11] Lowering the temperature and increasing the polarity of the surrounding medium are also known to stabilize the colored merocyanine-state.[1, 2] Addition of an appropriate metal forming a chelate with the merocyanine-state, eliminates the thermal decoloration almost entirely.[12] If the molecular switch is incorporated into a polymeric matrix, its photochromic behavior strongly depends on the free volume in the matrix and the polarity of the polymer. In a soft matrix with a big free volume, switching is easier than in a rigid matrix with a low free volume.[2, 13, 14]

Spiropyrans are slowly decomposed when exposed to light. Especially the UV-light used to switch the molecule from its SP- into its MC-state has a big impact on the decomposition of the molecular switch. Decreasing coloration of a material due to decomposition of the dye is called fading. Up to now, it has not been ultimately clarified, what mechanisms are involved in the decomposition of photochromic spiro-compounds. The formation of highly reactive singlet oxygen during the illumination of the molecular switches was discussed[15] as well as the formation of radicals due to homolytic ring-opening reactions.[16] What is known from literature is the fact that integration of spiropyran into polymeric matrices lowers the fading rate.[17] Spirooxazines are also known to have lower fading rates than spiropyrans.[1, 3, 4, 18] Spiropyrans often still have high fading rates after implementation into polymeric matrices. Therefore it is reasonable to use spirooxazines to improve the durability of developed systems. Nevertheless, for the production of prototypes, spiropyrans are often used due to the well-known straightforward syntheses and purifications of these structures.

Although a lot of data has been collected for a variety of photochromic spiro-compounds, no universally valid concept to predict the impact of substituents and the surroundings on the decoloration and the fading rate of the molecular switches has been found. Simple models (e.g.

electron donor/acceptor) only allow limited predictions of the molecular switches' behavior, since there are always exceptions to these models.[1]

Nowadays, spiropyrans are often simply compounded into polymeric matrices to create photochromic materials.[4] Drawback of that approach is the leaking of spiropyran in such systems. Especially for swelling polymers (e.g. hydrogels) and in close contact with good solvents for spiropyrans, this approach is not suitable.

To optimally benefit not only from the color-change but also from the polarity-change of spiropyran (e.g. switchable solubility of a polymer), it is advantageous to covalently link the molecular switch to its matrix. Covalent linkage also solves the leaking-problem. Therefore, a linker has to be introduced to the spiropyran structure during the synthesis. Two strategies were followed to incorporate spiropyran into the matrix. In the first strategy, the structures of the linker were chosen such, that spiropyran were linked to a functional side chain of a polymer via esterification after polymerization. In the second strategy, a transformation of the linker into a methacrylate or an acrylate was performed, which allowed the direct copolymerization of spiropyran with other monomers.

To gain information not only about the electrostatic but also the steric impact of photochromic spiro-compounds on polymeric matrices, a spirooxazine with two linkers was synthesized. Incorporation of that molecule as cross-linker into a polymeric matrix is expected to result in a mechanochromic material.[19]

Contemporary publications usually report on the incorporation of only one type of spiropyran or spirooxazine into a material. No comparison of different spiro-compounds has been reported and barely any data concerning fading rates have been shown. Comparing the behavior of different spiropyrans reported in different studies is problematic due to differences in the production or the analysis setup (e.g. irradiation intensity for determination of fading rates). The in-house synthesis of several spiropyrans and spirooxazines allowed producing and analyzing materials with different molecular switches. Fading behavior was measured under identical conditions (see Chapter 3 – 6).

2.2. RESULTS AND DISCUSSION

Synthesis of photochromic spiropyrans with different linkers was successfully performed (Figure 2.4). Several grams of corresponding acrylic and methacrylic derivatives of spiropyran were achieved in high purity. These photochromic monomers were all tested as potential candidates for copolymerization with other monomers to obtain photochromic materials. Additionally, the synthesis of three photochromic spirooxazines was elaborated (Figure 2.4). One of them has two acrylic groups and is therefore a potential crosslinking species to achieve mechanochromic materials.[19] Furthermore, functional groups at the spiropyran backbone and the position and length of the linker have been altered to investigate the impact on the photochromic behavior of the corresponding spiro-compound.

It is known from literature, that changing the linker-length has a significant impact on the photochromic behavior of spiropyrans that are covalently bound to a matrix material.[20] Short linkers do not allow the spiropyran structure to move far apart from its matrix. Therefore, a higher impact

from the matrix on the photochromic behavior can be expected for short linkers. Photochromism of different spiropyrans and spirooxazines was first investigated in different solvents at room temperature. Not all synthesized spiro-compounds showed photochromic behavior at room temperature. Whether these structures were non-photochromic at all or whether ring-closing reaction was too fast to be detected by eye cannot be stated. From literature it is known that some spiropyrans show photochromic behavior only at low temperatures (e.g. at -200°C).[1]

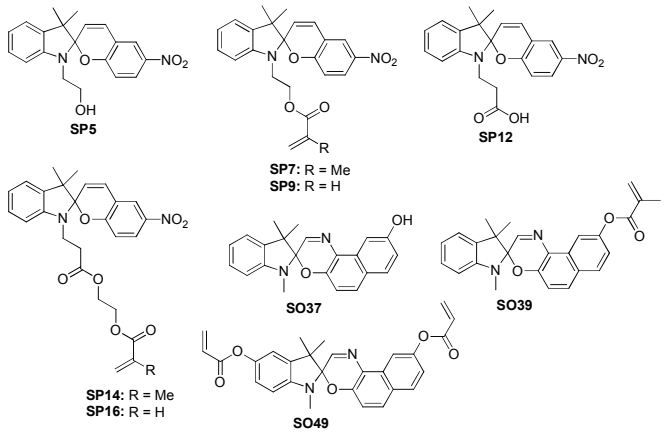

Figure 2.4 Synthesized spiro-compounds that show photochromic behavior at room temperature.

For the application in a transdermal caffeine delivery setup, only molecules with photochromic behavior at room temperature are of interest. Therefore, all molecules showing no photochromic behavior at room temperature in any solvent were excluded from further investigations and are not listed in Figure 2.4.

The most prominently reported spiropyran including a monomeric unit is methacrylate **7**.[21-23] Since copolymerization of spiropyran was not only planned with methacrylates but also with acrylates, molecule **9** was synthesized similarly. The three step syntheses were performed with an overall yield of 23% (**SP7**) and 56% (**SP9**) (Figure 2.5). Not only molecules **7** and **9** but also spiropyran **5** showed photo- and solvatochromic behavior at room temperature. Replacing acetonitrile (reported in two published syntheses[22, 24]) by toluene increased the yield of the first step significantly. In toluene, product **3** precipitated during the reaction whereas it stayed dissolved in acetonitrile. That difference in solubility can be an explanation for the increased yield.

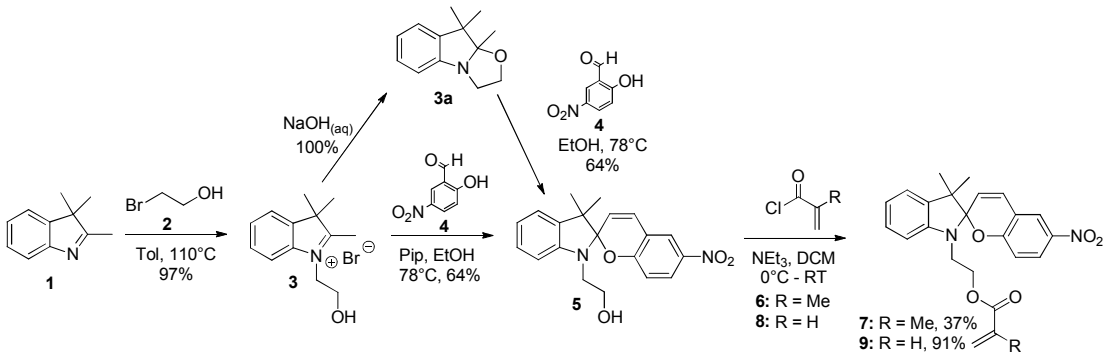

Figure 2.5 Three step synthesis of spiropyran **7** and **9** via photochromic intermediate **5**.

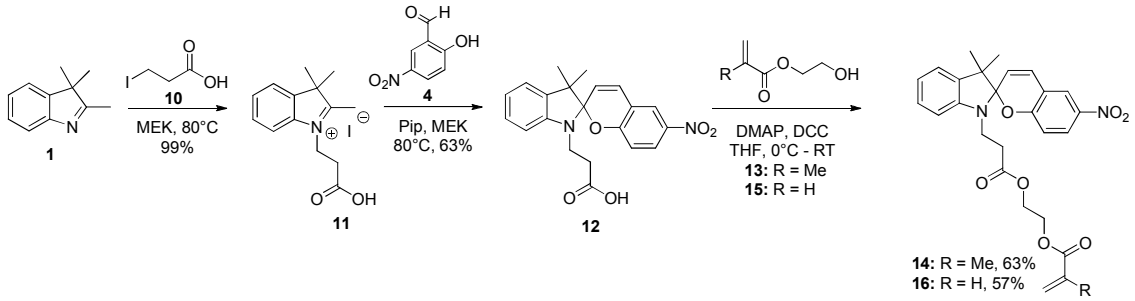

Figure 2.6 Three step synthesis of spiropyran **14** and **16** via photochromic intermediate **12**.

Using piperidine as base for the condensation of benzaldehyde **4** with indoline salt **3** resulted in a slightly higher yield of spiropyran **5** than using triethylamine. Additionally, it was easier to remove piperidine than triethylamine during the work-up.

In general, purification of spiro-compounds was the most demanding part of the synthesis because of their adaptive character. On silica gel, the spiro-compounds switched into their MC-state. This highly polar structure did not allow separation from polar impurities and a lot of material stayed on the column. Also recrystallization caused difficulties. One of the different states of the spiro-compounds was almost always soluble in a certain solvent.

Deprotonation of indoline salt **3** allowed isolating structure **3a**. Condensation of molecule **3a** with aldehyde **4** resulted also in spiropyran **5**. No significant difference concerning yield and purity of spiropyran **5** was found for the two alternative routes (Figure 2.5).

Spiropyran **14** is a known photochromic monomer.[25] Reports about photochromic materials containing structure **14** are less common than reports about materials based on molecule **7**. Structure **16**, which cannot be found in literature, was synthesized similar to molecule **14**. The three step syntheses were performed with an overall yield of 39% (**SP14**) and 36% (**SP16**) (Figure 2.6). Concerning the yield of the condensation reaction of molecules **11** with aldehyde **4**, *in situ* deprotonation of indoline salt **11** was more effective than including a separate deprotonation step. Using piperidine as base for the *in situ* deprotonation resulted again in slightly higher yields than using triethylamine.

1-ethyl-3-(3-dimethylaminopropyl)carbodiimide (EDCI) was tested as coupling agent instead of *N,N'*-dicyclohexylcarbodiimide (DCC) for the esterification of spiropyran **12.** The approach with EDCI resulted in no product. Even after refluxing for 24 hours, only starting material was isolated. Molecule **12**, **14** and **16** are all photochromic substances at room temperature.

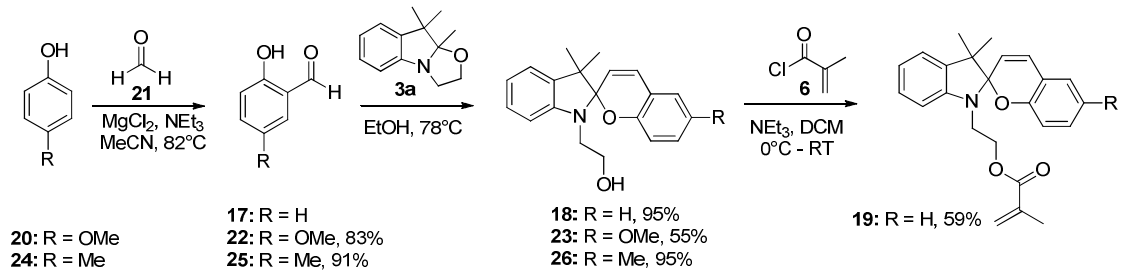

Figure 2.7 Synthesis of different spiro-compounds without a nitro-group showing no photochromic behavior at room temperature.

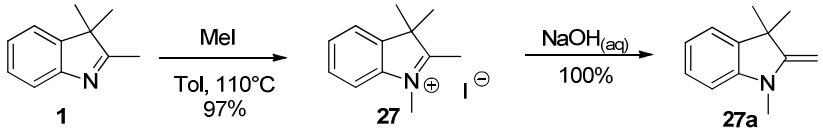

Figure 2.8 Synthesis of indoline **27** as precursor for spirooxazines and spiropyrans.

Since it is known from literature that the nitro-group plays a crucial role in the degradation process of spiropyrans under UV-irradiation[8, 26], three different spiro-structures without nitro-group were synthesized (Figure 2.7). Up to now, synthesis of spiropyran **26** has never been reported. It is expected that replacing a strong electron acceptor like NO_2 with an electron donor (e.g. OMe) has a major impact on the electron-distribution in the molecule, as explained in Chapter 2.1. The substitution of the nitro-group turned out to have such a big impact on the molecules that neither molecules **18**, **23**, **26** nor methacrylate **19** were photochromic at room temperature. Removing the nitro-group without adequate replacement with another strong electron withdrawing group seems to eliminate the photochromic behavior of spiropyrans.

Not only replacing substituents at the spiropyran backbone but also changes in length, structure or position of the linker from the spiropyran-unit to the (meth)acrylic unit can have a significant impact on the photochromic behavior of spiropyrans.[20] Therefore, spiropyrans with different linker positions were synthesized. Molecule **27** was synthesized as nonfunctional precursor for spiropyrans with its linker on the benzopyran-part (Figure 2.8).[27]

Spiropyran **30** was prepared according to literature.[8] In the present case, methacryloyl chloride was replaced by acryloyl chloride **8**. The overall yield for the three steps was found to be 12% (Figure 2.9). According to literature, molecule **30** was expected to show inversed photochromic behavior and improved photo-stability under UV-irradiation compared to nitro-containing spiropyrans.[8] However, spiro-compound **30** did not show any photochromic behavior at room temperature, neither as solute in different solvents (MeOH, EtOH, H_2O, Et_2O, EtOAc, Hx, MEK, TBME, Tol, THF, MeCN, DMF, DMSO, and acetone) nor in a polymeric structure copolymerized with 2-hydroxyethyl acrylate.

Since replacing the nitro-group did not result in any photochromic molecule at room temperature, it seems to be more meaningful to develop spirooxazine containing materials for long term applications with low fading rates. However, for the development of simple prototypes, working with nitro-spiropyrans provides enough stability.

Precursor **34** was synthesized according to literature with a slightly modified procedure (Figure 2.10).[28] The three-step synthesis gave an overall yield of 44%. This indoline derivative allowed us to introduce a linker on the indoline part of the spiropyran. Creation of crosslinking-molecules is possible, if there is a second linker introduced in the pyran or oxazine part.

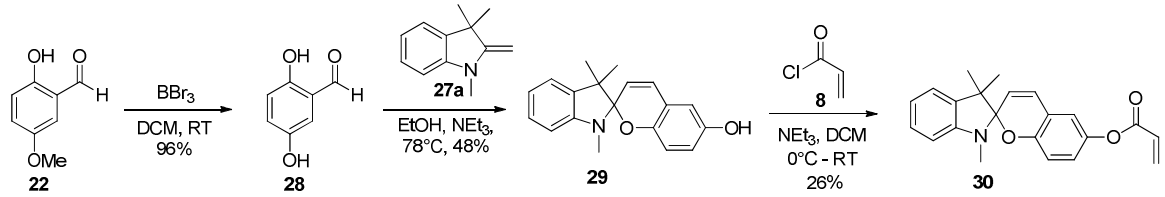

Figure 2.9 Synthesis of nitro-free acrylic spiropyran **30.**

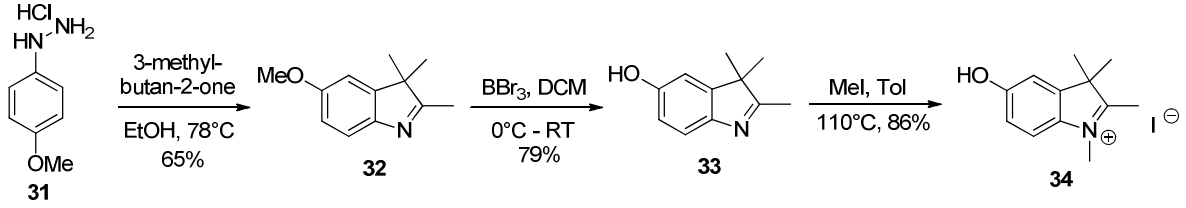

Figure 2.10 Synthesis of indoline salt **34** as functional precursor for spiropyrans and spirooxazines.

Spirooxazine **39** was synthesized in 3 steps. Two alternative routes were investigated. One approach was the condensation of nitroso-compound **36** with indoline salt **27** to obtain spirooxazine **37.**[29] *In situ* oxidation of amino-compound **38** with DMSO followed by condensation with indoline salt **27** to obtain spirooxazine **37** was the second approach. From literature it is known that using amino-compounds with *in situ* oxidation generally results in higher yields of spirooxazines.[30] But in the present case, working with amine **38** resulted in an overall yield of 3% whereas condensation with nitroso-compound **36** gave an overall yield of 11% (Figure 2.11). Molecule **37** as well as molecule **39** was photochromic at room temperature.

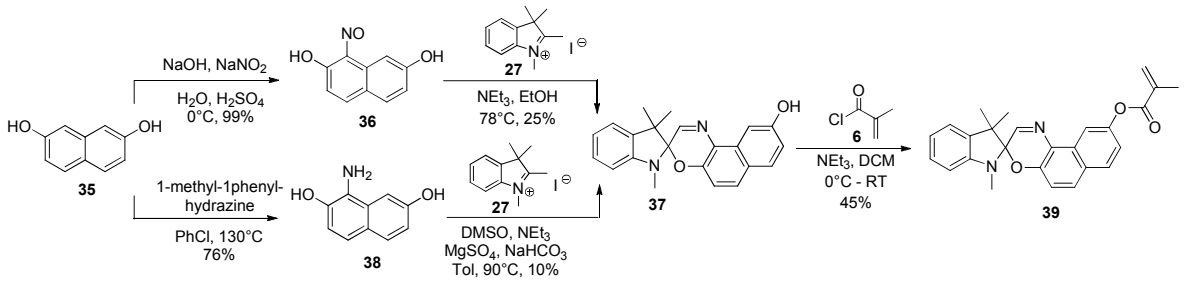

Figure 2.11 Three step synthesis of methacrylic spirooxazine **39.**

To compare spirooxazines with spiropyrans, the same indoline-unit as for spiropyran **5** was used for spirooxazine **40**. Unexpectedly, the free alcohol of the linker reacted after condensation-reaction in a favored 6-exo-trig pattern (Baldwin-rule) with the created electrophilic imine, resulting in an additional morpholinic group that eliminated the photochromic behavior of the molecule (Figure 2.12). No reports on structure **40** or similar intramolecular reactions of functional groups with the imine of spirooxazines can be found in literature. The additional ring-closure was confirmed by HMBC and NOESY measurements. It was not possible to reopen the undesired ring to functionalize the alcohol. Transforming the alcohol into a methacrylate before performing the condensation reaction was tested without any success.

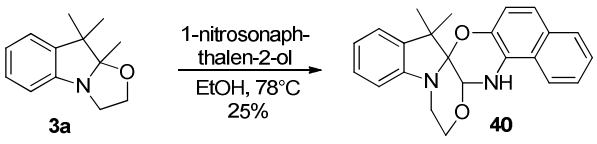

Figure 2.12 Condensation reaction to obtain spiro-compound **40** with interfering linker.

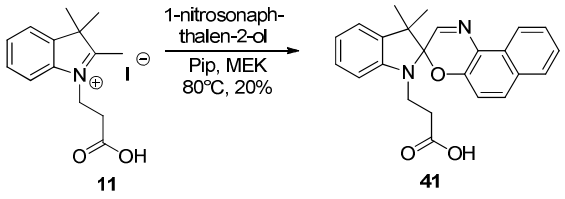

Figure 2.13 Condensation reaction to obtain spirooxazine **41** that shows photochromic behavior on silica gel.

Synthesis of spirooxazine **41** was successfully performed (Figure 2.13). Structure **41** was found to be photochromic on silica gel but no photochromic behavior was observed in a variety of solvents (MeOH, EtOH, H_2O, Et_2O, EtOAc, Hx, MEK, TBME, Tol, THF, MeCN, DMF, DMSO, acetone) or after linking to pHEMA. Up to now, molecule **41** has only been reported as starting material in literature without any synthetic details shown.[31, 32]

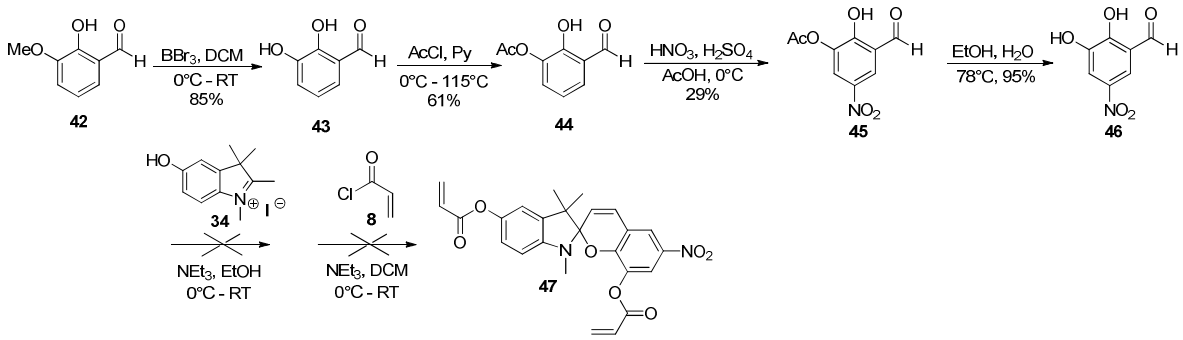

Figure 2.14 Unsuccessful synthetic approach to obtain biacrylic spiropyran **47.**

Crosslinking spiro-compound **47** is known from literature to lead to photo- and mechanochromic polymers.[19] Since in a polymeric matrix not only electrostatic but also steric aspects play an important role, the idea was to synthesize such a biacrylate derivative to investigate the impact of a second linker on the photochromic and structural properties of polymers. Syntheses of the precursors were performed as reported in literature. However, all attempts to isolate the bi-alcoholic spiropyran after condensation in a sufficient purity for further studies failed. Taking the crude product to the next step neither solved the problem. Although photochromic behavior of molecule **47** was detectable, no pure spiropyran **47** was isolated (Figure 2.14).

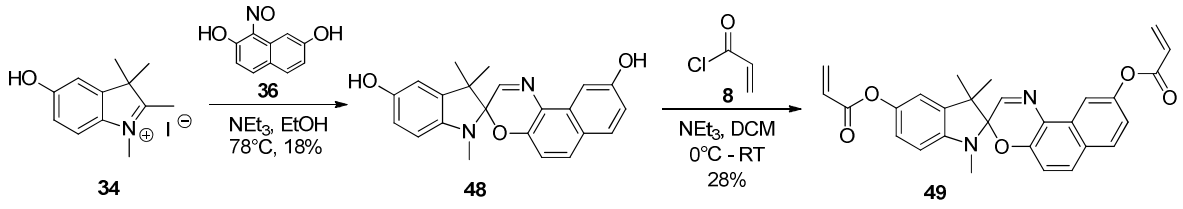

Figure 2.15 Synthetic approach to produce photochromic biacrylic spirooxazine **49.**

As an alternative approach to synthesizing a crosslinking-spiro-compound, synthesis of biacrylic spirooxazine **49** was performed (Figure 2.15). Molecules **48** and **49** have not been described yet in literature. The overall-yield for spirooxazine **49** was modest but three synthetic steps and two purifications by column chromatography could be avoided compared to the synthetic rout of spiropyran **47**. An additional plus for spirooxazine **49** is its lower fading rates (see Chapter 3).[1, 4]

2.3. EXPERIMENTAL

All reactions were performed under an inert gas atmosphere. Magnesium chloride ($MgCl_2$) was delivered by Fluka. Boron tribromide (BBr_3, 99%), ethanol (EtOH, absolute, 99.0%, dried over molecular sieve), dichloromethane (DCM, 99.8%, dried over molecular sieve) and toluene (Tol, 99.8%, dried over molecular sieve) were purchased from Acros. Acetonitrile (MeCN, HPLC grade) was delivered by Fisher Chemical. Deuterated chloroform ($CDCl_3$, 99.8%) and deuterated DMSO (d_6-DMSO, 99.8%) were obtained from Armar Chemicals. All other chemicals were delivered from Sigma Aldrich, e.g. 2-butanone (MEK, 99.0%) and THF (99.8%, dried). All reagents and solvents were used without further purification if not stated otherwise. Deionized water was obtained from the in-house purification system. For rotary evaporation, the temperature was set to 40°C. Organic layers after extractions were dried over $MgSO_4$ x 2 H_2O. Column chromatography was performed on silica gel 60 (70 – 230 mesh) from Merck. Thin layer chromatography (TLC) was performed on Silicagel 60W F_{254S} TLC glass plates from Merck. Preparative layer chromatography (PLC) was performed on PLC Silicagel 60 F_{254} glass plates with a layer thickness of 2 mm from Merck.
^{1}H-NMR and ^{13}C-NMR were measured with a Bruker 400 MHz. The signal of non-deuterated solvent was used as internal reference for the ^{1}H-spectra. For the ^{13}C-spectra the carbon signal of the deuterated solvent was used as internal reference. Coupling constants are reported in Hertz (Hz). For the assignment of the signals in the ^{13}C-NMR spectra, HMBC and HSQC experiments were performed. Infrared (IR) spectra were recorded with a BioRad FTS 6000 using an ATR Golden Gate. Ultraviolet and visible (UV/VIS) absorption measurements were performed on a Varian 50Bio/50MPR. Low resolution mass spectroscopy (LRMS) was performed on a Bruker Daltonics esquire HCT. All LRMS-samples were dissolved in acetonitrile and filtered over titan HPLC-nylon filter (0.45 μm) from Infochroma AG. Elemental analysis (EA) was recorded on an Elementar Vario Micro Cube at the measuring service of the University of Basel.

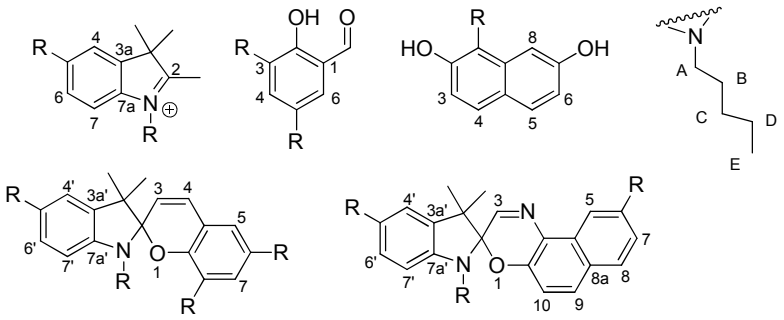

Figure 2.16 Numbering of molecules relevant for NMR-signal assignments.

1-(2-hydroxyethyl)-2,3,3-trimethyl-3H-indol-1-ium bromide (3). A dry round-bottom flask was charged with indoline **1** (5.0 g, 31 mmol) and 50 mL toluene. After addition of bromide **2** (4.7 g, 38 mmol) the reaction mixture was heated to 110°C and stirred for 12 h. After cooling to room temperature, the precipitated material was isolated by vacuum filtration and washed with cold toluene followed by Et_2O to obtain product **3** (8.7 g, 30 mmol, 97%) as a light pink salt.
^{1}H-NMR (400 MHz, d_6-DMSO) δ: 7.98 (dd, J = 5.6, 3.4 Hz, 1H, H7), 7.85 (dd, J = 5.8, 2.9 Hz, 1H, H4), 7.63 – 7.55 (m, 2H, H5, H6), 4.64 – 4.58 (t, J = 5.1 Hz, 2H, HA), 3.90 – 3.84 (t, J = 5.1 Hz, 2H, HB), 2.83 (s, 3H, C2-**Me**), 1.55 (s, 6H, C3-**Me$_2$**).
^{13}C-NMR (101 MHz, d_6-DMSO) δ: 197.73 (C2), 141.80 (C3a), 141.14 (C7a), 129.27 (C6), 128.78 (C5), 123.45 (C4), 115.61 (C7), 57.74 (CB), 54.24 (C3), 50.31 (CA), 22.01 (2C, C3-**Me$_2$**), 14.50 (C2-**Me**).
IR (cm^{-1}): 3251, 1607, 1463, 1379, 1092, 1062, 721.
LRMS-ESI$_{pos}$ (*m/z*): $[M-Br]^+$ calc. for $C_{13}H_{18}NO$ 204.1; found 203.7

9,9,9a-trimethyl-2,3,9,9a-tetrahydrooxazolo[3,2-a]indole (3a). When bromide salt **3** was suspended in DCM and washed with 1 M NaOH, structure **3a** was isolated as dark violet oil in 100% yield.
^{1}H-NMR (400 MHz, $CDCl_3$) δ: 7.15 (dd, J = 7.8, 7.7 Hz, 1H, H6), 7.08 (d, J = 7.4 Hz, 1H, H4), 6.93 (dd, J = 7.7, 7.4 Hz, 1H, H5), 6.77 (d, J = 7.8 Hz, 1H, H7), 3.89 – 3.81 (m, 1H, HB), 3.77 – 3.69 (m, 1H, HA), 3.65 – 3.48 (m, 2H, HA,HB), 1.44 (s, 3H, C3-**Me$_2$**), 1.40 (s, 3H, C2-**Me**), 1.19 (s, 3H, C3-**Me$_2$**).
^{13}C-NMR (101 MHz, $CDCl_3$) δ: 150.48 (C7a), 139.95 (C3a), 127.45 (C6), 122.36 (C4), 121.65 (C5), 111.93 (C7), 108.92 (C2), 62.93 (CB), 50.03 (CA), 46.90 (C3), 28.05 (C3-**Me$_2$**), 20.75 (C3-**Me$_2$**), 17.54 (C2-**Me**).
IR (cm^{-1}): 2962, 2879, 1606, 1579, 1455, 1293, 1030, 746.
LRMS-ESI$_{pos}$ (*m/z*): $[MH]^+$ calc. for $C_{13}H_{18}NO$ 204.1; found 203.7

2-(3',3'-dimethyl-6-nitrospiro[chromene-2,2'-indolin]-1'-yl)ethanol (5). Bromide salt **3** (2.0 g, 7.0 mmol) was dissolved in 20 mL ethanol. Piperidine (0.77 mL, 7.7 mmol) and benzaldehyde **4** (1.78 g, 10.7 mmol) were added in one portion. The reaction mixture was refluxed for 5 h. After cooling to room temperature, the mixture was stirred for an additional hour. Precipitated material was then isolated at 0°C and washed with cold ethanol to obtain spiropyran **5** (1.6 g, 4.5 mmol, 64%) as violet powder.
^{1}H-NMR (400 MHz, $CDCl_3$) δ: 8.02 (m, 2H, H5, H7), 7.20 (dd, J = 7.8, 7.6 Hz, 1H, H6'), 7.11 (d, J = 7.1 Hz, 1H, H4'), 6.91 (m, 2H, H4, H5'), 6.77 (d, J = 8.7 Hz, 1H, H8), 6.68 (d, J = 7.8 Hz, 1H, H7'), 5.90 (d, J = 10.4 Hz, 1H, H3), 3.91 – 3.67 (m, 2H, HA), 3.58 – 3.42 (m, 1H, HB), 3.41 – 3.28 (m, 1H, HB), 1.30 (s, 3H, C3'-**Me$_2$**), 1.20 (s, 3H, C3'-**Me$_2$**).
^{13}C-NMR (101 MHz, $CDCl_3$) δ: 159.28 (C8a), 146.93 (C7a'), 141.10 (C6), 135.78 (C3a'), 128.22 (C4), 127.81 (C6'), 125.93 (C7), 122.73 (C5), 121.90 (2C, C3 and C4'), 119.95 (C5'), 118.51 (C4a), 115.49 (C8), 106.87 (C7'), 106.69 (C2), 60.81 (CA), 52.80 (C3'), 46.07 (CB), 25.87 (C3'-**Me$_2$**), 19.98 (C3'-**Me$_2$**).
IR (cm^{-1}): 2958, 2926, 1609, 1480, 1334, 1272, 1088, 952, 722.
UV/VIS (MeCN): ε_{366} = 2684 M^{-1}cm^{-1} $\lambda_{max,UV}$ = 560 nm
LRMS-ESI$_{pos}$ (*m/z*): $[MH]^+$ calc. for $C_{20}H_{21}N_2O_4$ 353.1; found 352.9

2-(3',3'-dimethyl-6-nitrospiro[chromene-2,2'-indolin]-1'-yl)ethyl methacrylate (7). A dry round-bottom flask was charged with spiropyran **5** (5.0 g, 14.2 mmol) and 40 mL DCM. After wrapping the flask with aluminum foil, the reaction mixture was cooled to 0°C. NEt_3 (2.4 mL, 17.0 mmol) was added in one portion followed by drop-wise addition of acid chloride **6** (1.7 mL, 17.0 mmol). After keeping the reaction at 0°C for an additional hour, the mixture was stirred at room temperature for 12 h.
Purification by column chromatography (3:2 DCM:Hx) allowed isolation of methacrylate **7** (2.2 g, 5.2 mmol, 37%) as dark-red, sticky substance.
^{1}H-NMR (400 MHz, $CDCl_3$) δ: 8.09 – 7.93 (m, 2H, H5, H7), 7.21 (dd, *J* = 7.7, 7.5 Hz, 1H, H6'), 7.09 (d, *J* = 7.3 Hz, 1H, H4'), 6.94 – 6.83 (m, 2H, H4, H5'), 6.76 (d, *J* = 8.2 Hz, 1H, H8), 6.70 (d, *J* = 7.7 Hz, 1H, H7') 6.07 (s, 1H, CE=**CH_2**), 5.88 (d, *J* = 10.3 Hz, 1H, H3), 5.56 (s, 1H, CE=**CH_2**), 4.30 (m, 2H, HB), 3.60 – 3.40 (m, 2H, HA), 1.92 (s, 3H, CE-**Me**), 1.28 (s, 3H, C3'-**Me_2**), 1.16 (s, 3H, C3'-**Me_2**).
^{13}C-NMR (101 MHz, $CDCl_3$) δ: 167.33 (CD), 159.53 (C8a), 146.79 (C7a'), 141.22 (C6), 136.17 (CE), 135.83 (C3a'), 128.43 (C4), 127.98 (C6'), 126.07 (2C, C7 and CE=**CH2**), 122.91 (C5), 121.93 (2C, C3 and C4') 120.06 (C5'), 118.55 (C4a), 115.69 (C8), 106.89 (C7'), 106.65 (C2), 62.76 (CB), 52.94 (C3'), 42.56 (CA), 25.97 (C3'-**Me_2**), 19.96 (C3'-**Me_2**), 18.48 (CE-**Me**).
IR (cm^{-1}): 2927, 1734, 1608, 1522, 1456, 1336, 1089, 1025, 950, 744.
UV/VIS (MeCN): ε_{366} = 1776 $M^{-1}cm^{-1}$ $\lambda_{max,UV}$ = 565 nm
LRMS-ESI_{pos} (*m/z*): $[MH]^+$ calc. for $C_{24}H_{25}N_2O_5$ 421.2; found 421.2
EA: calc. [C] 68.6%, [H] 5.8%, [N] 6.7%; found [C] 67.2%, [H] 5.7%, [N] 6.3%.

2-(3',3'-dimethyl-6-nitrospiro[chromene-2,2'-indolin]-1'-yl)ethyl acrylate (9). Spiropyran **5** (5.6 g, 15.9 mmol) was dissolved in 50 mL DCM. After wrapping the flask with aluminum foil, the reaction mixture was cooled to 0°C. NEt_3 (2.8 mL, 19.1 mmol) was added in one portion followed by drop-wise addition of acid chloride **8** (1.6 mL, 19.1 mmol). After stirring for an additional hour at 0°C the reaction mixture was stored for 12 h at room temperature. The crude product was then dissolved in DCM and washed with 0.1 M HCl solution, saturated $NaHCO_3$ solution and brine. Acrylate **9** (5.9 g, 14.5 mmol, 91%) was isolated as a red sticky substance.
^{1}H-NMR (400 MHz, *d_6*-DMSO) δ: 8.20 (s, 1H, H5), 7.98 (d, *J* = 9.0 Hz, 1H, H7), 7.18 (d, *J* = 10.4 Hz, 1H, H4), 7.12 (m, 2H, H4', H6'), 6.86 (d, *J* = 9.0 Hz, 1H, H8), 6.78 (dd, *J* = 7.3, 7.3 Hz, 1H, H5'), 6.71 (d, *J* = 7.9 Hz, 1H H7'), 6.26 (d, *J* = 17.2 Hz, 1H, CE=**CH_2**), 6.09 (dd, *J* = 17.2, 10.3 Hz, 1H, CE-**H**), 5.97 (d, *J* = 10.4 Hz, 1H, H3), 5.89 (d, *J* = 10.3 Hz, 1H, CE=**CH_2**), 4.35 – 4.15 (m, 2H, HB), 3.70 – 3.25 (m, 2H, HA), 1.18 (s, 3H, C3'-**Me_2**), 1.06 (s, 3H, C3'-**Me_2**).
^{13}C-NMR (101 MHz, *d_6*-DMSO) δ: 165.30 (CD), 159.05 (C8a), 146.35 (C7a'), 140.55 (C6), 135.42 (C3a'), 131.70 (CE=**CH_2**), 128.12 (2C, C4 and CE), 127.58 (C4' or C6'), 125.73 (C7), 122.83 (C5), 121.63 (2C, C3 and C4' or CC6'), 119.37 (C5'), 118.71 (C4a), 115.46 (C8), 106.52 (C7'), 106.23 (C2), 62.07 (CB), 52.36 (C3'), 41.87 (CA), 25.55 (C3'-**Me_2**), 19.44 (C3'-**Me_2**).
IR (cm^{-1}): 2960, 2927, 1719, 1479, 1333, 1272, 1185, 1089, 953, 805, 715.
UV/VIS (MeCN): ε_{366} = 3069 $M^{-1}cm^{-1}$ $\lambda_{max,UV}$ = 569 nm
LRMS-ESI_{pos} (*m/z*): $[MH]^+$ calc. for $C_{23}H_{23}N_2O_5$ 406.2; found 406.9
EA: calc. [C] 68.0%, [H] 5.5%, [N] 6.9%; found [C] 68.5%, [H] 5.6%, [N] 7.1%.

1-(2-carboxyethyl)-2,3,3-trimethyl-3H-indol-1-ium iodide (11). Indoline **1** (4.0 g, 25 mmol) was dissolved in 4 mL MEK. After addition of iodide **10** (5.4 g, 27 mmol) the reaction mixture was refluxed and stirred for 12 h. After cooling to room temperature, the precipitated material was isolated and washed with cold hexane followed by Et_2O to obtain iodide salt **11** (9.1 g, 25 mmol, 99%) as a light-brown salt.
^{1}H-NMR (400 MHz, d_6-DMSO) δ: 8.05 – 7.90 (dd, J = 5.8, 3.1 Hz, 1H, H7), 7.83 (dd, J = 4.0, 2.1 Hz, 1H, H4), 7.61 (m, 2H, H5, H6), 4.64 (t, J = 7.0 Hz, 2H, HA), 2.97 (t, J = 7.0 Hz, 2H, HB), 2.86 (s, 3H, C2-**Me**), 1.52 (s, 6H, C3-**Me$_2$**).
^{13}C-NMR (101 MHz, d_6-DMSO) δ: 197.88 (C2), 171.50 (CC), 141.73 (C3a), 140.80 (C8), 129.32 (C6), 128.89 (C5), 123.47 (C4), 115.55 (C7), 54.24 (C3), 43.55 (CB), 31.09 (CA), 21.86 (2C, C3-**Me$_2$**), 14.44 (C2-**Me**).
IR (cm^{-1}): 3032, 1727, 1397, 1171, 768.
LRMS-ESI$_{pos}$ (*m/z*): $[M-I]^+$ calc. for $C_{14}H_{18}NO_2$ 232.1; found 231.7

3-(3',3'-dimethyl-6-nitrospiro[chromene-2,2'-indolin]-1'-yl)propanoic acid (12). A dry round-bottom flask was wrapped with aluminum foil and then charged with iodide salt **11** (4.5 g, 12.6 mmol) and 20 mL MEK. Piperidine (1.3 mL, 13.2 mmol) and benzaldehyde **4** (2.1 g, 12.6 mmol) were added in one portion. The reaction mixture was heated to 80°C and stirred for 3 h. Then the reaction mixture was cooled to room temperature and stored for 12 h without stirring. After cooling to 0°C, the precipitated material was isolated and washed with cold MEK followed by MeOH to obtain spiropyran **12** (3.0 g, 7.9 mmol, 63%) as yellow powder.
^{1}H-NMR (400 MHz, d_6-DMSO) δ: 12.22 (s, 1H, COO**H**), 8.20 (s, 1H, H5), 7.99 (d, J = 9.0 Hz, 1H, H7), 7.20 (d, J = 10.4 Hz, 1H, H4), 7.10 (m, 2H, H4', H6'), 6.85 (d, J = 9.0 Hz, 1H, H8), 6.79 (dd, J = 7.4, 7.4 Hz, 1H, H5'), 6.65 (d, J = 8.0 Hz, 1H, H7'), 5.98 (d, J = 10.4 Hz, 1H, H3), 3.60 – 3.21 (m, 2H, HA), 2.66 – 2.26 (m, 2H, HB), 1.17 (s, 3H, C3-**Me$_2$**), 1.06 (s, 3H, C3-**Me$_2$**).
^{13}C-NMR (101 MHz, d_6-DMSO) δ: 172.85 (CC), 159.07 (C8a), 146.10 (C7a'), 140.54 (C6), 135.64 (C3a'), 128.15 (C4), 127.63 (C4' or C6)', 125.70 (C7), 122.79 (C5), 121.77 (2C, C3 and C4' or C6'), 119.22 (C5'), 118.83 (C4a), 115.48 (C8), 106.63 (C7'), 106.49 (C2), 52.41 (CA), 38.85 (C3'), 33.15 (CB), 25.57 (C3'-**Me$_2$**), 19.45 (C3'-**Me$_2$**).
IR (cm^{-1}): 1705, 1480, 1328, 1268, 944, 914, 747.
UV/VIS (MeCN): ε_{366} = 1387 M^{-1}cm^{-1} $\lambda_{max,UV}$ = 565 nm
LRMS-ESI$_{pos}$ (*m/z*): $[MH]^+$ calc. for $C_{21}H_{21}N_2O_5$ 381.1; found 380.9

2-((3-(3',3'-dimethyl-6-nitrospiro[chromene-2,2'-indolin]-1'-yl)propanoyl)oxy)ethyl methacrylate (14). Spiropyran **12** (2.0 g, 5.3 mmol), HEMA **13** (0.67 g, 5.8 mmol) and DMAP (122 mg, 1.0 mmol) were dissolved in 50 mL THF. After cooling to 0°C, DCC (1.2 g, 5.8 mmol) was added in one portion. The reaction mixture was then stirred at room temperature for additional 12 h. After removing the solvent, the crude mixture was dissolved in DCM and washed with brine. Recrystallization from EtOAc/Hx resulted in product **14** (1.6 g, 3.3 mmol, 63%) as yellow crystals.
^{1}H-NMR (400 MHz, $CDCl_3$) δ: 8.03 – 7.98 (m, 2H, H5, H7), 7.19 (dd, J = 7.7, 7.5 Hz, 1H, H6'), 7.09 (d, J = 7.3 Hz, 1H, H4'), 6.95 – 6.88 (m, 2H, H4, H5'), 6.73 (d, J = 8.3 Hz, 1H, H8), 6.61 (d, J = 7.7 Hz, 1H, H7'), 6.08 (s, 1H, CI=**CH$_2$**), 5.86 (d, J = 10.4 Hz, 1H, H3), 5.56 (s, 1H, CI=**CH$_2$**), 4.32 –

4.23 (m, 4H, HE, HF), 3.70 – 3.47 (m, 2H, HA), 2.78 – 2.55 (m, 2H, HB), 1.91 (s, 3H, CI-**Me**), 1.26 (s, 3H, C3'-**Me$_2$**), 1.14 (s, 3H, C3'-**Me$_2$**).
^{13}C-NMR (101 MHz, $CDCl_3$) δ: 171.69 (CC), 167.15 (CH), 159.47 (C8a), 146.30 (C7a'), 141.19 (C6), 136.08 (C3a'), 135.96 (CI), 128.48 (C4), 127.92 (C6'), 126.10 (2C, C7 and CI=**CH2**), 122.87 (C5), 122.03 (2C, C3 and C4'), 119.99 (C5'), 118.71 (C4a), 115.64 (C8), 106.86 (2C, C2 and C7'), 62.40 (2C, CE and CF), 53.04 (C3'), 39.29 (CA), 33.55 (CB), 25.86 (C3'-**Me$_2$**), 19.88 (C3'-**Me$_2$**), 18.35 (CI-**Me**).
IR (cm^{-1}): 2929, 1728, 1480, 1328, 1272, 1155, 946, 746.
UV/VIS (MeCN): $\varepsilon_{366} = 1219\ M^{-1}cm^{-1}$ $\lambda_{max,UV} = 566$ nm
LRMS-ESI$_{pos}$ (*m/z*): $[MH]^+$ calc. for $C_{27}H_{29}N_2O_7$ 493.2; found 493.0
EA: calc. [C] 65.8%, [H] 5.7%, [N] 5.7%; found [C] 66.4%, [H] 5.9%, [N] 6.6%.

2-((3-(3',3'-dimethyl-6-nitrospiro[chromene-2,2'-indolin]-1'-yl)propanoyl)oxy)ethyl acrylate (16). A dry round-bottom flask was charged with spiropyran **12** (1.0 g, 2.6 mmol), HEA **15** (0.34 g, 2.9 mmol), DMAP (64 mg, 0.5 mmol) and 15 mL THF. After cooling to 0°C, DCC (597 mg, 2.9 mmol) was added in one portion. The reaction mixture was stirred for additional 12 h at room temperature. After removing the solvent the crude product was dissolved in DCM and washed with brine. Recrystallization from EtOAc/Hx allowed the isolation of product **16** (0.71 g, 1.5 mmol, 57%) as yellow crystals.
^{1}H-NMR (400 MHz, $CDCl_3$) δ: 8.08 – 7.88 (m, 2H, H5, H7), 7.20 (dd, *J* = 7.7, 7.5 Hz, 1H, H6'), 7.10 (d, *J* = 7.3 Hz, 1H, H4'), 6.96 – 6.86 (m, 2H, H4, H5'), 6.73 (d, *J* = 9.1 Hz, 1H, H8), 6.62 (d, *J* = 7.7 Hz, 1H, H7'), 6.40 (d, *J* = 17.3 Hz, 1H, CI=**CH$_2$**), 6.09 (dd, *J* = 17.3, 10.5 Hz, 1H, CI-**H**), 5.86 (d, *J* = 10.6 Hz, 1H, H3), 5.84 (d, *J* = 10.5 Hz, 1H, CI=**CH$_2$**) 4.36 – 4.20 (m, 4H, HE, HF), 3.74 – 3.44 (m, 2H, HA), 2.81 – 2.55 (m, 2H, HB), 1.26 (s, 3H, C3'-**Me$_2$**), 1.14 (s, 3H, C3'-**Me$_2$**).
^{13}C-NMR (101 MHz, $CDCl_3$) δ: 171.54 (CC), 165.76 (CH), 159.33 (C8a), 146.16 (C7a'), 141.04 (C6), 135.92 (C3a'), 131.45 (CI=**CH$_2$**), 128.32 (C4), 127.80 (2C, C6' and CI), 125.84 (C7), 122.71 (C5), 121.87 (2C, C3 and C4'), 119.83 (C5'), 118.56 (C4a), 115.49 (C8), 106.72 (C7), 106.66 (C2), 62.12 (2C, CE and CF), 52.88 (C3'), 39.12 (CA), 33.39 (CB), 25.70 (C3'-**Me$_2$**), 19.71 (C3'-**Me$_2$**).
IR (cm^{-1}): 2930, 2116, 1726, 1480, 1332, 1269, 1165, 948, 746.
UV/VIS (MeCN): $\varepsilon_{366} = 1110\ M^{-1}cm^{-1}$ $\lambda_{max,UV} = 568$ nm
LRMS-ESI$_{pos}$ (*m/z*): $[MH]^+$ calc. for $C_{26}H_{27}N_2O_7$ 479.2; found 478.9
EA: calc. [C] 65.3%, [H] 5.5%, [N] 5.9%; found [C] 65.6%, [H] 5.6%, [N] 6.1%.

2-(3',3'-dimethylspiro[chromene-2,2'-indolin]-1'-yl)ethanol (18). Substance **3a** (0.83 g, 4.1 mmol) was dissolved in 20 mL EtOH. Benzaldehyde **17** (0.50 g, 4.1 mmol) was added in one portion and the reaction mixture was heated to 78°C and stirred for 12 h. After removing the solvent the crude product was purified by column chromatography (4:1 Hx:EtOAc). Spiropyran **18** (1.2 g, 3.9 mmol, 95 %) was isolated as an oily substance.
^{1}H-NMR (400 MHz, $CDCl_3$) δ: 7.17 (dd, *J* = 7.7, 7.5 Hz, 1H, H6'), 7.12 – 7.08 (m, 2H, H5, H7), 7.05 (d, *J* = 7.5 Hz, 1H, H4'), 6.92 – 6.79 (m, 3H, H4, H8, H5'), 6.71 (d, *J* = 8.1 Hz, 1H, H6), 6.64 (d, *J* = 7.8 Hz, 1H, H7'), 5.68 (d, *J* = 10.2 Hz, 1H, H3), 3.80 – 3.72 (m, 2H, HB), 3.59 – 3.25 (m, 2H, HA), 1.32 (s, 3H, C3'-**Me$_2$**), 1.18 (s, 3H, C3'-**Me$_2$**).

^{13}C-NMR (101 MHz, $CDCl_3$) δ: 153.84 (C8a), 147.33 (C7a'), 136.39 (C3a'), 129.85 (C5), 129.48 (C8), 127.54 (C6'), 126.80 (C7), 121.82 (C4'), 120.40 (C5'), 119.56 (C3), 119.28 (C4), 118.57 (C4a), 115.01 (C6), 106.57 (C7'), 104.50 (C2), 60.79 (CB), 52.26 (C3'), 46.06 (CA), 25.82(C3'-**Me_2**), 20.30(C3'-**Me_2**).
IR (cm^{-1}): 2928, 2802, 2735, 2510, 2411, 1583, 1456, 1030, 932, 860.
UV/VIS (MeCN): ε_{366} = 389 $M^{-1}cm^{-1}$
LRMS-ESI_{pos} (*m/z*): $[MH]^+$ calc. for $C_{20}H_{22}NO_2$ 308.2; found 308.2

2-(3',3'-dimethylspiro[chromene-2,2'-indolin]-1'-yl)ethyl methacrylate (19). A dry round-bottom flask was charged with spiropyran **18** (0.70 g, 2.2 mmol), NEt_3 (0.39 mL, 2.7 mmol) and 5 mL DCM. After wrapping the flask with aluminum foil, the reaction mixture was cooled to 0°C. Acid chloride **6** (0.29 g, 2.7 mmol) was added drop-wise. After stirring at 0°C for an additional hour, the reaction mixture was stirred for 12 h at room temperature. The crude product was then dissolved in DCM and washed with 0.1 M HCl solution, saturated $NaHCO_3$ solution and brine. The crude product was purified by column chromatography (2:3 Hx:DCM). Methacrylate **19** (0.48 g, 1.3 mmol, 59%) was isolated as an orange, oily substance.
^{1}H-NMR (400 MHz, $CDCl_3$) δ: 7.18 (dd, *J* = 7.7, 7.6 Hz, 1H, H6'), 7.13 – 6.99 (m, 3H, H5, H7, H4'), 6.91 – 6.78 (m, 3H, H4, H8, H5'), 6.68 (m, 2H, H6, H7'), 6.10 (s, 1H, CE=**CH_2**), 5.69 (d, *J* = 10.2 Hz, 1H, H3), 5.56 (s, 1H, CE=**CH_2**), 4.31 (t, *J* = 6.4 Hz, 2H, HB), 3.70 – 3.30 (m, 2H, HA), 1.94 (s, 1H, CE-**Me**), 1.3a (s, 1H, C3'-**Me_2**), 1.14 (s, 1H, C3'-**Me_2**).
^{13}C-NMR (101 MHz, $CDCl_3$) δ: 167.25 (CD), 154.05 (C8a), 147.18 (C7a'), 136.31 (2C, C3a' and CE), 129.76 (C4), 129.42 (C7), 127.52 (C6'), 126.73 (C5), 125.68 (CE=**CH_2**), 121.68 (C4'), 120.15 (C5'), 119.48 (C8), 119.19 (C3), 118.42 (C4a), 115.02 (C6), 106.41 (C7'), 104.40 (C2), 62.96 (CB), 52.16 (C3'), 42.36 (CA), 25.79 (C3'-**Me_2**), 20.02 (C3'-**Me_2**), 18.34 (CE-**Me**).
IR (cm^{-1}): 2961, 1716, 1482, 1155, 1108, 964, 743.
UV/VIS (MeCN): ε_{366} = 95 $M^{-1}cm^{-1}$
LRMS-ESI_{pos} (*m/z*): $[MH]^+$ calc. for $C_{24}H_{26}NO_3$ 376.2; found 376.2

2-hydroxy-5-methoxybenzaldehyde (22). Alcohol **20** (3.0 g, 24.2 mmol), $MgCl_2$ (3.5 g, 37 mmol), and NEt_3 (12.8 mL, 92 mmol) were dissolved in 100 mL MeCN. Formaldehyde **21** (5.0 g, 167 mmol) was added in one portion and the reaction mixture was heated to 82°C. After stirring for 12 h the reaction was quenched with 1 M HCl solution, extracted with Et_2O and washed with brine. The crude product was purified by column chromatography (4:1 Hx:EtOAc). Aldehyde **22** (3.3 g, 19.9 mmol, 83%) was isolated as a red-brown liquid.
^{1}H-NMR (400 MHz, $CDCl_3$) δ: 10.65 (s, 1H, C1-C**H**O), 9.86 (s, 1H, C2-O**H**), 7.15 (d, *J* = 9.0, 1H, H4), 7.00 (s, 1H, H6), 6.93 (d, *J* = 9.0 Hz, 1H, H3), 3.82 (s, 3H, C5-O**Me**).
^{13}C-NMR (101 MHz, $CDCl_3$) δ: 196.10 (C1-**C**HO), 156.02 (C2), 152.69 (C5), 125.22 (C4), 119.99 (C1), 118.68 (C3), 115.13 (C6), 55.88 (C5-O**Me**).
IR (cm^{-1}): 2837, 1655, 1482, 1267, 1150, 1035, 772.
LRMS-ESI_{pos} (*m/z*): $[MH]^+$ calc. for $C_8H_9O_3$ 153.1; found 153.1

2-(6-methoxy-3',3'-dimethylspiro[chromene-2,2'-indolin]-1'-yl)ethanol (23). A dry round-bottom flask was charged with substance **3a** (2.20 g, 11.6 mmol) and 50 mL EtOH. Aldehyde **22** (1.67 g, 11.0

mmol) was added in one portion and the reaction-mixture was heated to 78°C and stirred for 12 h. After removing the solvent, the crude product was purified by column chromatography (2:1 Hx:EtOAc). Product **23** (2.1 g, 6.1 mmol, 55 %) was isolated as an oily substance.
^{1}H-NMR (400 MHz, $CDCl_3$) δ: 7.16 (dd, *J* = 7.7, 7.5 Hz, 1H, H6'), 7.07 (d, *J* = 7.3 Hz, 1H, H4'), 6.85 (dd, *J* = 7.5, 7.3 Hz, 1H, H5'), 6.79 (d, *J* = 10.2 Hz, 1H, H4), 6.75 – 6.51 (m, 4H, H5, H6, H7, H7'), 5.70 (d, *J* = 10.2 Hz, 1H, H3), 3.80 – 3.72 (m, 5H, C6-O**Me**, HB), 3.60 – 3.25 (m, 2H, HA), 1.32 (s, 3H, C3'-**Me$_2$**), 1.16 (s, 3H, C3'-**Me$_2$**).
^{13}C-NMR (101 MHz, $CDCl_3$) δ: 153.37 (C6), 147.85 (C8a), 147.26 (C7a'), 136.39 (C3a'), 129.37 (C4), 127.51 (C6'), 121.79 (C4'), 120.55 (C3), 119.16 (C5'), 118.91 (C4a), 115.40 (2C, C7 and C8), 111.63 (C5), 106.49 (7'), 104.20 (C2), 60.68 (CB), 55.71 (C6-O**Me**), 52.19 (C3'), 46.05 (CA), 25.77 (C3'-**Me$_2$**), 20.37 (C3'-**Me$_2$**).
IR (cm^{-1}): 3404, 2958, 1605, 1483, 1456, 1245, 1160, 1023, 964, 819, 741.
UV/VIS (MeCN): ε_{366} = 238 $M^{-1}cm^{-1}$
LRMS-ESI$_{pos}$ (*m/z*): $[MH]^+$ calc. for $C_{21}H_{24}NO_3$ 338.2; found 338.2

2-hydroxy-5-methylbenzaldehyde (25). Alcohol **24** (2.0 g, 18.5 mmol), $MgCl_2$ (2.1 g, 22 mmol) and NEt_3 (8.5 mL, 55 mmol) were dissolved in 75 mL MeCN. Formaldehyde **21** (3.0 g, 102 mmol) was added in one portion and the reaction mixture was heated to 82°C. After stirring for 12 h, the reaction wash quenched with 1 M HCl solution, extracted with Et_2O and washed with brine. The crude product was purified by column chromatography (10:1 Hx:EtOAc). Aldehyde **25** (2.3 g, 16.8 mmol, 91%) was isolated as off-white crystals.
^{1}H-NMR (400 MHz, $CDCl_3$) δ: 10.83 (s, 1H, C1-C**H**O), 9.85 (s, 1H, C2-O**H**), 7.33 (m, 2H, H4, H6), 6.91 (d, *J* = 9.2 Hz, 1H, H3), 2.34 (s, 3H C5-**Me**).
^{13}C-NMR (101 MHz, $CDCl_3$) δ: 196.69 (C1-**C**HO), 159.67 (C2), 138.16 (C6), 133.53 (C4), 129.25 (C5), 120.47 (C1), 117.51 (C3), 20.35 (C5-**Me**).
IR (cm^{-1}): 3029, 2919, 2855, 1644, 1588, 1482, 1277, 1207, 1149, 826, 737, 667.
LRMS-ESI$_{pos}$ (*m/z*): $[MH]^+$ calc. for $C_8H_9O_2$ 137.1; found 137.1

2-(3',3',6-trimethylspiro[chromene-2,2'-indolin]-1'-yl)ethanol (26). A dry round-bottom flask was charged with substance **3a** (0.51 g, 2.7 mmol) and 9.0 mL EtOH. Aldehyde **25** (0.39 g, 2.9 mmol) was added in one portion and the reaction mixture was heated to 78°C and stirred for 12 h. After removing the solvent, the crude product **26** was analyzed without further purification. Spiropyran **26** was isolated as red-brown oil (0.85 g, 2.6 mmol, 95%).
^{1}H-NMR (400 MHz, $CDCl_3$) δ: 7.16 (dd, *J* = 7.7, 7.5 Hz, 1H, H6'), 7.07 (d, *J* = 7.2 Hz, 1H, H4'), 6.93 – 6.82 (m, 3H, H5', H7, H8), 6.79 (d, *J* = 10.2 Hz, 1H, H4), 6.61 (m, 2H, H5, H7'), 5.65 (d, *J* = 10.2 Hz, 1H, H3), 3.76 – 3.67 (m, 2H, HB), 3.55 – 3.25 (m, 2H, HA), 2.24 (s, 3H, C6-**Me**), 1.30 (s, 3H, C3'-**Me$_2$**), 1.16 (s, 1H, C3'-**Me$_2$**).
^{13}C-NMR (101 MHz, $CDCl_3$) δ: 151.67 (C8a), 147.34 (C7a'), 136.45 (C3a'), 130.37 (C7), 129.56 (2C, C4 and C4a) 127.52 (C6'), 127.17 (C8), 121.82 (C4'), 119.60 (C3), 119.20 (C5), 118.28 (C6), 114.72 (C7'), 106.53 (C5), 104.34 (C2), 60.77 (CB), 52.21 (C3'), 46.05 (CA), 25.82 (C3'-**Me$_2$**), 20.37 (2C, C3'-**Me$_2$** and C6-**Me**).
IR (cm^{-1}): 3371, 2960, 2923, 2867, 1605, 1483, 1249, 1020, 964, 815, 739.
UV/VIS (MeCN): ε_{366} = 414 $M^{-1}cm^{-1}$

LRMS-ESI$_{pos}$ (*m/z*): $[MH]^+$ calc. for $C_{21}H_{24}NO_2$ 322.2; found 322.0

1,2,3,3-tetramethyl-3H-indol-1-ium iodide (27). Indoline **1** (3.0 g, 18.9 mmol) and iodomethane (3.2 g, 22.6 mmol) were dissolved in 13 mL toluene. The reaction mixture was heated to 110°C and stirred for 12 h. After cooling to room temperature, the precipitated material was isolated and washed with cold toluene followed by Et_2O to obtain product **27** (5.5 g, 18.3 mmol, 97%) as a light-pink salt.
^{1}H-NMR (400 MHz, $CDCl_3$) δ: 7.91 (d, *J* = 8.6, 1H, 7H), 7.82 (d, *J* = 8.4, 1H, 4H), 7.64 – 7.57 (m, 2H, 6H, 5H), 3.96 (s, 3H, N-**Me$_2$**), 2.76 (s, 3H, C2-**Me$_2$**), 1.52 (s, 6H, C3-**Me$_2$**)
^{13}C-NMR (101 MHz, d_6-DMSO) δ: 195.99 (C2), 142.10 (C7a), 141.59 (C3a), 129.30 (C5), 128.80 (C6), 123.28 (C4), 115.11 (C7), 53.91 (C3), 34.68 (N-**Me**), 21.68 (2C, C3'-**Me$_2$**), 14.11 (C2-**Me**).
IR (cm^{-1}): 3024, 2969, 2929, 1455, 773.
LRMS-ESI$_{pos}$ (*m/z*): $[M-I]^+$ calc. for $C_{12}H_{16}N$ 174.1; found 174.0

1,3,3-trimethyl-2-methyleneindoline (27a). When indolium salt **27** was suspended in DCM and washed with 1 M NaOH, structure **27a** was isolated as dark violet oil in 100% yield.
^{1}H-NMR (400 MHz, $CDCl_3$) δ: 7.26 – 7.07 (m, 2H, H4, H6), 6.83 (dd, *J* = 7.5, 7.4 Hz, 1H, H5), 6.61 (d, *J* = 7.8 Hz, 1H, H7), 3.93 (s, 2H, C2=**CH$_2$**), 3.10 (s, 3H, N-**Me**), 1.42 (s, 6H, C3-**Me$_2$**).
^{13}C-NMR (101 MHz, $CDCl_3$) δ: 162.73 (C2), 146.34 (C7a), 137.50 (C3a), 127.48 (C6), 121.69 (C4), 118.29 (C5), 104.84 (C7), 73.00 (C2=**CH$_2$**), 44.04 (C3), 29.90 (3C, C3-**Me$_2$** and N-**Me**).
IR (cm^{-1}): 2962, 2879, 1607, 1579, 1456, 1294, 1030, 747.
LRMS-ESI$_{pos}$ (*m/z*): $[MH]^+$ calc. for $C_{12}H_{16}N$ 174.1; found 174.1

2,5-dihydroxybenzaldehyde (28). A dry round-bottom flask purged with N_2 was charged with aldehyde **22** (0.20 g, 1.3 mmol) and 4 mL DCM. BBr_3 (0.65 g, 2.6 mmol) was added carefully and the reaction mixture was stirred at room temperature for 12 h. The reaction was then quenched with water and extracted with DCM. Aldehyde **28** (0.17 g, 1.2 mmol, 96%) was isolated as a green powder without further purification.
^{1}H-NMR (400 MHz, $CDCl_3$) δ: 10.61 (s, 1H, C1-C**H**O), 9.80 (s, 1H, C2-O**H**), 7.07 (d, *J* = 8.9 Hz, 1H, H4), 7.01 (s, 1H, H6), 6.89 (d, *J* = 8.9 Hz, 1H, H3), 5.32 (s, 1H, C5-O**H**).
^{13}C-NMR (101 MHz, $CDCl_3$) δ: 196.21 (C1-**C**HO), 155.72 (C2), 148.52 (C5), 125.62 (C4), 120.22 (C1), 118.67 (C3), 118.05 (C6).
IR (cm^{-1}): 3244, 1646, 1626, 1480, 1273, 1143, 800, 634.
LRMS-ESI$_{pos}$ (*m/z*): $[MH]^+$ calc. for $C_7H_7O_3$ 139.0; found 139.0

1',3',3'-trimethylspiro[chromene-2,2'-indolin]-6-ol (29). Aldehyde **28** (870 mg, 2.9 mmol) was dissolved in 10 mL EtOH. After the addition of NEt_3 (450 μL, 3.2 mmol), indoline **27a** was added in one portion. The reaction mixture was heated to 78°C for 12 h. After extraction (DCM/NH_4Cl/brine) the crude product was purified by column chromatography (4:1 Hx:EtOAc). Spiropyran **29** (410 mg, 1.4 mmol, 48%) was isolated as green-brown oil.
^{1}H-NMR (400 MHz, $CDCl_3$) δ: 7.16 (dd, *J* = 7.5, 7.3 Hz, 1H, H6'), 7.07 (d, *J* = 7.1 Hz, 1H, H4'), 6.80 (dd, *J* = 7.3, 7.1 Hz, 1H, H5'), 6.75 (d, *J* = 10.2 Hz, 1H, H4), 6.50 – 6.60 (m, 4H, H5, H7, H8,

H7'), 5.69 (d, *J* = 10.2 Hz, 1H, H3), 4.51 (s, 1H, OH), 2.71 (s, 3H, N-**Me**), 1.29 (s, 3H, C3'-**Me$_2$**), 1.15 (s, 3H, C3'-**Me$_2$**).
^{13}C-NMR (101 MHz, $CDCl_3$) δ: 149.25, 148.95, 148.60, 137.00, 129.40, 127.97, 122.01, 120.85, 119.52, 119.33, 116.80, 115.97, 113.30, 107.77, 104.35, 52.10, 29.64, 26.37, 20.49.
IR (cm^{-1}): 3051, 1582, 1456, 1255, 1213, 1160, 1116, 749.
UV/VIS (MeCN): $\varepsilon_{366} = 5538\ M^{-1}cm^{-1}$
LRMS-ESI$_{pos}$ (*m/z*): $[MH]^+$ calc. for $C_{19}H_{20}NO_2$ 294.2; found 294.0

1',3',3'-trimethylspiro[chromene-2,2'-indolin]-6-yl acrylate (30). A dry round-bottom flask was charged with spiropyran **29** (250 mg, 0.85 mmol), NEt_3 (185 μL, 1.2 mmol) and 3.0 mL DCM. After cooling to 0°C, acid chloride **8** (170 μL, 1.7 mmol) was added slowly. The reaction was stirred for 12 h at room temperature. The crude product was diluted with DCM and washed with 1 M HCl and brine. After drying over Na_2SO_4, further purification was achieved by column chromatography over silica (4:1 Hx:EtOAc). Methacrylate **30** (80 mg, 0.22 mmol, 26%) was isolated as a dark red crystalline material.
^{1}H-NMR (400 MHz, $CDCl_3$) δ: 7.18 (dd, *J* = 7.6, 7.5 Hz, 1H, H6'), 7.08 (d, *J* = 7.3 Hz, 1H, H4'), 6.91 – 6.74 (m, 4H, H4, H5, H7, H5'), 6.71 (d, *J* = 8.4 Hz, 1H, H8), 6.56 (m, 2H, H7', -O(CO)-CH=**CH$_2$**), 6.30 (dd, *J* = 17.3, 10.4 Hz, 1H, -O(CO)-C**H**=CH2), 5.99 (d, *J* = 10.4 Hz, 1H, -O(CO)-CH=**CH$_2$**), 5.72 (d, *J* = 10.2 Hz, 1H, H3), 2.73 (s, 3H, N-**Me**), 1.31 (s, 3H, C3'-**Me$_2$**), 1.17 (s, 3H, C3'-**Me$_2$**).
^{13}C-NMR (101 MHz, $CDCl_3$) δ: 164.91 (-O(**C**O)-CH=CH_2), 152.04 (C8a), 148.11 (C7a'), 143.33 (C6), 136.65 (C3a'), 132.37 (-O(CO)-CH=**CH$_2$**), 128.85 (C4 or C5 or C7) , 127.96 (-O(CO)-**C**H=CH_2), 127.59 (C6'), 122.29 (C4 or C5 or C7), 121.48 (C4'), 120.31 (C3), 119.15 (3C, C4a and C5' and C4 or C5 or C7), 115.58 (C8), 106.79 (C7), 104.39 (C2), 51.80 (C3'), 28.94 (N-**Me**), 25.82 (C3'-**Me$_2$**), 20.18(C3'-**Me$_2$**).
IR (cm^{-1}): 3055, 1583, 1456, 1257, 1216, 1116, 968, 747.
UV/VIS (MeCN): $\varepsilon_{366} = 292\ M^{-1}cm^{-1}$
LRMS-ESI$_{pos}$ (*m/z*): $[MH]^+$ calc. for $C_{22}H_{22}NO_3$ 348.2; found 348.2

5-methoxy-2,3,3-trimethyl-3H-indole (32). Hydrazine hydrochloride **31** (2.0 g, 11.5 mmol) and 3-methylbutan-2-one (0.8 mL, 11.5 mmol) were dissolved in 40 mL ethanol. After refluxing for 5.5 h, the crude product was purified by column chromatography (2:1 Hx:EtOAc). Indoline **32** (1.4 g, 7.5 mmol, 65%) was isolated as an off-withe solid.
^{1}H-NMR (400 MHz, $CDCl_3$) δ: 7.42 (d, *J* = 8.2 Hz, 1H, H7), 6.84 – 6. 79 (m, 2H, H4, H6), 3.83 (s, 3H, O**Me**), 2.24 (s, 3H, C2-**Me**), 1.28 (s, 6H, C3-**Me$_2$**).
^{13}C-NMR (101 MHz, $CDCl_3$) δ: 185.9 (C2), 157.9 (C5), 147.3 (2C, C3a and C7a), 120.1 (C7), 112.1 (C4 or C6), 108.2 (C4 or C6), 55.7 (OMe), 53.8 (C3), 23.3 (2C, C3-**Me$_2$**), 15.3 (C2-**Me**).
IR (cm^{-1}): 2964, 1573, 1461, 1213, 1068, 1031.
LRMS-ESI$_{pos}$ (*m/z*): $[MH]^+$ calc. for $C_{12}H_{16}NO$ 190.1; found 190.1

2,3,3-trimethyl-3H-indol-5-ol (33). A dry round-bottom flask was charged with indoline **32** (300 mg, 1.6 mmol) and 2.0 mL DCM. After cooling to 0°C, a 1 M BBr_3 solution in DCM (3.0 mL, 3.0 mmol)

was added slowly. The mixture was stirred for additional 12 h at room temperature. Afterwards, the solution was quenched with saturated $NaHCO_3$ solution. After diluting with water, the solution was extracted with DCM and a tiny amount of MeOH. After column chromatography (5% MeOH in DCM), indoline **33** (260 mg, 1.5 mmol, 79%) was obtained as yellow crystals.
^{1}H-NMR (400 MHz, $CDCl_3$) δ: 7.26 (d, J = 8.2 Hz, 1H, H7), 6.77 (d, J = 2.3 Hz, 1H, H4), 6.72 (dd, J = 8.2, 2.3 Hz, 1H, H6), 2.39 – 1.94 (m, 3H, C2-**Me**), 1.24 (s, 6H, C3-**Me$_2$**).
^{13}C-NMR (101 MHz, $CDCl_3$) δ: 185.74 (C2), 155.14 (C5), 147.12 (C3a), 145.43 (C7a), 119.79 (C7), 113.94 (C6), 109.28 (C4), 53.55 (C3), 23.04 (2C, C3-**Me$_2$**), 14.65 (C2-**Me**).
IR (cm^{-1}): 2967, 1581, 1461, 1386, 1357, 1292, 1060, 815, 460.
LRMS-ESI$_{pos}$ (*m/z*): $[MH]^+$ calc. for $C_{11}H_{14}NO$ 176.1; found 176.1

5-hydroxy-1,2,3,3-tetramethyl-3H-indol-1-ium iodide (34). To a solution of indoline **33** (0.50 g, 2.9 mmol) in 12 ml Toluene, methyl iodide (0.75 mL, 12 mmol) was added drop-wise. Then the reaction mixture was refluxed for 12 h. After cooling to room temperature, the precipitated material was isolated by filtration and washed with EtOAc to yield indoline salt **34** (0.79 g, 2.5 mmol, 86%) as light brown solid.
^{1}H-NMR (400 MHz, d_6-DMSO) δ: 10.22 (s, 1H, OH), 7.67 (d, J = 8.7 Hz, 1H, H7), 7.11 (d, J = 2.3 Hz, 1H, H4), 6.93 (dd, J = 8.7, 2.3 Hz, 1H, H6), 3.89 (s, 3H, N-**Me**), 2.67 (s, 3H, C2-**Me**), 1.46 (s, 6H, C3-**Me$_2$**).
^{13}C-NMR (101 MHz, d_6-DMSO) δ: 191.87 (C2), 158.96 (C5), 143.69 (C3a), 134.11 (C7a), 116.06 (C7), 114.99 (C6), 110.28 (C4), 53.41 (C3), 34.54 (N-Me), 21.83 (2C, C3-**Me$_2$**), 13.64 (C2-**Me**).
IR (cm^{-1}): 3174, 1596, 1495, 1470, 1354, 1296, 1193, 1054, 947, 899, 800, 647, 551.
LRMS-ESI$_{pos}$ (*m/z*): $[M-I]^+$ calc. for $C_{12}H_{16}NO$ 190.1; found 190.0

1-nitrosonaphthalene-2,7-diol (36). A round-bottom flask was charged with diol **35** (4.0 g, 25 mmol) suspended in 0.6 M aqueous NaOH (43 mL). After cooling to 0°C, $NaNO_2$ (1.73 g, 25 mmol) was added in one portion. The reaction mixture was then acidified with concentrated H_2SO_4 (3.0 mL) and stirred for 1 h at 0°C. The precipitated material was isolated and washed with 0.1 M aqueous HCl followed by water to obtain nitroso-compound **36** (4.8 g, 25 mmol, 99%) as a dark brown solid.
^{1}H-NMR (400 MHz, d_6-DMSO) δ: 10.25 (s, 1H, OH), 8.47 (s, 1H, OH), 7.61 (s, 1H), 7.41 (d, J = 7.8 Hz, 1H), 6.90 (d, J = 7.8 Hz, 1H), 6.18 (s, 1H).
^{13}C-NMR (101 MHz, d_6-DMSO) δ: 159.93, 155.62, 136.33, 132.05, 129.09, 124.03, 123.39, 117.16, 115.22, 107.20.
IR (cm^{-1}): 3149, 1524, 1199, 1224, 1023, 827.
LRMS-ESI$_{pos}$ (*m/z*): $[MH]^+$ calc. for $C_{10}H_8NO_3$ 190.0; found 190.0

1,3,3-trimethylspiro[indoline-2,3'-naphtho[2,1-b][1,4]oxazin]-9'-ol (37). Nitroso-compound **36** (1.9 g, 10 mmol) was dissolved in 20 mL EtOH. The mixture was heated to 78°C and a premixed solution of indoline **34** (3.0 g, 10 mmol) and NEt_3 (2.7 mL, 20 mmol) in 10 mL EtOH was added drop-wise. After refluxing for 2 h, the solvent was removed. Recrystallization from EtOH resulted in spirooxazine **37** (860 mg, 2.5 mmol, 25%) as a light brown powder.
^{1}H-NMR (400 MHz, $CDCl_3$) δ: 10.04 (s, 1H, OH), 7.90 (d, J = 2.5 Hz, 1H, H5), 7.69 (s, 1H, H3), 7.63 (d, J = 8.8 Hz, 1H, H8), 7.56 (d, J = 8.8 Hz, 1H, H9), 7.21 (dd, J = 7.7, 7.0 Hz, 1H, H6'), 7.07

(m, 2H, H7, H4'), 6.89 (dd, *J* = 7.2, 7.0 Hz, 1H, H5'), 6.82 (d, *J* = 8.8 Hz, 1H, H10), 6.56 (d, *J* = 7.7 Hz, 1H, H7'), 2.75 (s, 3H, N-Me), 1.34 (s, 6H, C3'-**Me$_2$**).
^{13}C-NMR (101 MHz, $CDCl_3$) δ: 155.23 (C6), 150.29 (C3), 147.51 (C7a'), 144.87 (C10a), 135.79 (C3a'), 132.35 (C4b), 130.14 (C8), 129.86 (C9), 127.94 (C6'), 124.56 (C8a), 121.88 (C4a), 121.42 (C4'), 119.76 (C5'), 115.94 (C7), 114.00 (C10), 107.06 (C7'), 103.69 (C5), 98.53 (C2), 51.71 (C3'), 29.58 (N-Me), 25.38 (C3'-**Me$_2$**), 20.73(C3'-**Me$_2$**).
IR (cm^{-1}): 3309, 2968, 2361, 1630, 1448, 1081, 965, 829, 737.
UV/VIS (MeCN): ε_{366} = 1990 $M^{-1}cm^{-1}$ $\lambda_{max,UV}$ = 575 nm
LRMS-ESI$_{pos}$ (*m/z*): $[MH]^+$ calc. for $C_{22}H_{21}N_2O_2$ 345.2; found 345.2

1-aminonaphthalene-2,7-diol (38). A dry round-bottom flask was charged with diol **35** (400 mg, 2.5 mmol), 1-methyl-1-phenylhydrazine (305 mg, 2.5 mmol) and 2.5 mL chlorobenzene. After refluxing for 3 h, the crude product was purified by column chromatography (3:2 Hx:EtOAc followed by 5:1 DCM:MeOH). Amine **38** (334 mg, 1.9 mmol, 76%) was isolated as an oily substance.
^{1}H-NMR (400 MHz, *d$_6$*-DMSO) δ: 7.49 (d, *J* = 8.8 Hz, 1H, H5), 7.08 (d, *J* = 2.3 Hz, 1H, H8), 6.96 (d, *J* = 8.6 Hz, 1H, H4), 6.83 (d, *J* = 8.6 Hz, 1H, H3), 6.79 (dd, *J* = 8.8, 2.3 Hz, 1H, H6).
^{13}C-NMR (101 MHz, *d$_6$*-DMSO) δ: 154.10 (C7), 139.45 (C2), 129.31 (C5), 126.84 (C4a), 125.73 (C8a), 123.36 (C1), 116.72 (C4), 114.99 (C6), 114.53 (C3), 103.12 (C8).
IR (cm^{-1}): 3390, 3006, 2362, 1624, 1405, 1288, 1012, 949.
LRMS-ESI$_{pos}$ (*m/z*): $[MH]^+$ calc. for $C_{10}H_{10}NO_2$ 176.1; found 176.2

1,3,3-trimethylspiro[indoline-2,3'-naphtho[2,1-b][1,4]oxazin]-9'-ol (37). Indoline **34** (200 mg, 0.66 mmol) was dissolved in NEt_3 (81 mg, 0.80 mmol) and 5 mL Tol. After stirring for 10 min, amine **38** (116 mg, 0.66 mmol), DMSO (104 mg, 1.33 mmol), $MgSO_4$ (160 mg, 1.33 mmol) and $NaHCO_3$ (112 mg, 1.33 mmol) were added in one portion. The reaction mixture was heated to 90°C and stirred for 12 h. After removing the solvent, the crude product was dissolved in DCM and washed with 0.1 M HCl solution. Recrystallization from EtOH allowed further purification. Product **37** (25 mg, 0.07 mmol, 10%) was isolated as brown powder.
^{1}H-NMR (400 MHz, $CDCl_3$) δ: 10.04 (s, 1H, OH), 7.90 (d, *J* = 2.5 Hz, 1H, H5), 7.69 (s, 1H, H3), 7.63 (d, *J* = 8.8 Hz, 1H, H8), 7.56 (d, *J* = 8.8 Hz, 1H, H9), 7.21 (dd, *J* = 7.7, 7.0 Hz, 1H, H6'), 7.07 (m, 2H, H7, H4'), 6.89 (dd, *J* = 7.2, 7.0 Hz, 1H, H5'), 6.82 (d, *J* = 8.8 Hz, 1H, H10), 6.56 (d, *J* = 7.7 Hz, 1H, H7'), 2.75 (s, 3H, N-Me), 1.34 (s, 6H, C3'-**Me$_2$**).
^{13}C-NMR (101 MHz, $CDCl_3$) δ: 155.23 (C6), 150.29 (C3), 147.51 (C7a'), 144.87 (C10a), 135.79 (C3a'), 132.35 (C4b), 130.14 (C8), 129.86 (C9), 127.94 (C6'), 124.56 (C8a), 121.88 (C4a), 121.42 (C4'), 119.76 (C5'), 115.94 (C7), 114.00 (C10), 107.06 (C7'), 103.69 (C5), 98.53 (C2), 51.71 (C3'), 29.58 (N-Me), 25.38 (C3'-**Me$_2$**), 20.73(C3'-**Me$_2$**).
IR (cm^{-1}): 3309, 2968, 2361, 1630, 1448, 1081, 965, 829, 737.
UV/VIS (MeCN): ε_{366} = 1990 $M^{-1}cm^{-1}$ $\lambda_{max,UV}$ = 575 nm
LRMS-ESI$_{pos}$ (*m/z*): $[MH]^+$ calc. for $C_{22}H_{21}N_2O_2$ 345.2; found 345.2

1,3,3-trimethylspiro[indoline-2,3'-naphtho[2,1-b][1,4]oxazin]-9'-yl methacrylate (39). A dry round-bottom flask was charged with spirooxazine **37** (250 mg, 0.73 mmol), NEt_3 (160 μL, 1.1 mmol) and

3.0 mL DCM. After cooling to 0°C, methacryloyl chloride **6** (150 μL, 1.4 mmol) was added drop-wise. The mixture was stirred for 18 h at room temperature. The reaction was quenched with 1 M HCl solution and extracted with DCM. The organic layers were combined and washed with brine and dried over Na_2SO_4. Product **39** was then purified by preparative TLC. Methacrylate **39** (0.33 mmol, 45%) was isolated as an off-white powder.
^{1}H-NMR (400 MHz, $CDCl_3$) δ: 8.29 (d, J = 2.4 Hz, 1H, H5), 7.77 (d, J = 8.8 Hz, 1H, H8), 7.72 (s, 1H, H3), 7.66 (d, J = 8.9 Hz, 1H, H9), 7.24 – 7.18 (m, 2H, H7, H6'), 7.09 (d, J = 8.2 Hz, 1H, H4'), 7.00 (d, J = 8.9 Hz, 1H, H10), 6.91 (dd, J = 7.4 Hz, 1H, H5'), 6.59 (d, J = 7.7 Hz, 1H, H7'), 6.42 (s, 1H, -O(CO)C=**CH$_2$**Me), 5.80 (s, 1H, -O(CO)C=**CH$_2$**Me), 2.77 (s, 3H, N-Me), 2.12 (s, 3H, -O(CO)C=CH$_2$**Me**), 1.36 (s, 6H, C3'-**Me$_2$**).
^{13}C-NMR (101 MHz, $CDCl_3$) δ: 166.08 (-O(**C**O)R), 150.78 (C3), 149.99 (C7a'), 147.54 (C10a), 144.73 (C6), 135.94 (2C, C3a' and -O(CO)**C**=CH$_2$Me), 131.76 (C4b), 129.99 (C9), 129.28 (C8), 128.00 (C6'), 127.25 (2C, C8a and -O(CO)C=**CH$_2$**Me), 122.86 (C4a), 121.47 (C4'), 119.86 (C5'), 119.38 (C7), 116.53 (C10), 112.95 (C5), 107.11 (C7'), 98.75 (C2), 51.84 (C3'), 29.59 (N-Me), 25.37 (C3'-**Me$_2$**), 20.74 (C3'-**Me$_2$**), 18.42 (-O(CO)C=CH$_2$**Me**).
IR (cm^{-1}): 2971, 2360, 1728, 1121, 740.
UV/VIS (MeCN): ε_{366} = 1764 M^{-1}cm^{-1} $\lambda_{max,UV}$ = 580 nm
LRMS-ESI$_{pos}$ (*m/z*): [MH]$^+$ calc. for $C_{26}H_{25}N_2O_3$ 413.2; found 413.4
EA: calc. [C] 75.7%, [H] 5.9%, [N] 6.8%; found [C] 74.9%, [H] 6.0%, [N] 6.5%.

14,14-dimethyl-5a,7,8,14-tetrahydro-5H-naphtho[1",2":5',6'][1,4]oxazino[3',2':2,3][1,4]-oxazino[4,3-a]indole (40). Compound 3a (500 mg, 1.75 mmol) was dissolved in 4 mL EtOH and heated to 78°C. 1-nitrosonaphthalen-2-ol (350 mg, 2.0 mmol) was added in one portion. After stirring for 15 h, the solvent was removed, the crude product dissolved in EtOAc and washed with brine. Further purification was achieved by column chromatography (2:1 Hx:EtOAc). Product **40** (156 mg, 0.44 mmol, 25%) was isolated as light brown crystals.
^{1}H-NMR (400 MHz, $CDCl_3$) δ: 7.75 (d, J = 8.2 Hz, 1H, H8), 7.67 (d, J = 8.5 Hz, 1H, H5), 7.45 (ddd, J = 8.3, 6.9, 1.2 Hz, 1H, H6), 7.36 – 7.28 (m, 2H, H7, H9), 7.21 (td, J = 7.7, 1.2 Hz, 1H, H6'), 7.09 (dd, J = 7.3, 0.8 Hz, 1H, H4'), 7.04 (d, J = 8.8 Hz, 1H, H10), 6.87 (td, J = 7.5, 0.8 Hz, 1H, H5'), 6.59 (d, J = 7.7 Hz, 1H, H7'), 5.24 (s, 1H, H4), 5.06 (d, J = 3.4 Hz, 1H, H3), 4.12 – 3.90 (m, 2H, HA), 3.60 – 3.20 (m, 2H, HB), 1.30 (s, 3H, C3'-**Me$_2$**), 1.22 (s, 3H, C3'-**Me$_2$**).
^{13}C-NMR (101 MHz, $CDCl_3$) δ: 146.7 (C7a'), 140.0 (C10a), 136.5 (C3a'), 129.1 (C8a), 128.5 (C8), 127.6 (C6'), 125.3 (C6), 123.3 (C4b), 123.1 (C7), 121.8 (C4'), 121.1 (C4a), 120.8 (C9), 119.3 (C5'), 118.3 (C5), 117.7 (C10), 105.8 (C7'), 95.0 (C2), 77.5 (C3), 65.1 (CB), 49.1 (C3'), 38.3 (CA), 23.6 (C3'-**Me$_2$**), 20.0 (C3'-**Me$_2$**).
IR (cm^{-1}): 3380, 2972, 2361, 1600, 1481, 1256, 1076, 748.
UV/VIS (MeCN): ε_{366} = 1059 M^{-1}cm^{-1}
LRMS-ESI$_{pos}$ (*m/z*): [MH]$^+$ calc. for $C_{23}H_{23}N_2O_2$ 359.2; found 359.2

3-(3,3-dimethylspiro[indoline-2,3'-naphtho[2,1-b][1,4]oxazin]-1-yl)propanoic acid (41). A dry round-bottom flask was charged with indoline salt **11** (500 mg, 1.4 mmol), piperidine (140 μL, 1.4 mmol) and 2.5 mL 2-butanone. The mixture was heated to 80°C and 1-nitrosonaphthalen-2-ol (250 mg, 1.4 mmol) was added in one portion. After refluxing for 13 h, the solvent was removed. The crude

product was dissolved in EtOAc and washed with 1 M HCl followed by brine. Further purification was achieved by column chromatography (5:2 Hx:EtOAc). Spirooxazine **41** was isolated as an off-white powder (110 mg, 0.28 mmol, 20%).

^{1}H-NMR (400 MHz, d_6-DMSO) δ: 8.45 (d, J = 8.5 Hz, 1H, H5), 7.87 (s, 1H, H3), 7.84 (d, J = 8.2 Hz, 1H, H8), 7.78 (d, J = 8.9 Hz, 1H, H9), 7.57 (dd, J = 7.7 Hz, 1H, H6), 7.41 (dd, J = 7.5 Hz, 1H, H7), 7.15 – 7.10 (m, 2H, H4', H6'), 7.07 (d, J = 8.9 Hz, 1H, H10), 6.82 (dd, J = 7.4 Hz, 1H, H5'), 6.69 (d, J = 7.7 Hz, 1H, H7'), 3.59 – 3.36 (m, 2H, HA), 2.71 – 2.44 (m, 2H, HB), 1.22 (s, 3H, C3'-**Me$_2$**), 1.22 (s, 3H, C3'-**Me$_2$**).

^{13}C-NMR (101 MHz, d_6-DMSO) δ: 173.12 (COOH), 152.14 (C3), 146.15 (C7a'), 143.39 (C10a), 135.26 (C3a'), 130.25 (C9), 130.16 (C4b), 128.92 (C8a), 127.92 (2C, C8 and C4' or C6'), 127.18 (C6), 124.18 (C7), 122.25 (C4a), 121.74 (C4' or C6'), 121.07 (C5), 119.47 (C5'), 116.81 (C10), 106.85 (C7'), 98.82 (C2), 52.05 (C3'), 39.61 (CA), 32.95 (CB), 25.18 (C3'-**Me$_2$**), 20.57 (C3'-**Me$_2$**).

IR (cm^{-1}): 2934, 2758, 2678, 2477, 1462, 1420, 1397, 1032, 800.

LRMS-ESI$_{pos}$ (*m/z*): [MH]$^+$ calc. for $C_{24}H_{23}N_2O_3$ 387.2; found 387.2

2,3-dihydroxybenzaldehyde (43). A solution of *o*-vanillin **42** (500 mg, 3.3 mmol) in 10 mL of DCM was cooled to 0°C. BBr_3 (0.35 mL, mmol) in 3.5 mL DCM was slowly added. The solution was stirred for 12 h at room temperature. The reaction was then quenched with water. The solvent was removed and the product was extracted with EtOAc. The crude product was further purified by column chromatography (1% MeOH in DCM). Aldehyde **43** (390 g, 2.8 mmol, 85%) was isolated as a yellow solid.

^{1}H-NMR (400 MHz, $CDCl_3$) δ: 11.08 (s, 1H, OH), 9.88 (s, 1H, CHO), 7.19 (dd, J = 7.9, 7.8 Hz, 1H, H5), 7.14 (d, J = 7.8 Hz, 1H, H6), 6.94 (d, J = 7.9 Hz, H4), 5.78 (s, 1H, OH).

^{13}C-NMR (101 MHz, $CDCl_3$) δ: 196.75 (CHO), 148.28 (C3), 144.79 (C2), 124.35 (C5), 121.56 (C6), 120.53 (C1), 120.22 (C4).

IR (cm^{-1}):3325, 1651, 1481, 1227, 967, 781, 731, 548, 483.

LRMS-ESI$_{pos}$ (*m/z*): [MH]$^+$ calc. for $C_7H_7O_3$ 139.0; found 139.2

3-formyl-2-hydroxyphenyl acetate (44). An acetyl chloride-pyridine complex was prepared by adding acetyl chloride (570 μL, 7.9 mmol) to 0.65 mL dry pyridine at 0°C. This premix was added with the help of 3.6 mL pyridine to a rigorously stirred solution of benzaldehyde **43** (1.0 g, 7.2 mmol) in 1.2 mL pyridine. After stirring for 1 h at room temperature, the solution was refluxed for 3 h. After cooling to room temperature, the precipitated material was removed by filtration and the solution was concentrated. This concentrate was diluted with DCM and washed with 0.5 M HCl followed by brine. Recrystallization from hexane yielded benzaldehyde **44** (800 mg, 4.4 mmol, 61%) as yellow crystals.

^{1}H-NMR (400 MHz, $CDCl_3$) δ: 11.13 (s, 1H, OH), 9.93 (s, 1H, CHO), 7.48 (d, 7.8 Hz, 1H, H6), 7.33 (d, J = 7.6 Hz, H4), 7.03 (dd, J = 7.8, 7.6 Hz, 1H, H5), 2.36 (s, 3H, Ac).

^{13}C-NMR (101 MHz, $CDCl_3$) δ: 196.30 (CHO), 168.53 (Ac), 153.27 (C2), 138.86 (C3), 130.95 (C6), 129.89 (C5), 121.89 (C1), 119.49 (C4), 20.45 (Ac).

IR (cm^{-1}): 1757, 1657, 1457, 1274, 1186, 1152, 848, 797, 668.

LRMS-ESI$_{pos}$ (*m/z*): [MH]$^+$ calc. for $C_9H_9O_4$ 180.0; found 180.2

3-acetoxy-2-hydroxy-5-nitro-benzaldehyde (45). A round-bottom flask was charged with benzaldehyde **44** (1.0 g, 5.6 mmol) and 10 mL of acetic acid. After cooling to 0°C, a prepared mixture of 1.85 mL HNO_3 (70%) and 1.0 mL H_2SO_4 (conc.) was added slowly. After stirring at 0°C for an additional hour, the precipitate was isolated, washed with diethyl ether, and recrystallized from EtOAc and diethyl ether. Nitrobenzaldehyde **45** (350 mg, 1.6 mmol, 29%) was obtained as yellow crystals.
^{1}H-NMR (400 MHz, d_6-DMSO) δ: 10.30 (s, 1H, CHO), 8.35 (s, 1H, H6), 8.30 (s, 1H, H4), 2.32 (s, 3H, Ac).
^{13}C-NMR (101 MHz, d_6-DMSO) δ: 189.24 (CHO), 168.87 (Ac), 158.34 (C2), 139.57 (C3), 138.79 (C5), 124.13 (C4), 123.59 (C1), 121.75 (C6), 20.87 (Ac).
IR (cm^{-1}): 3099, 1777, 1652, 1520, 1343, 1302, 1257, 1184, 953, 908, 716.
LRMS-ESI$_{pos}$ (*m/z*): $[MH]^+$ calc. for $C_9H_8NO_6$ 226.0; found 226.2

2,3-dihydroxy-5-nitrobenzaldehyde (46). A solution of benzaldehyde **45** (285 mg, 1.3 mmol) in 6.0 mL ethanol and 5.0 mL water was refluxed for 4 h. After cooling to 0°C, the crude product precipitated. After recrystallized from EtOAc and diethyl ether, benzaldehyde **46** (220 mg, 1.2 mmol, 95%) was isolated as pale crystals.
^{1}H-NMR (400 MHz, d_6-DMSO) δ: 11.18 (s, 1H, OH), 10.28 (s, 1H, CHO), 7.96 (s, 1H, H6), 7.76 (s, 1H, H4).
^{13}C-NMR (101 MHz, d_6-DMSO) δ: 189.77 (CHO), 155.91 (C2), 147.17 (C3), 139.22 (C5), 121.79 (C1), 114.55 (C6), 113.17 (C4).
IR (cm^{-1}): 3086, 1662, 1516, 1456, 1346, 1264, 1182, 950, 903, 756, 742.
LRMS-ESI$_{pos}$ (*m/z*): $[MH]^+$ calc. for $C_7H_6NO_5$ 184.0; found 184.0

1',3',3'-trimethyl-6-nitrospiro[chromene-2,2'-indoline]-5',8-diyl bis(2-methylacrylate) (47). Indoline **34** (173 mg, 0.5 mmol) and benzaldehyde **46** (100 mg, 0.5 mmol) were dissolved in 5.4 mL ethanol. Piperidine (0.1 mL, 1.0 mmol) was added in one portion. The reaction was refluxed for 2.5 h. The solvent was then removed. The residue was taken up in 2.4 mL anhydrous DCM, Et_3N (0.14 ml, 1.0 mmol) was added and the solution was cooled to 0°C. A solution of acryloyl chloride **8** (0.1 mL, 1.0 mmol) was added drop-wise. After stirring for 14 h, the solution was dissolved with DCM. The organic layer was then washed with 0.1 M HCl solution, saturated $NaHCO_3$ solution and brine. Removal of the solvent resulted in an oily residue. TLC indicated the presence of a photochromic substance, but all attempts to isolate pure product **47** failed.

1,3,3-trimethylspiro[indoline-2,3'-naphtho[2,1-b][1,4]oxazine]-5,9'-diol (48). Diol **36** (1.0 g, 4.9 mmol) was dissolved in 11.0 mL EtOH and refluxed for 1 h. Indoline **34** (1.7 g, 5.3 mmol) and 1.4 mL NEt_3 (1.4 mL, 10 mmol) were premixed in 5.0 mL EtOH and then added drop-wise to the reaction mixture. After refluxing for 12 h, the solvent was removed and the crude product was recrystallized from EtOAc/Hx. Spirooxazine **48** (0.67 g, 1.9 mmol, 18%) was isolated as dark red solid.
^{1}H-NMR (400 MHz, d_6-DMSO) δ: 9.83 (s, 1H, OH), 8.75 (s, 1H, OH), 7.79 – 7.52 (m, 4H, H3, H5, H8, H9), 6.92 (d, J = 11.0 Hz, 1H, H7), 6.77 (d, J = 8.8 Hz, 1H, H10), 6.62 – 6.48 (m, 2H, H4', H6'), 6.40 (d, J = 8.2 Hz, 1H, H7'), 2.54 (s, 3H, N-Me), 1.24 (s, 3H, C3'-**Me$_2$**), 1.16 (s, 3H, C3'-**Me$_2$**).

^{13}C-NMR (101 MHz, d_6-DMSO) δ: 156.58 (C3), 151.37 (C5‘), 150.30 (C6), 144.27 (C10a), 139.90 (C7a’), 136.82 (C3a’), 132.23 (C4b), 129.85 (2C, C8 and C9), 123.52 (C8a), 121.40 (C4a), 116.34 (C7), 113.17 (C10 and C6’), 109.61 (C4’), 107.63 (C7’), 102.83 (C5), 98.40 (C2), 51.29 (C3’), 29.61 (N-Me), 25.11(C3’-**Me$_2$**), 20.29(C3’-**Me$_2$**).
IR (cm^{-1}): 3283, 2969, 1621, 1492, 1439, 1360, 1294, 1181, 1081, 1024, 976, 836.
UV/VIS (MeCN): ε_{366} = 1032 M^{-1}cm^{-1} $\lambda_{max,UV}$ = 620 nm
LRMS-ESI$_{pos}$ (*m/z*): [M]$^+$ calc. for $C_{22}H_{20}N_2O_3$ 360.2; found 360.2

1,3,3-trimethylspiro[indoline-2,3'-naphtho[2,1-b][1,4]oxazine]-5,9'-diyl diacrylate (49). A dry round-bottom flask was charged with spirooxazine **48** (1.0 g, 2.8 mmol) and 14.0 mL DCM. NEt_3 (0.82 mL, 5.8 mmol) was added in one portion at 0°C before acryloyl chloride **8** (0.48 mL, 5.8 mmol) was added slowly. The reaction was stirred at room temperature for additional 12 h. After removing the solvent, recrystallization from EtOAc/Hx was performed. Subsequent preparative TLC allowed isolation of pure diacrylate **49** (0.37 g, 0.8 mmol, 28%) as white crystals.
^{1}H-NMR (400 MHz, d_6-DMSO) δ: 8.16 (d, *J* = 2.4 Hz, 1H, H5), 7.93 (d, *J* = 8.8 Hz, 1H, H8), 7.87 (s, 1H, H3), 7.85 (d, *J* = 8.8 Hz, 1H, H9), 7.25 (dd, *J* = 8.8, 2.4 Hz, 1H, H7), 7.17 (d, *J* = 8.9 Hz, 1H, H10), 7.01 (d, *J* = 2.4 Hz, 1H, H4’), 6.94 (dd, *J* = 8.3, 2.4 Hz, 1H, H6’), 6.66 (d, *J* = 8.4 Hz, 1H, H7’), 6.65 – 6.30 (m, 4H, -O(CO)CH=**CH$_2$** and, -O(CO)**CH**=CH$_2$), 6.18 (dd, *J* = 10.2, 1.4 Hz, 1H, -O(CO)CH=**CH$_2$**), 6.12 (dd, *J* = 10.2, 1.4 Hz, 1H, -O(CO)CH=**CH$_2$**), 2.69 (s, 3H, N-Me), 1.29 (s, 3H, C3’-**Me$_2$**), 1.25 (s, 3H, C3’-**Me$_2$**).
^{13}C-NMR (101 MHz, d_6-DMSO) δ: 164.75 (-O(**C**O)CH=CH$_2$), 164.32 (-O(**C**O)CH=CH$_2$), 151.32 (C3), 149.32 (C6), 145.00 (C7a’), 144.32 (C10a), 143.71 (C5’), 136.66 (C3a’), 133.73 (-O(CO)CH=**CH$_2$**), 133.17 (-O(CO)CH=**CH$_2$**), 130.93 (C4b), 130.29 (C9), 129.78 (C8), 127.85 (-O(CO)**CH**=CH$_2$), 127.67(-O(CO)**CH**=CH$_2$), 126.90 (C8a), 122.19 (C4a), 120.60 (C6’), 119.48 (C7), 116.59 (C10), 115.73 (C4’), 112.28 (C5), 107.22 (C7’), 98.72 (C2), 51.57 (C3’), 29.42 (N-Me), 24.94 (C3’-**Me$_2$**), 20.17 (C3’-**Me$_2$**).
IR (cm^{-1}): 1733, 1622, 1483, 1407, 1248, 1164, 1023, 964, 911, 837, 797.
UV/VIS (MeCN): ε_{366} = 901 M^{-1}cm^{-1} $\lambda_{max,UV}$ = 585 nm
LRMS-ESI$_{pos}$ (*m/z*): [MH]$^+$ calc. for $C_{28}H_{25}N_2O_5$ 469.2; found 469.2
EA (**49** + 1 x EtOAc): calc. [C] 69.05%, [H] 5.79%, [N] 5.98%; found [C] 68.11%, [H] 5.29%, [N] 5.39%.

2.4. CONCLUSION AND OUTLOOK

The synthesis of different spiropyrans and spirooxazines was successfully achieved. A spirooxazine with two acrylic units was synthesized for the first time. Although reported in literature, the synthesis of a spiropyran with two acrylic units failed, due to problems with purifying the final product. In general, purification of spiro-compounds was the most demanding part of the synthesis because of their adaptive character. Not all synthesized spiro-compounds showed photochromic behavior at room temperature. These non-photochromic molecules were excluded from further investigation. Yields of the spiropyrans-syntheses differ tremendously. Production of several grams of highly pure spiropyrans was achieved for molecules **5**, **7**, **9**, **12**, **14** and **16**. Highest yields are obtained if the product precipitated during the synthesis. This is especially the case for the condensation reaction forming the spiro-unit. Testing different solvents and solvent-mixtures could therefore improve the yields of the syntheses significantly. Position of the linker also had an influence on the synthetic success. Introducing the linker at the indoline-nitrogen was most successful for spiropyrans. For spirooxazines it was more successful to introduce the linker at the naphthol-ring. Depending on the length and the chemical structure of the linker, it can happen that the linker interferes with the imine of the spirooxazine. If the imine is converted into a secondary amine, the photochromic behavior of spirooxazine is quenched. Therefore it is important to carefully choose the right linker structure for spirooxazines. For long-term applications of spiro-compounds in materials, it is more meaningful to develop spirooxazine-containing materials than working with spiropyrans due to lower fading rates of spirooxazines. To be able to work with spirooxazines, it is important to improve the purification methods. Since spirooxazines – similar to spiropyrans – do not behave well on silica, recrystallization is the most promising approach to purify large quantities of spirooxazines, which are needed to prepare and analyze light-responsive materials.

2.5. REFERENCES

1. G. H. Brown, R. Livingston and R. C. Bertelson, *Potochromism*, Wiley-Interscience, New York, 1971.
2. H. Dürr, H. Bouas-Laurent, R. Guglielmetti and N. Y. C. Chu, *Photochromism – molecules and systems*, Elsevier, Amsterdam, 1990.
3. J. C. Crano and R. J. Guglielmetti, *Main Photochromic Families*, Plenum Press, New York, 1999.
4. C. B. McArdle, J. C. Crano, W. S. Kwak, C. N. Welch and M. Irie, *Applied Photochromic Polymer Systems*, Blackie & Son Ltd, Glasgow, 1992.
5. Y. Hirschberg and E. Fischer, *J. Chem. Soc.*, 1952, 4522 - 4524.
6. K. Kinashi, S. Nakamura, Y. Ono, K. Ishida and Y. Ueda, *Journal of Photochemistry and Photobiology A: Chemistry*, 2010, **213**, 136-140.
7. P. H. Vandewyer and G. Smets, *Journal of Polymer Science Part A-1: Polymer Chemistry*, 1970, **8**, 2361-2374.
8. D. S. Achilleos and M. Vamvakaki, *Macromolecules*, 2010, **43**, 7073-7081.
9. C. Beyer, in *Naturwissenschaftlichen Fakultät IV*, Universität Regensburg, Regensburg, 2010.
10. J. T. C. Wojtyk, A. Wasey, P. M. Kazmaier, S. Hoz and E. Buncel, *The Journal of Physical Chemistry A*, 2000, **104**, 9046-9055.
11. T. Satoh, K. Sumaru, T. Takagi, K. Takai and T. Kanamori, *Physical Chemistry Chemical Physics*, 2011, **13**, 7322-7329.
12. H. Oda, *Dyes and Pigments*, 1998, **38**, 243-254.
13. G. Such, R. A. Evans, L. H. Yee and T. P. Davis, *Journal of Macromolecular Science, Part C*, 2003, **43**, 547-579.
14. R. A. Evans, T. L. Hanley, M. A. Skidmore, T. P. Davis, G. K. Such, L. H. Yee, G. E. Ball and D. A. Lewis, *Nat Mater*, 2005, **4**, 249-253.
15. C. Salemi, G. Giusti and R. Guglielmetti, *Journal of Photochemistry and Photobiology A: Chemistry*, 1995, **86**, 247-252.
16. A. K. Chibisov and H. Görner, *The Journal of Physical Chemistry A*, 1997, **101**, 4305-4312.
17. R. Matsushima, M. Nishiyama and M. Doi, *Journal of Photochemistry and Photobiology A: Chemistry*, 2001, **139**, 63-69.
18. J. Ratner, N. Kahana, A. Warshawsky and V. Krongauz, *Industrial & Engineering Chemistry Research*, 1996, **35**, 1307-1315.
19. S. L. Potisek, D. A. Davis, N. R. Sottos, S. R. White and J. S. Moore, *Journal of the American Chemical Society*, 2007, **129**, 13808-13809.
20. A. Zelichenok, F. Buchholtz, S. Yitzchaik, J. Ratner, M. Safro and V. Krongauz, *Macromolecules*, 1992, **25**, 3179-3183.
21. D. S. Achilleos, T. A. Hatton and M. Vamvakaki, *Journal of the American Chemical Society*, 2012, **134**, 5726-5729.
22. S. Friedle and S. W. Thomas, *Angewandte Chemie International Edition*, 2010, **49**, 7968-7971.
23. D. Wang, P. Jiao, J. Wang, Q. Zhang, L. Feng and Z. Yang, *Journal of Applied Polymer Science*, 2012, **125**, 870-875.
24. F. M. Raymo and S. Giordani, *Journal of the American Chemical Society*, 2001, **123**, 4651-4652.
25. J. Chen, P. Zhang, G. Fang, P. Yi, X. Yu, X. Li, F. Zeng and S. Wu, *The Journal of Physical Chemistry B*, 2011, **115**, 3354-3362.
26. H. Görner, *Chemical Physics Letters*, 1998, **282**, 381-390.
27. Y. Ueno, J. Jose, A. Loudet, C. Pérez-Bolívar, P. Anzenbacher and K. Burgess, *Journal of the American Chemical Society*, 2010, **133**, 51-55.
28. S.-H. Kim, S.-W. Choi, H.-J. Suh, S.-H. Jin, Y.-S. Gal and K. Koh, *Dyes and Pigments*, 2002, **55**, 17-25.
29. S. Wang, M.-S. Choi and S.-H. Kim, *Journal of Photochemistry and Photobiology A: Chemistry*, 2008, **198**, 150-155.
30. V. Lokshin, A. Samat and R. Guglielmetti, *Tetrahedron*, 1997, **53**, 9669-9678.

3. PLASMA INDUCED COATING OF POROUS POLYCARBONATE MEMBRANES

3.1. INTRODUCTION

A powerful and easy process to get a covalently bound coating on a membrane is to activate the membrane surface by a plasma treatment followed by a polymerization process in solution.[1]

To create plasma, an electrical field is applied on a gas sample. Practical glow discharges are complex environments, and they are far from being well understood.[2] It is known that the electric field induces two pairs of main processes, namely excitation and relaxation as well as ionization and recombination. Energy from the electric field causes the transportation of electrons into energetically higher orbitals within the same molecule (excitation). When the electrons are falling back into energetically lower orbitals, light is emitted (relaxation). Since the difference of energy levels are characteristic for different molecules, the emitted light is composed of characteristic wavelengths.[2, 3] In practice, the gas tightness of a plasma setup can easily be checked by monitoring the characteristic wavelengths of nitrogen.[4] If an electron is entirely removed from a gas molecule, an ion pair is created (ionization) that experiences acceleration in opposite directions in the electric field. If a cation meets an electron, they recombine to a neutral gas molecule (recombination). Steady state plasma is reached when ionization-rate matches the recombination-rate.[2, 5] A typical low-temperature plasma consists mostly of non-charged gas molecules.[3, 6] The degree of ionization is only about 10^{-4} and the current density is in the order of 1 mA/cm^2.[2, 3, 5] Although only a minority of gas molecules is ionized, these ions are crucial for all modification processes that take place during plasma treatment of a material.[2, 3] Different processes make use of ionization in different ways. For sputtering-processes, it is important that a high number of ions are accelerated towards the target surface. In plasma etching, the creation of chemically active species which can react with the substrate is essential.[6] For the creation of radicals, the number of electrons that are able to hit the target surface is relevant.[2] Although the macroscopic temperature of the plasma is low, the temperature of the free electrons is extremely high. The mass of an electron is much smaller than the mass of the cation that gets created during ionization. Therefore, electrons get much more accelerated in the applied electrical field. They obtain a kinetic energy of about 2 eV in average which corresponds to a temperature of 23'200 K.[2, 3] The majority of gas molecules in a plasma process stays neutral and are not accelerated by the electric field. Collisions of neutral molecules with electrons transmits energy from the accelerated electrons to the neutral species.[6] But due to the significant difference in mass, the macroscopic temperature of the gas increases only by some kelvins.[2]

Plasma modification has some advantages compared to other surface technologies. It is a fast, dry and environmentally friendly technology which has become an important process step in many industrial fields. It enables the tailored surface-functionalization of polymers, while maintaining their desirable bulk properties.[7-9] Besides the creation of active surface species, cleaning of the surface is an additional beneficial process which makes plasma a promising approach for creating homogenously coated polymer-surfaces in a reproducible manner.[7, 10-12]

In order to optimize the plasma-activation of polycarbonate membranes, the number of reactive species created in the plasma and their lifetime has to be regarded. Hence, the gas mixture and the pressure are important parameters beside power input and treatment time. Especially, argon/oxygen gaseous mixtures were found to improve the adhesion of coatings on polycarbonate substrates.[13, 14]

In this work, the polycarbonate membranes were treated with an argon/oxygen ratio of 6:1 and moderate pressure (52 Pa). Similar plasma parameters have been previously reported for the treatment of different porous media such as textiles, non-wovens and membranes.[15, 16] Polycarbonate is a polymer which typically shows linear etching rates with plasma exposure time.[12]

In this study, a novel plasma setup is reported, which allows the modification of the activated membranes in solution under inert conditions. Thus nonvolatile monomers can be used in contrast to convenient gas deposition processes.[17]

Two strategies are possible to create photochromic coatings based on a plasma initiated polymerization process. Strategy number one includes the creation of a polymeric coating with functional side chains followed by a postmodification of these functional side chains in a separate reaction.[18, 19] Strategy number two is the random copolymerization of photochromic monomer with the main coating-monomer in a one-step approach.[20]

Up to now, only one report has been published on a plasma-induced photochromic surface coating with spiropyran.[20] The plasma-induced surface-grafting performed by Chung *et al.*, followed the copolymerization strategy to coat a porous PTFE-membrane in a single reaction step. They showed that the flow of a methanol/water-mixture through the light responsive membrane was depending on the spiropyran state. More solution was flowing through the membrane under UV-irradiation than at daylight.[20]

For this study it was decided to focus on the modification of PC-membranes since they are more environmental friendly and can be plasma-activated at lower energies than PTFE-membranes.

The herein reported surface-modification method allows first of all the adjustment of the surface hydrophilicity of polycarbonate, which leads to non-responsive membranes with a range of permeability resistances towards caffeine solution. Postmodification of functional coatings with spiropyran resulted in photochromic membranes with switchable permeability resistance towards caffeine. The same was achieved using a copolymerization process yielding photochromic coatings in a single reaction step. To improve the long-term stability of the membrane, a spirooxazine-containing photochromic coating for porous materials was developed for the first time.

3.2. EXPERIMENTAL

Materials and general methods

Polycarbonate (PC) Membranes Cyclopore and Nanopore Track Etched (TE) (1.0 μm, 0.2 μm, 0.1 μm, 50 nm, 30 nm and 15 nm pore diameter; 47 mm or 25 mm membrane diameter) were purchased from Whatman. Polyethersulfone (PESF) Membranes Supor-200 (0.2 μm pore diameter; 47 mm membrane diameter) were obtained from Pall. Polyvinylidene fluoride (PVDF) Membranes Durapore (0.22 μm pore diameter; 47 mm membrane diameter) were purchased from Millipore. PC-wafers (thickness: 1.5 mm) were obtained from Microfluidic Chip Shop. Silicon-wafers were delivered by Powatec GmbH. Methacrylic Acid (MAA, 98%) and ethanol (EtOH, absolute, 99%, dried over molecular sieve) was delivered by Acros Organics. Octanoic Acid (Oct, purris) was obtained from Riedel-de Haën. Hexane (Hx, 99%) was obtained from Biosolve. Methanol (MeOH, 99%, dried over molecular sieve), 2-Hydroxyethyl methacrylate (HEMA, 97%), 2-Hydroxyethyl acrylate (HEA, 96%) methyl methacrylate (MMA, 99%), 2-Aminoethyl methacrylate (AEMA, 90%), 2-Acrylamido-2-methyl-1-propane sulfonic acid sodium salt (AMPS-Na, 96%), N,N-Dicyclohexylcarbodiimide (DCC, 99%), dimethyl aminopyridine (DMAP, 99%), ethyl acetate (EtOAc, puriss) and aluminum oxide (Type CG20) were obtained from Sigma Aldrich. Caffeine (reagent plus) and *tert*-butylmetylether (TBME, 98%) was purchased by Fluka. All chemicals, unless stated otherwise, were used as delivered without further purification. Spiropyrans and spirooxazine were synthesized and named according to Chapter 2. The relevant structures for this can be seen in Figure 3.1.

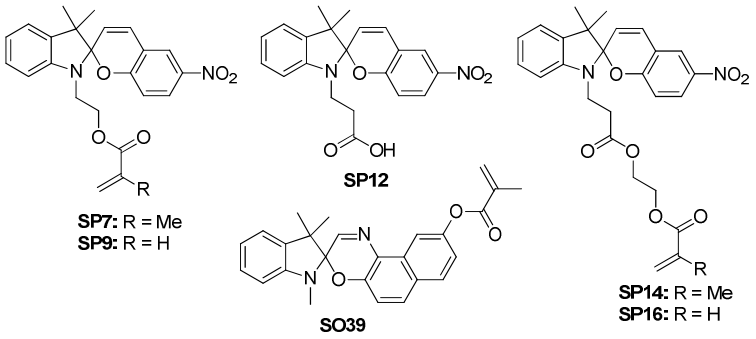

Figure 3.1 Used photochromic spiropyrans and spirooxazine for the different coatings.

Argon (99.9995%) and Oxygen (99.9995%) were purchased from Alphagaz. Distilled water from the in-house supply was used unless stated otherwise. UV-Vis measurements of all liquid samples were performed on a Varian 50Bio/50MPR. For weighing, a Mettler Toledo AB204-S and a Mettler ME30 were used. IR measurements were performed on a BioRad FTS 6000 equipped with an ATR Golden Gate. NMR spectra were recorded on a Bruker 400 MHz. Scanning electron Microscopy (SEM) pictures were recorded on a Hitachi S4800. All SEM-samples were coated with a gold layer of about 3 nm. Membranes for SEM cross-section images were cut in liquid nitrogen. Pore diameters were determined by measuring 30 pores of each sample. Only single round-shaped pores that were not fused to other pores were therefor considered. Membrane thickness was measured at

ten different positions. Standard X-ray photoelectron spectroscopy (XPS) was performed on a PHI 5600 spectrometer. Investigated emission angle was 45°. XPS data were analyzed using the program CasaXPS. Profilometric measurements were performed on a Dektak 150 from Veeco.

Plasma chamber

Scheme 3.1 shows the plasma chamber used to produce the surface modified membranes.[17] A Dressler Cesar RF Power Generator, a MKS Multi Gas Controller 647C, two MKS Mass-Flo controllers and a Vacuubrand RE 2.5 rotary vane vacuum pump were used for the setup. A glass tube (length: 16 cm, diameter: 4.5 cm) was equipped with three copper bands (length: 15 cm with: 2 cm). The first band was wrapped around the central part of the tube. The two others were fixed in a distance of 6.0 cm each on the left and right part of the tube to get a symmetrical setup. The central band (electrode) was connected to the RF power generator via a matching network, while the outer two bands (counter electrodes) were connected to the grounded coaxial shield of the RF coupling. At one end, the glass tube was connected via a gas flow controller to argon and oxygen gas bottles. At the other end, a three-way valve connected the glass tube with the vacuum pump. There was a free connection, which allowed flooding the plasma chamber under defined conditions without opening the chamber. For these experiments, a round-bottom flask with a monomer solution was attached to this connection.

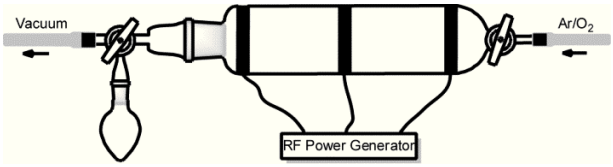

Scheme 3.1 Homemade plasma-setup for surface activation and modification in liquid phase.

To initiate the plasma, the vacuum pump was at full power and gas flow was set to 15.0 sccm argon and 2.5 sccm oxygen to reach a pressure of 52 Pa in the chamber. With 25 W and a radio frequency of 13.56 MHz, the plasma could then be ignited. After initiating the plasma, it was possible to lower the power to a minimum of 10 W. The plasma expands symmetrically to both sides of the central electrode up to the outer electrodes.

Etching of PC-membranes

In order to examine the etching effect of the applied plasma conditions on the PC membranes, one membrane was positioned in the plasma chamber, with the shiny side pointing to the gas phase. While the vacuum pump was at full power, the gas flow was set to 15 sccm argon and 2.5 sccm oxygen. The chamber was rinsed under these conditions for two hours to remove other gases from the chamber and to stabilize the gas flow. Immediately after initiating the plasma (25 W, 13.56 MHz), the applied power was reduced to 12 W. The membrane was etched for a designated time span (between one and four minutes), removed from the chamber and then analyzed without further treatment.

Preparation of monomer solutions

To remove inhibitors, HEA and HEMA were dissolved in water and washed with hexane. Subsequently, the aqueous phase was saturated with sodium chloride and extracted with Et_2O. The organic layers were dried over $MgSO_4$. After removing the solvent, the monomer was distilled under reduced pressure.[21] Inhibitors of MAA and MMA were removed by column chromatography over aluminum oxide. AEMA and AMPS-Na were used as delivered.

For homo-polymerization/post-modification with octanoic acid: 30 mL of a 3.17 M methanolic solution of the monomer was placed in the round-bottom flask and degased for 1 hour by argon bubbling.

For copolymerization and homo-polymerization/post-modification with SPs: As described above but monomer concentration of the comonomer was only 0.62 M. For copolymerization, **SP7**, **SP9**, **SP14, SP16** or **SO39** were added to the mixture. Dissolving of spiropyrans and spirooxazines was accelerated by an ultrasonic bath.

Coating of PC-membranes and PC-wafers

Two membranes were positioned in the plasma chamber next to each other, with the shiny side pointing to the gas phase. The chamber was evacuated and purged for four hours with 15 sccm argon and 2.5 sccm oxygen until a constant gas flow was obtained. After the plasma was initiated at 25 W, the power was immediately reduced to 12 W. After 4 minutes of plasma treatment, the power and the gas flow were switched off and the chamber was evacuated. Afterwards, the chamber was flooded with the prepared monomer solution and subsequently filled with argon. The flooded chamber was then stored for 12 hours at 20°C in a conditioned room. After removal of the left-over monomer solution, the membranes were washed with ethanol and water in an ultrasonic bath for 5 minutes each to remove residual monomers. Finally, the membranes were dried *in vacuo* over molecular sieves for at least 2 hours before being analyzed.

Post-modification of coated PC-membranes

For HE(M)A coated membranes: A round-bottom flask was equipped with a stirrer and a protecting grid. The flask was dried under reduced pressure with a heat gun and flooded with argon. **SP12** (100 mg, 0.27 mmol), DCC (55 mg, 0.27 mmol), DMAP (33 mg, 0.27 mmol) and 12 mL TBME were added to the flask. The coated membrane was added and the whole mixture was gently stirred at room temperature for 12 hours.

For AEMA coated membranes: As described above but without DMAP. Either octanoic acid or **SP12** was linked to the AEMA-coated surface. *For octanoic acid coupling:* As described above but octanoic acid (1.0 mL, 6.3 mmol) and DCC (1.3 g, 6.3 mmol) were dissolved in 12 mL TBME.

Preparation of silicon wafers as model systems

Silicon wafers were cleaned with Acetone, Ethanol and Hexane before plasma treatment. Plasma parameters and monomer solutions were the same as for the PC-Membranes modification except the plasma power that was set to 75W in order to create reactive species on the Si-surface.

Preparation of PC-wafers as model systems

PC-wafers were coated as the PC-membranes with identical plasma activation followed by surface polymerization in 30 mL of a degased 3.17 M methanolic solution of the corresponding monomer. The wafers were washed with ethanol and water in an ultrasonic bath for 5 minutes each. Finally, the membranes were dried *in vacuo* over molecular sieves.

Permeability measurements

All measurements were performed in a Franz diffusion-cell purchased from SES Analyse Systeme with a receptor volume of 12.0 mL and an orifice area of 1.77 cm^2. Mass transfer rates of caffeine were measured under UV irradiation (366 nm, 15 W/m^2) and at daylight (DL). After filling the receptor chamber with water (12.0 mL), the membrane was fixed in the diffusion cell. The donor chamber was charged with a caffeine or glucose solution (20 mM; 3.0 mL). Samples (200 μL) were collected from the receptor part of the cell after 1, 10, 20, 30, 45, and 60 minutes. The caffeine concentrations of these samples were assigned by measuring its UV absorption at 293 nm. (calibration curve: $c_{caff} = 1.0859x + 0.0056$, x: measured absorption)
Resistance R of a membrane was calculated according to Fick's law using the formula

$$R = \frac{\Delta c}{F} \quad (1)$$

where Δc represents the difference of caffeine concentration comparing the donor compartment with the receptor part of the used franz cell. Δc was assumed to be constant over the time frame of the measurement. F was the molecular flux in amount per time per area. Permeability measurements for all treated membranes were performed directly after the production. Nonresponsive membranes were either dried *in vacuo* (dry) or dipped into water (wet) for at least 5 hours to precondition the membranes for the permeability measurements. Photochromic membranes were stored at ambient conditions unless stated otherwise.

Contact angle measurements

All measurements were performed on a Krüss G10. A membrane was fixed with a standard tape on a metal O-ring. A drop of nanopure water (3.3 µL) was positioned on that part of the membrane surface, which was not in contact with the O-ring. For testing the long term stability of the samples, the contact angles were measured at three different spots of the membranes after 0, 1, 2, 3, 7, 14, and 21 days. For measuring the impact of switching SP on the surface tension of the membrane, the CA was measured first at day light. Then the membrane was illuminated with UV-light (366 nm, 80 W/m^2) for 1 minute and the contact angle was measured again. For measuring the repeatability of switching the surface tension, the membrane was illuminated with white light (500 W bulb) until no coloration was visible anymore before contact angle was measured again. This circle was repeated at least three times. The method allowed measurement with an accuracy of ±2°.

Solid state UV-Vis measurements

All measurements were performed on a Lambda 9 in the reflection mode. UV illumination was always at 366 nm with an intensity of 80 W/m^2. The untreated membrane – stored at daylight – was used for the base line measurements. After illuminating the membrane for 1 minute with UV light, the spectrum of that membrane was measured and the maximal absorbance was detected. The

membrane was then illuminated with UV-light for five more minutes. Afterwards, the absorption at the assigned maximum was measured over a time span of 90 minutes to get information about the ring-closing kinetics of the spiro-compounds under dark conditions at room temperature. Subsequently, the membrane was illuminated for 5 hours with UV-light. After 15, 30, 45, 60, 90, 120, 180 and 300 minutes, the absorption at the assigned maximum was measured to get information about the speed of decomposition of the spiro-compounds under UV-irradiation. Since fading and ring closing reaction did not follow a simple reaction mechanism a linear fit was applied as a rough approximation. For fading rates, the measurements of the first 60 minutes were considered for the linear fitting. For ring closing rates, all measurements between minute 20 and 40 were considered for the estimation of the reaction speed.

Multi-angle XPS measurements

The measurements were performed by SuSoS AG, Dübendorf, using a PhI5000 VersaProbe spectrometer equipped with a 180° spherical capacitor energy analyzer and a multi-channel detection system with 16 channels. All spectra were obtained at a base pressure of 10^{-8} Pa using a focused scanning monochromatic Al-Ca source (1486.6 eV) with a spot size of 200 μm, scanning an area of 1000x500 μm. Charge neutralization utilizing both, a cool cathode electron flood source (1.2 eV) and very low energy Ar^+–ions (10 eV), was applied throughout the analysis. All data were analyzed by SuSoS AG, Dübendorf, using the program CasaXPS. As a result, the measured amounts are given as apparent normalized atomic concentration and the accuracy under the chosen condition is approximately ±10%.

ToF-SIMS measurements

The measurements were performed on a ToF-SIMS 5 from ION-TOF GmbH. Negative secondary ions and elements from 1 to 800 mu were analyzed in the high mass resolution spectra mode (dual beam mode). For the primary analysis, Bi_3^{2+} ions (50keV) were used and an area of 300 x 300 μm was analyzed. For sputtering, Cs^+-ions at 500 eV were used on an area of 600 x 600 μm.

Ellipsometry

By using a multi angle ellipsometer (EP3SW system, Accurion, Göttingen, Germany) it was possible to measure not only the thicknesses of the silicon oxide layer after plasma treatment, but also to estimate the thickness of the HEMA and the PMMA coatings on silicon wafers. All samples were measured at least at two different positions and at eleven different angles (from 55° to 75°) per position. For each coating, four different samples were measured as a minimum. All samples were stored under dry conditions over molecular sieve for at least 24 hours before being measured. For measuring the thickness of the HEMA coating under wet condition, the samples were stored in water for 30 minutes and then air dried. For measuring the coating in its MC state, the samples were irradiated with UV light (366 nm, 80 W/m^2) for 1 minute. The refractive index of the HEMA coatings was assumed to be 1.51 for all angles.[22] For the PMMA coating a value of 1.49 was assumed.[23]

Amount of spiropyran on the membrane

A coated PC membrane was dissolved in DCM. The UV-absorption at 375 nm was caused by spiropyran and was therefore used to determine the amount of spiropyran that was incorporated during the modification of the membrane. For the calibration, the corresponding spiropyran-monomer was dissolved in DCM together with an untreated PC-membrane (**SP7** and **SP9:** $\varepsilon_{375} = 245$ $cm^{-1}M^{-1}$ and **SP12**, **SP14** and **SP16:** $\varepsilon_{375} = 226$ $cm^{-1}M^{-1}$).

Two-photon microscopy

The samples were fixed on a glass slide and covered with a second glass slide. To assure that the measured fluorescence really originates from spiropyran, an original PC-membrane, a plasma-treated PC-membrane, and a HEMA-coated PC-membrane were measured before SP-containing PC-membranes were analyzed.

3.3. RESULTS AND DISCUSSION

Etching of PC-Membranes

The time dependent mass loss of polycarbonate membranes (1.0 μm pore diameter) in an argon/oxygen plasma (15.0/2.5 sccm, 52 Pa, 12 W, 13.56 MHz) was measured. Plotting etching times versus mass losses of the treated membranes showed a linear correlation of these two parameters (Figure 3.2).[12] The slope of the straight line indicated an etching rate of 477 μg per minute. Assuming an intermediate membrane density of 0.9 g/cm^3 and a membrane surface of 17.3 cm^2, the etch rate was calculated to be 310 nm/min.

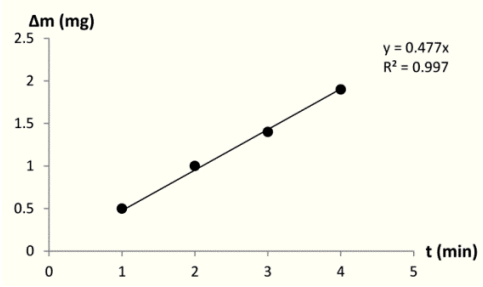

Figure 3.2 Etch rate over time of polycarbonate in argon/oxygen plasma at 12 W.

In former experiments with polycarbonate polymers, an etching rate of 120 nm min^{-1} was observed using a pure argon discharge at a pressure of 20 Pa and a comparable power density.[12] Thus, the enhanced pressure and the addition of oxygen increase the etching rate of polycarbonate due to a higher number of reactive species. Five membranes were all etched independently for four minutes at 12 W. The average mass loss was found to be 1.78 ± 0.28 mg after four minutes of plasma treatment.

Similar experiments were performed with polyethersulfone (PESF) and polyvinylidene fluoride (PVDF) membranes. PESF lost its mechanical stability due to the plasma treatment resulting in very fragile membranes. PVDF had a high etching rate (1.5 mg/min at 12 W) but showed very low

chemical reactivity in subsequent coating experiments. Therefore it was decided to use only PC-membranes for the subsequent experiments.

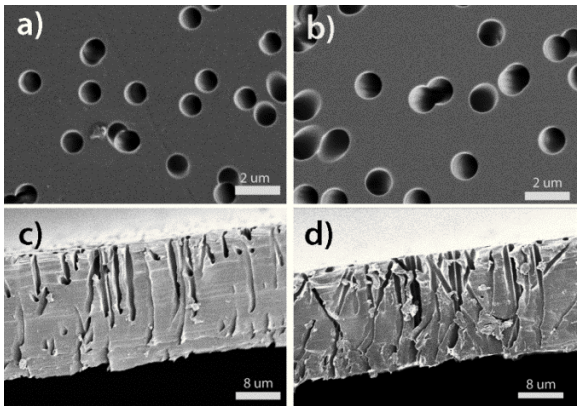

Figure 3.3 SEM micrographs of **a)** untreated PC membrane; **b)** PC membrane after plasma treatment; **c)** side view – untreated PC membrane; **d)** side view – Plasma treated membrane.

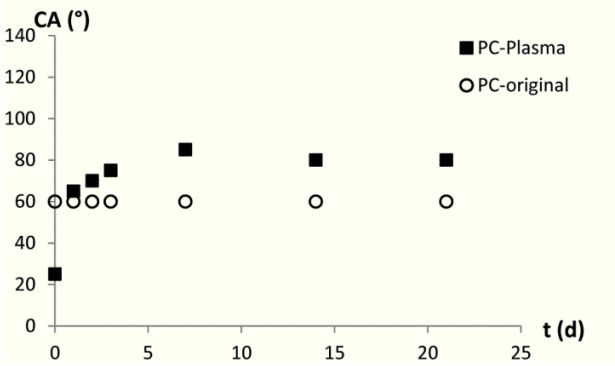

Figure 3.4 Contact angle measurements showing the long-time stability of untreated PC and clear aging effects already after one day for plasma treated PC-membranes.

SEM measurements of PC-membranes (1.0 μm pore diameter) before and after plasma treatment showed an increase in the average pore diameter from 1.03 ± 0.04 μm to 1.22 ± 0.05 μm and a decrease in the membrane thickness from 22.0 ± 0.2 μm to 19.5 ± 0.6 μm caused by the plasma treatment (Figure 3.3).

Besides the etching effect, PC-membranes were also more hydrophilic after the argon/oxygen plasma treatment due to the fact that radicals were created which react with oxygen forming different oxygen-containing functionalities.[24] The change of surface hydrophilicity after the plasma treatment was investigated by contact angle measurements over time. As shown in Figure 3.4, this hydrophilic modification lacked long term stability. Each sample was measured at three different positions each time. There was no local dependence detectable.

Commercial available PC membranes are coated with polyvinylpyrrolidone (PVP) to improve their wettability properties. The contact angle of such a PVP coated PC membrane was found to be 60°. Directly after plasma treatment with oxygen, the PC membrane was highly hydrophilic with a contact angle of 25°. During the first week after the treatment, the PC membrane became less and

less hydrophilic until its contact angle remained stable at around 80° which was obviously more than the original PVP-covered PC membrane.

Table 3.1 XPS measurements of untreated and plasma treated PC membrane. All result are shown in At.-%

Sample	C 1s	O 1s	N 1s
PC original	85.5	11.9	2.7
PC-Plasma (1d)	80.9	19.1	0
PC-Plasma (21d)	84.6	15.4	0
PC (calc.)	*84.2*	*15.8*	*0*

XPS measurement proved the removal of the PVP-layer during the plasma treatment. The initial nitrogen signal measured for the untreated PC-membrane disappeared after the plasma treatment (Table 3.1).

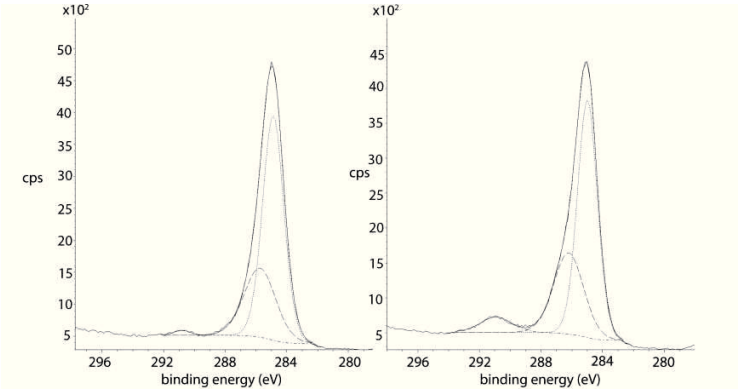

Figure 3.5 High resolution C 1s trace of an untreated (left) and a plasma treated (right) PC membrane. The peak at 291 eV corresponds to carbonate. The grey line and the dashed lines are the corresponding fitted signals. The intensity of the carbonate signal is lower on the untreated membrane due to a PVP-coating which disappears during the plasma treatment.

Additionally, the carbonate peak at 291 eV increases significantly from 0.9 % (rel.% for high resolution C 1s signal) for the original, PVP-coated membrane to 7.5% for the plasma-treated membrane (Figure 3.5). The measured oxygen content of about 19.1% after the plasma-treatment revealed the formation of oxygen functionalities on the membrane surface. The oxygen value decreases with time and reaches 15.4% after 21 days (Table 3.1). Additionally, the area from the peak at 286.4 eV (C-O) reduces from 31.9% (rel.% for high resolution C 1s signal) directly after plasma-treatment to 19.8% after storage for 21 days.

The plasma-induced polar oxygen groups resulted in a strongly improved wettability directly after treatment. Gradually, the oxygen functionalities can be reorganized and thus turn to the inwards yielding hydrophobic recovery, also known as aging.[25] A subsequent coating with polar monomers, however, minimizes aging effects (see below).[12]

Nonresponsive coating of PC-Membranes

More stable surfaces were achieved when the described plasma treatment was only used as surface activation followed by free radical surface induced polymerization to obtain coatings on the membrane surfaces. For this approach, the plasma chamber was flooded with a monomer solution immediately after the plasma treatment. Starting from the radicals that were created during the plasma activation, molecular chains started to grow as shown in Scheme 3.2.

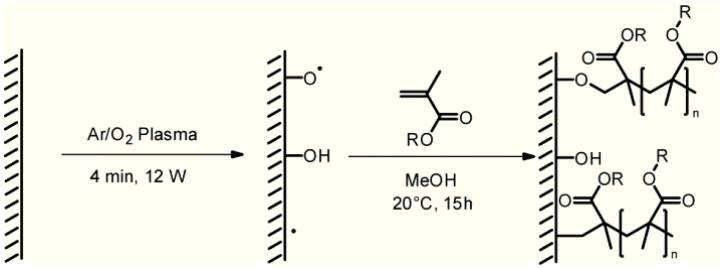

Scheme 3.2 PC-surface activation by plasma treatment and subsequent surface modification.

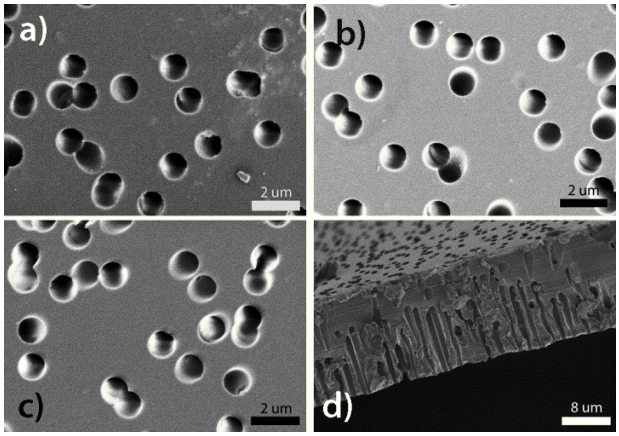

Figure 3.6 SEM pictures of PC membranes coated with **a)** HEMA; **b)** MMA; **c)** AMPS-NA; **d)** HEMA (side view) showing that the pore size was not affected by the coating. Therefore steric effects can be neglected when permeability resistances of the membranes are measured.

SEM pictures were recorded for all coated membranes. Since there was no significant change detectable between only plasma treated membranes and coated membranes (HEMA: pore diameter: 1.19 ± 0.06 μm / membrane thickness: 18.8 ± 1.0 μm. MMA: pore diameter: 1.25 ± 0.11 μm / membrane thickness: 19.3 ± 0.5 μm. AMPS-Na: pore diameter: 1.19 ± 0.08 μm / membrane thickness: 20.0 ± 0.8 μm) regarding the pore diameter, the thickness of the membrane and the surface morphology, a very thin coating with a low degree of polymerization was deduced (Fig. 3.6). Other than with oxygen plasma treatment alone, long term stable coatings of different hydrophilicities were achieved with MMA, HEMA and AMPS-Na (Figure 3.7). The latter allowed getting a hydrophilic surface with a contact angle of 40° whereas HEMA created a modestly hydrophobic surface with a contact angle of around 90°. MMA lead to a slightly higher hydrophobicity with a contact angle of 100° (Figure 3.8). Contact angle measurements at different positions on the membrane showed no local dependence of the surface tension.

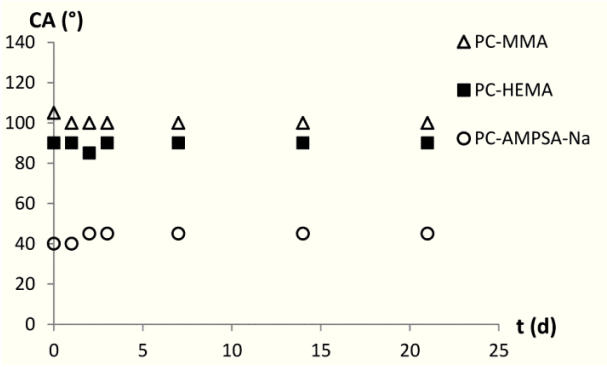

Figure 3.7 Contact angle measurements over time of coated PC-membranes showing the improved long-term stability of coated membranes compared to only plasma treated membranes.

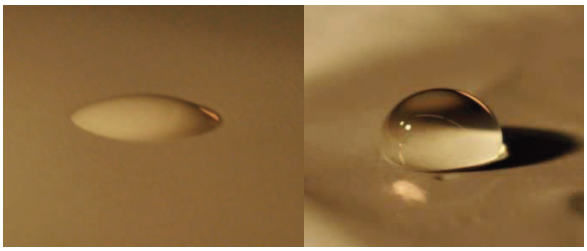

Figure 3.8 Contact angle of an AMPS-Na coated (left) and a MMA coated (right) porous PC-membrane.

XPS-measurements revealed that the carbon and oxygen content of the HEMA and MMA modified membranes was about the same as for pure polycarbonate. Nevertheless, the C(sp_2)-carbonate peak at 291 eV decreased after modification from 7.5% to 5.0% (HEMA), 5.6% (MMA), and 4.9% (AMPS), respectively. This is a clear indication of the presence of a coating. The fact, that the signal at 291 eV was still detectable after modification of the membrane indicated that the coating was thinner than 10 nm. The nitrogen and sulfur signals on the XPS spectrum of the AMPS-Na coated membrane revealed the presence of AMPS (Table 3.2).

Table 3.2 XPS measurements of coated PC-membranes. All results are shown in At.-%.

Sample	C 1s	O 1s	N 1s	S 2p
PC (calc.)	*84.2*	*15.8*	*0*	*0*
PC-HEMA	83.8	16.2	0	0
HEMA (calc.)	*66.6*	*33.3*	*0*	*0*
PC-MMA	84.5	15.6	0	0
MMA (calc.)	*71.4*	*28.6*	*0*	*0*
PC-AMPS-Na	73.6	22.1	2.4	2.0
AMPS-Na (calc.)	*50.0*	*28.6*	*7.1*	*7.1*

Moreover, FTIR- and NMR-measurements were not sensitive enough to evidentially detect any coating. Profilometry indicated a coating thickness of less than 10 nm. Measuring the weight gain during the coating process was not successful since the weight of the coating turned out to be smaller than the error of the plasma etching process.
The described method of surface induced modification can be further used to bring desired functionalities onto the surface. To demonstrate this, a PC membrane was plasma activated and AEMA coated as described above for other acrylates. The primary amino groups of this AEMA coating were then reacted with octanoic acid (Oct) activated with DCC under mild conditions (Scheme 3.3).

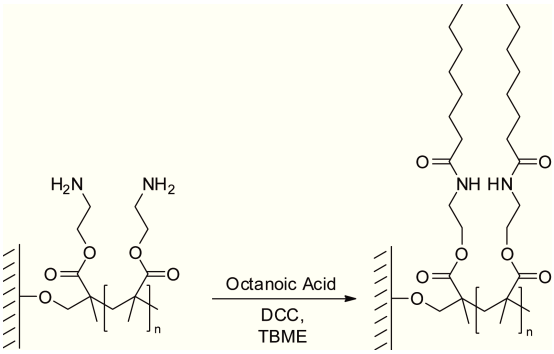

Scheme 3.3 Post-modification of AEMA-coated PC-membranes.

SEM-pictures showed an average pore size of 1.17 ± 0.04 μm with an average membrane thickness of 19.0 ± 0.3 μm for the AEMA-coated membrane and an average pore size of 1.16 ± 0.05 with an average membrane thickness of 19.1 ± 0.3 μm for the post modified membrane. Compared to only plasma treated membranes, no significant change in pore size or thickness was detected (Figure 3.9).
This post-modification allowed transforming the modestly hydrophilic PC-AEMA-membrane into a highly hydrophobic PC-AEMA-Oct-membrane. The AEMA-coated as well as the post-modified membrane were both long term stable as shown in Figure 3.10. Again, no difference in contact angle was observed by measuring at different positions.

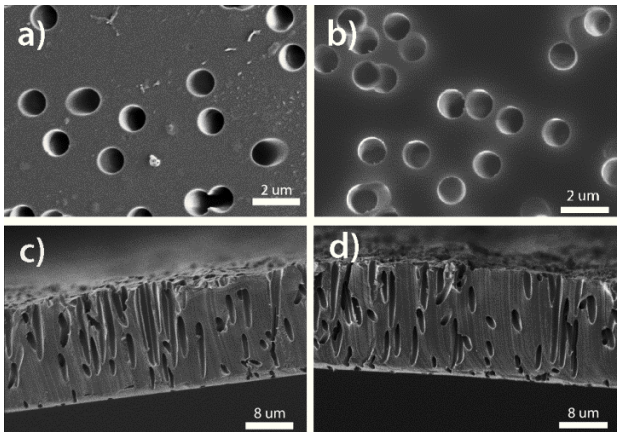

Figure 3.9 SEM-pictures of **a)** AEMA-coated PC-membrane; **b)** post modified AEMA-coated membrane **c)** side view of AEMA-coated membrane; **d)** side view of postmodified membrane. The pore size was unaffected by the surface modification.

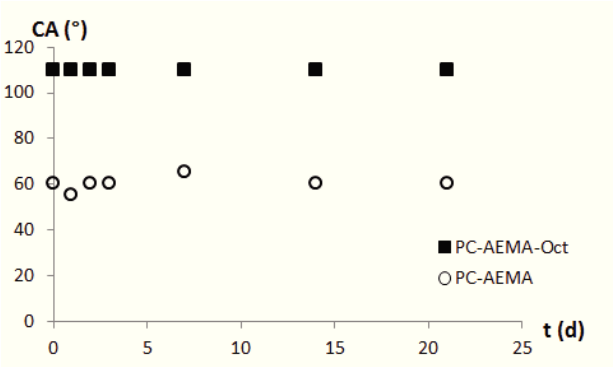

Figure 3.10 Contact angle measurements showing the long term stability and the change of hydrophilicity of AEMA coated PC-membrane and postmodified AEMA coated PC-membrane.

XPS-measurements showed that the AEMA-coated membrane had a nitrogen content of around 6.2% due to the primary amino groups of the pAEMA. The C(sp_2)-carbonate signal at 291 eV decreased after AEMA-grafting from 7.5% to 5.1% for the AEMA-coating. Again, the presence of the carbonate signal after grafting indicated a thin coating in the sub-10nm range. Post-modification with octanoic acid lowered the amount of nitrogen on the surface to 1.2% (Table 3.3) and the signal at 291 eV was found to be 4.2%.

Table 3.3 XPS measurements of AEMA coated and postmodified PC-membrane. All results shown in At.-%.

Sample	C 1s	O 1s	N 1s
PC (calc.)	*84.2*	*15.8*	*0*
PC-AEMA	73.9	19.9	6.2
AEMA (calc.)	*66.7*	*22.2*	*11.1*
PC-AEMA-Oct	78.4	20.4	1.2
Oct (calc.)	*80.0*	*20.0*	*0*

To gain more information about the thickness of the coatings, silicon wafers were coated with HEMA with the same process used to coat the PC-membranes. However, in order to activate the silicate surface, a higher plasma power was necessary. Ellipsometry measurements of dry HEMA coatings resulted in a median coating thickness of 1.9 nm (interquartile range: 1.2 nm to 3.6 nm). The median thickness for wet HEMA-coatings was found to be 3.0 nm (interquartile range: 2.7 nm to 3.8 nm). Allowing the sample to swell for more time in water did not increase the coating thickness anymore. Therefore, swelling was assumed to be completed after 30 minutes. A median thickness of 2.7 nm (interquartile range: 1.3 nm to 3.7 nm) was found for the PMMA coatings. These coating thicknesses on the silicon wafers indicate that oligomers consisting of between ten and twenty monomeric units were created during the plasma induced graft surface modification.

Table 3.4 XPS-measurements of AEMA coated PC-wafer. All results shown in At.-%.

Sample	C 1s	O 1s	N 1s	Si 2p	S 2p	Cl 2p	Na 1s	Ca 2p
PC plasma	74.8	22.4	0.0	2.2	0.6	0.0	0.0	0.0
PC-AEMA 20°	65.4	18.1	5.6	0.8	0.6	7.7	0.3	1.4
PC-AEMA 45°	65.9	18.3	5.9	0.6	0.8	6.7	0.5	1.4
PC-AEMA 70°	68.6	17.3	5.4	0.5	0.6	6.1	0.4	1.2
AEMA (calc.)	*66.7*	*22.2*	*11.1*	*0*	*0*	*0*	*0*	*0*

Since silicon wafers are not the most adequate model system, PC-wafers were activated with the same plasma process as the PC-membranes. The wafers were subsequently coated with AEMA, respectively HEMA under similar conditions as the PC-membranes. Angle dependent XPS measurements can provide information about the coating thickness if the x-ray beam is able to pass through the coating for several angles to measure coating and substrate simultaneously. The angle dependency of several signals can then be analyzed and with an adequate model, a coating thickness can be calculated. Chances to successfully perform such measurements are good, if the coating is thinner than 10 nm. For the AEMA-coating, no carbonate-signal at 291 eV was found, not even with a 70° detection angle, whereas for only plasma treated PC-wafers, a clear signal was detected for all angles (Figure 3.11 a) + b)). This indicates that the AEMA-coating is thicker than 10 nm.

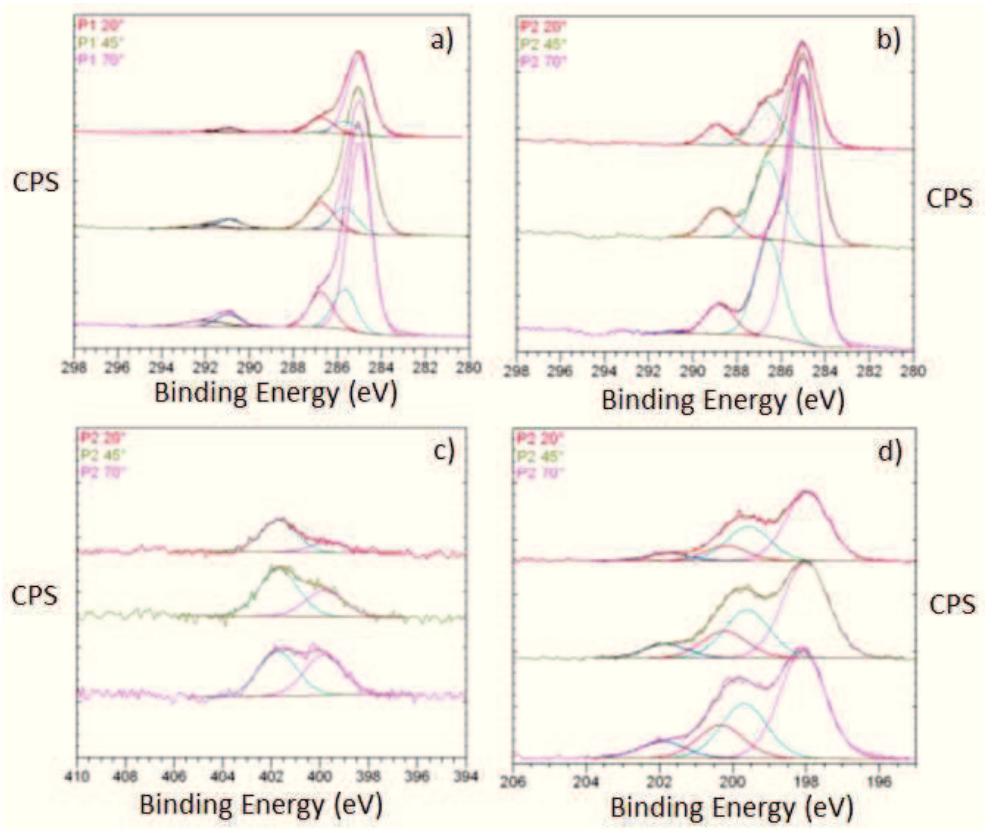

Figure 3.11 Angle dependant XPS-measurements: **a)** C-detail scan of a plasma treated PC membrane; **b)** C-detail scan of a AEMA-coated PC-membrane; **c)** N-detail scan of a AEMA coated PC-membrane; **d)** Cl-detail scan of a AEMA-coated PC-membrane.

Nevertheless, the elemental composition of the coating does not match the calculated composition of pure AEMA (Table 3.4). A possible explanation for the difference in the elemental composition is the occurrence of trans-esterification during the modification of the membrane. Assuming this hypothesis, the side chains of AEMA were replaced for example by methanol. This would explain the decreased N-signal.

XPS-measurements showed two signals at around 400 eV. The signal at 399 eV corresponded to free amine whereas the signal at 402 eV corresponded to protonated amines. The angle dependency of these signals showed that more protonated amines are on the outermost layers and more free amines can be found in inner layers of the coating (Figure 3.11 c)). Therefore, gradients in the coating rather than a homogenous coating have to be assumed. Several chemically different chloride species were detected at around 200 eV (Figure 3.11 d)). The signals at 200 eV and below were assumed to be the counter ions of the protonated amine and of impurities. The signal at 202 eV indicated most probably the presence of C-bound chlorine. This finding supports the hypothesis that some unpredictable radical chemistry was occurring during the coating process. Measurements of HEMA-coated PC-wafers showed that the coating of this polymer was thinner. It was possible to detect a clear carbonate peak at 291 eV after the coating process. Unfortunately, there was a large amount of Si (8.9%) detected on the surface. Since the source of this Si-signal remained unclear, applications of an adequate model for this coating was impossible. A Si-signal was also detected on

the only plasma treated PC-wafer but was not detected on HEMA-coated membranes. Therefore, it was assumed that the Si-containing species was already present in the original PC-wafer.
Comparing the signal intensity at 291 eV of a HEMA-coated PC-wafer with a HEMA-coated PC-membrane indicated that the coating on the membrane was even thinner than the one on the wafer. Therefore, measurements of coating-thickness on the PC-waver allowed only limited conclusions about the coating-thickness on the PC-membrane. Nevertheless, it can be concluded with a high probability that the HEMA-coating thickness on the PC-membrane was below 10 nm.
Time-of-flight secondary ion mass spectrometry (ToF-SIMS) of an AEMA-coated and a plasma-etched membrane allowed the assignment of characteristic mass-peaks for the coating and the polycarbonate. By measuring the signal intensity of these characteristic peaks while sputtering the sample layer by layer, information about the thickness of the coating were obtained. As can be seen from Figure 3.12, no sharp intensity step of the signals was detected, when the PC-matrix was reached. This can be caused by several reasons. The membrane is porous. All coating in the pores will be sputtered together with PC-matrix material only after removing of the surface coating. Therefore, a continuous change in signal intensity of the coating has to be expected rather than a sharp step. Additionally, the membrane surface is not completely flat. Some positions were sputtered first while others were sputtered later. Therefore, the sputtering already reached the matrix at some position while at other positions the sputtering still took place in the cladding and thus a mixture of coating and PC-matrix was measured. Other possible explanations for the slow change from coating to matrix signal are an inhomogeneous coating or a mixing of coating and PC-matrix during the coating process.
To obtain quantitative information about the coating thickness, it is necessary to know the sputter rate of the material. It was tried to determine the depth of the created crater by AFM-measurements to calculate the sputter rate. Since the crater-surface and the non-sputtered membrane surface were very bumpy, it was not possible to reliably quantify the crater depth. To obtain the sputter rate of pAEMA, it would be necessary to sputter a smooth layer of pAEMA.

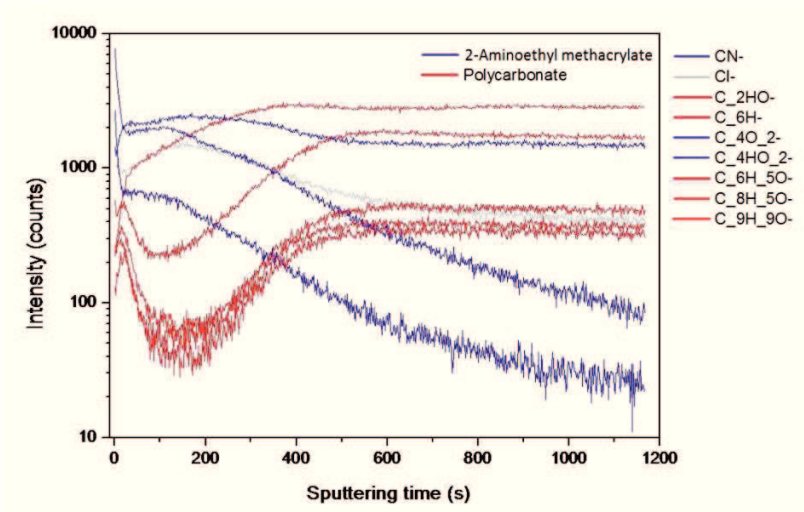

Figure 3.12 ToF-SIMS measurement of an AEMA-coated PC-membrane.

Permeability Measurements of nonresponsive membranes

The permeability resistance of PC-membranes with different pore-diameter was measured before and after plasma treatment (Table 3.5). There was no correlation of pore size to caffeine permeability resistance detected. In general, caffeine permeability resistance was somewhat lower after plasma treatment.

Table 3.5 Permeability resistance of PC-membranes with different pore diameters before (R_{orig}) and after (R_{plas}) plasma treatment.

Sample	R_{orig} (s/cm)	R_{plas} (s/cm)
PC 1.0 µm	9000	9000
PC 0.2 µm	11'000	10'000
PC 0.1 µm	20'000	19'000
PC 50 nm	13'000	11'000
PC 30 nm	15'000	12'000
PC 15 nm	28'000	24'000

As stated in the introduction, surface modifications of polymeric materials have a significant influence on the properties of the material. Therefore, the influence of the surface on the permeability of the membranes was studied. The permeability of caffeine through the treated membranes was measured and the permeability resistance R of each membrane was calculated. Permeability measurements were performed once with a dry membrane and once with a pre-wetted membrane. There was an evident impact of the conditioning of the membranes. If the membranes were stored in water, their permeability resistance decreased (Table 3.6).

Table 3.6 Membrane resistances for caffeine solution in dry and wet state.

Sample	R_{wet} (s/cm)	R_{dry} (s/cm)	CA (°)
PC original	6000 ± 240	7500 ± 300	60
PC-Plasma (0 d)	7600 ± 800	9400 ± 250	25
PC-Plasma (21 d)	8700 ± 960	10'700 ± 780	80
PC-AMPS-Na	5100 ± 550	9800 ± 1000	40
PC-MAA	6400 ± 620	9900 ± 350	50
PC-HEMA	6800 ± 640	11'800 ± 580	90
PC-MMA	11'300 ± 260	14'000 ± 140	105
PC-AEMA	7500 ± 350	10'200 ± 730	60
PC-AEMA-Oct	9800 ± 980	15'500 ± 240	110

In addition, a tendency was observed showing that membranes with a low contact angle also had a low resistance for caffeine. This means that hydrophilic membranes were highly permeable for caffeine whereas hydrophobic membranes had a significant lower permeability concerning caffeine (Figure 3.13).

This tendency and the fact that there was no change in pore size for the different membranes implies that the most important impact on the membrane resistance for caffeine in an aqueous solution is rather of electrostatic nature between surface and the solute than of a steric interaction of the solute with the membrane. This assumption is consolidated by the decreased permeability resistance of the membrane in wet state. If swelling would have an impact on the permeability resistance, it would be expected that a contrarious tendency is observed. (High resistance for wet membranes, low resistance for dry membranes)[26] Additionally, it is not surprising that swelling has no major impact on the permeability resistance since the observed swelling on silicon wafers was about 1.1 nm whereas the pore diameter was 1.2 μm. Profilometric measurements of dry and wet polycarbonate membranes showed that the used membranes were not swelling in water. Since the pore diameter is about 2000 times larger than the molecular radius of caffeine, it is stated that the wetting of the pores had the most prominent impact on the membrane resistance, as has already been reported for similar systems.[27]

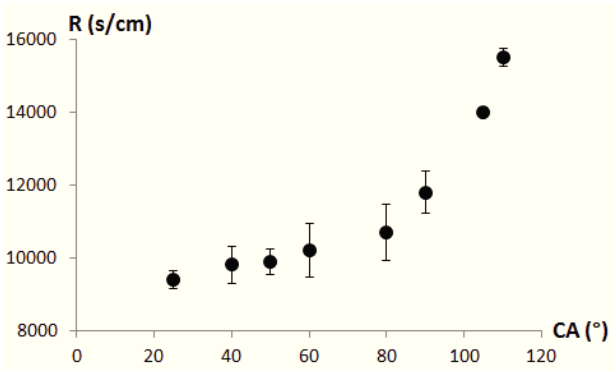

Figure 3.13 Membrane resistances for caffeine versus corresponding contact angles showing two domains. One domain for hydrophilic membranes with a CA lower than 80° and a second domain for hydrophobic membranes with a CA over 80°.

Based on classical theory of capillarity, membranes with a contact angle larger than 90° require pressure to push water into the pores.[28] This effect can be clearly seen in Figure 3.13. The impact of the contact angle on the membrane permeability resistance was much higher for hydrophobic membranes with contact angles larger than 90°.

Postmodification: Transforming nonresponsive coatings into light-responsive coatings

For this approach, PC-membranes with a pore diameter of 0.2 μm were coated similarly as described above but with a 0.62 M (instead of 3.17 M) methanolic monomer solution. It was possible to covalently link **SP12** to the HEA-, HEMA- and AEMA-coated membranes by creating an ester- or an amid-bond between the functional side chains of the polymeric coating and **SP12** (Scheme 3.4). This postmodification (PM) transformed nonresponsive membranes into photochromic membranes. UV-irradiation of the membrane resulted in a deep-blue coloration of the irradiated membrane (Figure 3.14).

Figure 3.14 Postmodified HEMA-coated PC-membrane – left: after UV irradiation; right: at daylight.

SEM-analysis showed that neither pore size nor thickness of the membrane is changed during the postmodification process. XPS-measurements showed only very little changes comparing postmodified membranes with only coated membranes. The N-signal corresponding to the spiropyran structure was not detectable. For the AEMA-coating, the amount of nitrogen was lowered (Table 3.7). Interpretation of the XPS values has to be made with caution since it is most probable that a mixture of PC, coating and **SP12** was measured. Since the changes are very small, no trustful statement can be made based on these measurements.

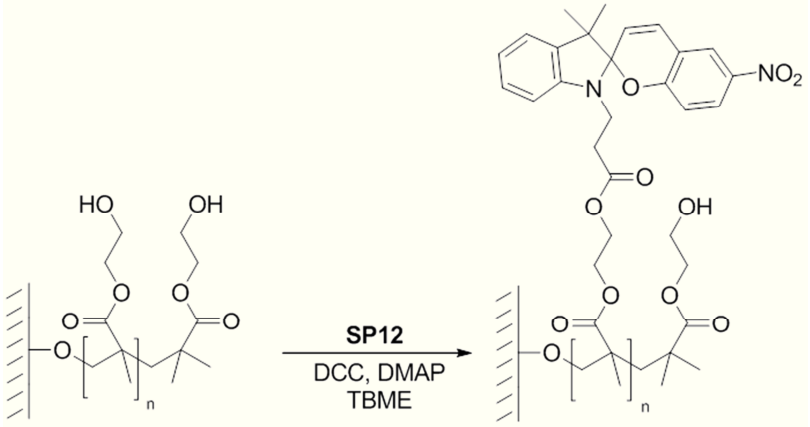

Scheme 3.4 Postmodification of a HEMA-coated PC-membrane via esterification.

Table 3.7 XPS-measurements of postmodified PC membranes. For comparison, XPS-values before postmodification are shown in italic. All results shown in At.-%.

Sample	C 1s	O 1s	N 1s
PC-HEMA-**SP12**	84.0	16.0	0
PC-HEMA	*83.8*	*16.2*	*0*
PC-HEA-**SP12**	83.2	16.8	0
PC-HEA	82.5	17.5	0
PC-AEMA-**SP12**	80.4	16.6	3.0
PC-AEMA	*73.9*	*19.9*	*6.2*

Contact angle measurements showed a decrease in surface tension for all photochromic coatings under UV-irradiation compared to its surface tension at daylight (Table 3.8). HEMA-SP was the

least hydrophilic coating changing its contact angle only by 10°. HEA-SP showed an intermediate contact angle of 95° and a change of 10°. AEMA-SP turned out to be the most hydrophilic coating with a change in contact angle of about 25°. This CA-switching can be repeated for at least three entire cycles with recovering the initial values for all reported coatings.
The amount of incorporated **SP12** was determined by UV-Vis absorption measurement at 375 nm after dissolving the coated PC-membrane in DCM. The most spiropyran was bound to the AEMA coating. HEA-coating incorporated about the same amount of **SP12** as the HEMA-coating. The different amounts of **SP12** found on the AEMA-coated membrane and on HE(M)A-coated membranes can either be explained by a higher reactivity of amines compared to alcohols or by the presence of more functional groups on the surface of the AEMA-coated membrane. The second explanation is supported by the angle dependent XPS-measurements discussed above that showed that AEMA-coatings are thicker than HEMA-coatings.

Table 3.8 Resistance towards caffeine, contact angles, spiropyran content and λ_{max} of postmodified PC-membranes. Membranes had been dried over molecular sieves before permeability measurements were performed.

Coating	R_{DL} (s/cm)	R_{UV} (s/cm)	CA_{DL} (°)	CA_{UV} (°)	SP on Mem (wt.%)	λ_{max} (nm)
HEMA-**SP12**	590'000 ± 98'000	15'700 ± 930	100	90	3.1	552
HEA-**SP12**	101'000 ± 3500	13'800 ± 2600	95	85	2.9	545
AEMA-**SP12**	13'900 ± 820	16'200 ± 810	75	50	4.2	543

For all coatings, the caffeine permeability resistance was lower under UV-irradiation than at daylight (Table 3.8 & Figure 3.15). The biggest switching potential concerning caffeine permeability resistance was found for the HEMA-coating. Postmodification of the HEA-coating provided a somewhat smaller but still evident change in caffeine permeability resistance as well. Postmodification of the AEMA-coating resulted in a photochromic membrane but the caffeine permeability resistance changed only little and a reversed switch was obtained.

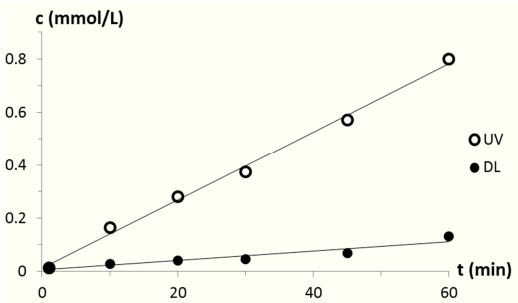

Figure 3.15 Caffeine permeability of a HEA-coated postmodified PC-membrane at daylight and under UV-irradiation.

Two-photon microscopy allowed the localization of spiropyran in and on the porous membranes. A HEMA-coated PC-membrane did not show any fluorescence at 546 nm and 647 nm (Figure 3.16 a)). Since the red fluorescence was not only measured on the surface of the membrane (Figure 3.16 b)) but also at the inner face (Figure 3.16 c) + d)), it can be concluded that spiropyran reacted not

only on the outside of the membrane but also on the pore-walls. An increased fluorescence in the pores can be seen compared to the PC-matrix (Figure 3.16 c) + d)). This is a clear indication of grafted spiropyran on the inner surface of the pores. The deeper in the membrane the focus plane was chosen, the less pores were clearly visible. This is due to light-scattering in the PC-matrix which leads to unfocused images.

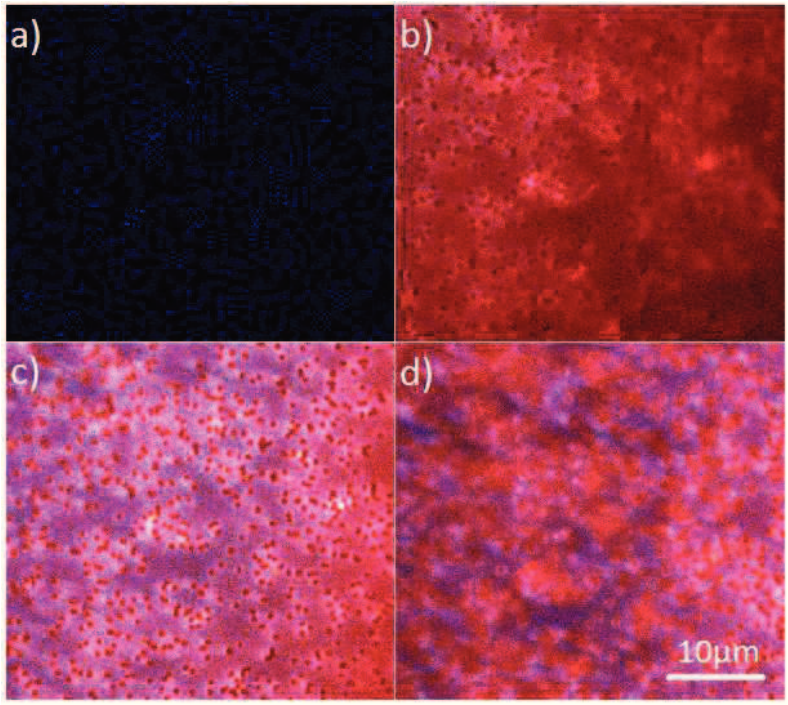

Figure 3.16 Two-photon microscopy pictures of **a)** a HEMA-coated PC-membrane; a postmodified HEMA-coated PC-membrane **b)** at the surface of the membrane; **c)** 6 µm below the surface; **d)** 10 µm below the surface.

Copolymerization

A one-step approach for the production of photochromic membranes was successfully developed. Instead of creating a nonresponsive coating followed by a postmodification to covalently link the photochromic molecule, spiropyran was transformed into a monomer and randomly copolymerized with the main coating monomer in a *grafting-from*-process in a single step (Scheme 3.5). UV-irradiation after the one-step coating process induced again a deep-blue coloration of the irradiated membrane (Figure 3.17).

Figure 3.17 Copolymerized HEMA-coated PC-membrane – left: at day light; right: under UV-irradiation.

For all samples, the measured caffeine permeability resistance was lower under UV-irradiation than at daylight (Table 3.9 & Figure 3.18). Switching potential was higher if monomeric **SP7** was copolymerized either with HEMA or HEA than if **SP7** was polymerized alone. Indeed, homopolymerization of **SP7** incorporated the highest amount of **SP7** on the membrane, but caffeine permeability resistance was only lowered by 33% under UV-irradiation. Copolymerizing HEMA with **SP7** resulted in a permeability resistance decrease of 87% (Table 3.9).

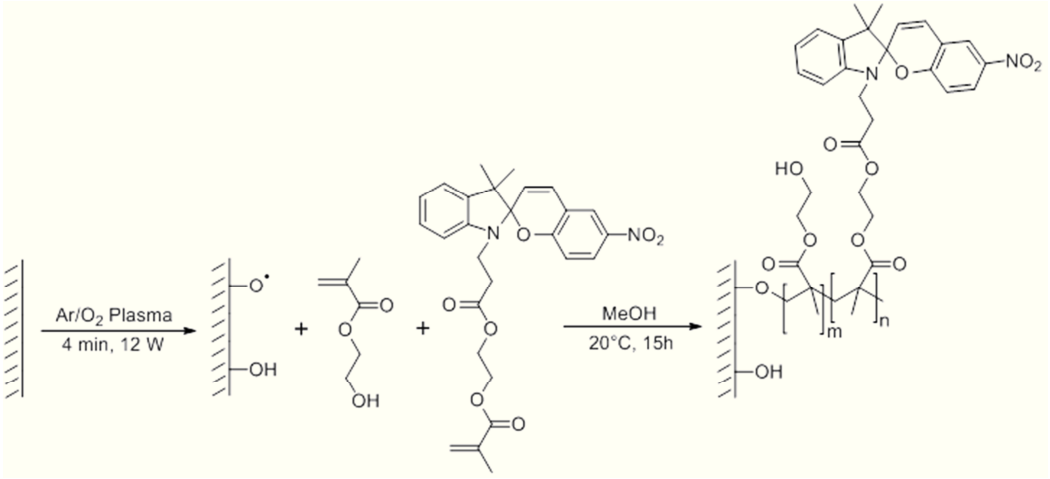

Scheme 3.5 Copolymerization of HEMA and **SP14** on a plasma-activated PC-surface.

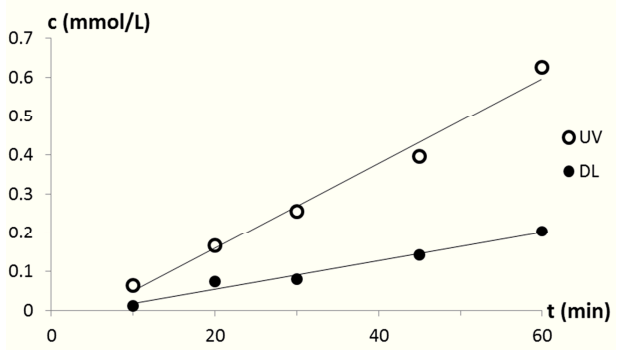

Figure 3.18 Caffeine permeability of a HEA-coated, copolymerized PC-membrane at daylight and under UV-irradiation.

Table 3.9 Resistance towards caffeine, contact angles, spiropyran content and λ_{max} of copolymerized PC-membranes. Membranes had been dried over molecular sieves before permeability measurements were performed.

Grafted monomers	SP in Rxn (mM)	R_{DL} (s/cm)	R_{UV} (s/cm)	CA_{DL} (°)	CA_{UV} (°)	SP on Mem (w%)	λ_{max} (nm)
PC original		11'300 ± 750	11'600 ± 860	60	60	-	-
HEMA; **SP7**	33.3	90'000 ± 22'000	11'600 ± 530	105	90	0.37	584
HEA; **SP7**	33.3	60'000 ± 17'000	17'300 ± 640	95	75	0.30	582
SP7	33.3	39'000 ± 4200	26'000 ± 3200	85	75	0.44	580

Measuring the surface tension at daylight and under UV-irradiation provides information about the hydrophilicity of a material. Contact angle measurements showed that the surface tension can be influenced by switching spiropyran from one to its other state (Table 3.9). This switching can be repeated for at least three entire cycles with recovering the initial values (Figure 3.19).

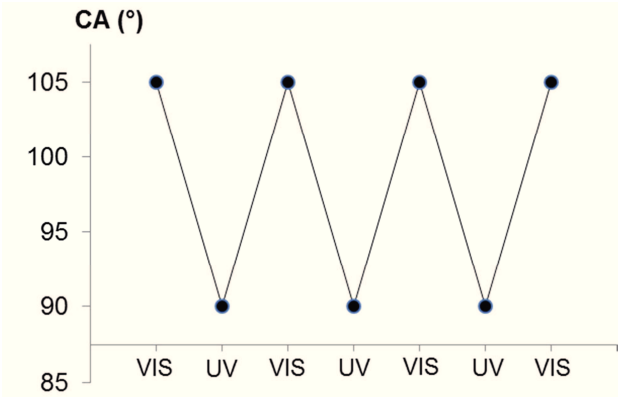

Figure 3.19 Reversibility of the surface tension switch of the copolymerized HEMA/**SP7**-coated PC-membrane.

Since the HEMA-**SP7** coating showed the biggest change in permeability resistance, this coating was chosen for the following investigation. The coating process remained unchanged except for the amount of **SP7**. The impact of changing the amount of **SP7** was found to be rather small. The best result concerning change of permeability resistance was achieved for a concentration of 25.0 mM **SP7** (Table 3.10). Reported values for R_{DL} were much larger in Table 3.8 than in Table 3.9 even for similar produced membranes. This difference resulted from unequal preconditioning of the membranes. Membranes reported in Table 3.9 were dried in a desiccator over molecular sieves before measuring their permeability resistances, whereas membranes reported in Table 3.10 were stored at ambient humidity. Preconditioning of a membrane has a big impact not only on the permeability resistance but also on the switching potential of the photochromic membranes. If a membrane is entirely dried before permeability measurements, R_{DL} is much higher and therefore the overall switching potential of the membrane appears to be larger. Therefore, preconditioning is essential for proper comparison of different membranes.

Table 3.10 Resistance towards caffeine, contact angles, spiropyran content and λ_{max} of PC-membranes; HEMA-coating copolymerized with different amounts of **SP7**.

Grafted monomers	SP in Rxn (mM)	R_{DL} (s/cm)	R_{UV} (s/cm)	CA_{DL} (°)	CA_{UV} (°)	SP on Mem (wt.%)	λ_{max} (nm)
HEMA; **SP7**	33.3	13'800 ± 440	10'800 ± 310	90	70	0.67	588
HEMA; **SP7**	25.0	15'200 ± 860	10'500 ± 360	95	75	0.72	595
HEMA;**SP7**	16.7	13'300 ± 370	11'100 ± 350	95	65	0.45	592

The amount of incorporated spiropyran is correlated to the switching potential of the membrane. More incorporated spiropyran resulted in a higher switching potential. Unexpectedly, the amount of incorporated spiropyran is not correlated to the concentration of spiropyran in the reaction mixture. As expected, the surface tension was lower under UV-irradiation than at daylight. Correlating the change in contact angle with the change in permeability resistance was not possible for this set of membranes. This indicates that there are also relevant interactions in the pores that cannot be judged by surface contact angle measurements.

For the next investigation step, the amount of spiropyran and comonomer remained unchanged but the impact of the linker length on membrane properties was compared (Figure 3.20).

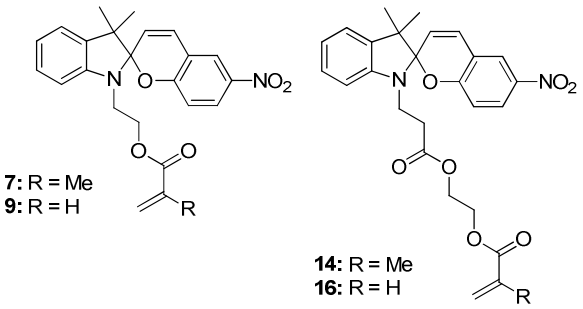

Figure 3.20 The impact of **SP7/9** with a short and **SP14/16** with a long linker on the membrane properties were investigated.

For the copolymerization with HEA, the acrylic derivative of the corresponding spiropyran was used whereas for approaches with HEMA the methacrylic derivative was copolymerized. It can be seen from Table 3.11 that using the longer linker (**SP14** and **SP16**) resulted in an increased amount of incorporated spiropyran. A long linker allows spiropyran to be rather far away from its reactive acrylic unit. This lowers the steric hindrance of the monomer and explains the easier incorporation of spiropyrans with long linkers into polymers. Nevertheless, HEA in combination with the short linked **SP9** resulted in the biggest change in permeability resistance followed by the HEMA coating with short-linked **SP7**. The impact of spiropyran on the permeability resistance of the membrane seems to decrease with increasing linker length. Lower surface tension was measured for all samples under UV-irradiation than at daylight. But it was again impossible to correlate changes in permeability resistance with contact angle changes.

Table 3.11 Resistance towards caffeine, contact angles, spiropyran content and λ_{max} of PC-membranes; HEA and HEMA-coating with two different SPs.

Grafted monomers	SP in Rxn (mM)	R_{DL} (s/cm)	R_{UV} (s/cm)	CA_{DL} (°)	CA_{UV} (°)	SP on Mem (wt.%)	λ_{max} (nm)
HEMA; **SP7**	25.0	15'200 ± 860	10'500 ± 360	95	75	0.72	595
HEMA; **SP14**	25.0	14'200 ± 1000	10'200 ± 700	70	55	1.15	590
HEA; **SP9**	25.0	58'000 ± 9000	17'500 ± 1400	100	85	0.64	591
HEA; **SP16**	25.0	15'900 ± 360	13'500 ± 2000	100	80	0.84	591

The following investigation focused on the impact of different comonomers on the membrane properties. Copolymerizing methyl methacrylate (MMA) with **SP7** resulted in a photochromic membrane (color change) but in no change of permeability resistance. Low free volume caused by high rigidity of a polymer is a common explanation in literature, if only little switching of photochromic molecules occurs.[29, 30] The high rigidity of pMMA compared to pHEMA or pHEA can also be an explanation for the non-existing change in permeability resistance in this case. Using AEMA as copolymer resulted in a membrane with only very little change in permeability resistance. Error margins show that this change is not even significant. Highest switching potential was provided by copolymerization of HEA with **SP9**. As before, no correlation of permeability resistance and contact angle was found (Table 3. 12).

Table 3.12 Resistance towards caffeine, contact angles, spiropyran content and λ_{max} of PC-membranes with different coatings copolymerized with spiropyran.

Grafted monomers	SP in Rxn (mM)	R_{DL} (s/cm)	R_{UV} (s/cm)	CA_{DL} (°)	CA_{UV} (°)	SP on Mem (wt.%)	λ_{max} (nm)
PC original		11'300 ± 750	11'600 ± 860	60	60	-	-
HEMA; **SP7**	25.0	15'200 ± 860	10'500 ± 360	95	75	0.72	595
HEA; **SP9**	25.0	58'000 ± 9000	17'500 ± 1400	100	85	0.64	591
AEMA; **SP7**	25.0	15'400 ± 620	14'100 ± 540	60	55	1.15	570
MMA; **SP7**	25.0	15'000 ± 510	15'200 ± 310	100	90	1.29	579

Not only spiropyrans but also **SO39** was copolymerized with HEMA. The resulting photochromic membrane showed a slightly higher switching potential concerning the caffeine permeability resistance compared to its spiropyran analogon **SP7** (Table 3.13). The incorporated amount of spiro-compounds was very similar. Copolymerization of **SO39** resulted in a lower surface tension at daylight as well as under UV-irradiation indicating that **SO39** is more hydrophilic than **SP7**.

Table 3.13 Resistance towards caffeine, contact angles, spiropyran content and λ_{max} of two photochromic, HEMA-coated PC-membranes. HEMA was copolymerized with **SP7** or **SO39**.

Grafted monomers	SP in Rxn (mM)	R_{DL} (s/cm)	R_{UV} (s/cm)	CA_{DL} (°)	CA_{UV} (°)	SP on Mem (wt.%)	λ_{max} (nm)
HEMA; **SP7**	25.0	15'200 ± 860	10'500 ± 360	95	75	0.72	595
HEMA; **SO39**	25.0	29'300 ± 750	12'300 ± 170	70	55	0.75	590

No XPS-measurement showed the elemental composition that was calculated for pure coating materials. This indicates that the coating was either thinner than 10 nm or inhomogeneous. A dependence of the linker length of spiropyran on the elemental composition was found (Table 3.14). If spiropyran with a long linker (**SP14/16**) was copolymerized, a higher content of O and a lower content of C were detected. The different elemental composition of the surface could be caused by different coating thicknesses. The longer linker allowed the spiropyran-backbone to be further away from the growing polymer-backbone. This reduced the steric hindrance and resulted probably in thicker coatings. As for the postmodified coatings, it is assumed that the XPS-signals resulted from a mixture of PC, copolymer and spiropyran. This made it impossible to carve out conclusive results or evident trends from XPS-measurements.

Table 3.14 XPS-measurements of different coated PC-membranes. All membranes are modified in a copolymerization process. All results shown in At.-%.

Sample	C 1s	O 1s	N 1s
PC (calc.)	*84.2*	*15.8*	*0*
HEMA; **SP7**	81.7	18.3	0
HEMA; **SP14**	75.3	24.7	0
HEMA (calc.)	*66.6*	*33.3*	*0*
HEA; **SP9**	84.2	15.8	0
HEA; **SP16**	82.7	17.3	0
HEA (calc.)	*62.5*	*37.5*	*0*
AEMA; **SP7**	76.8	21.2	2.0
AEMA (calc.)	*66.7*	*22.2*	*11.1*
MMA; **SP7**	80.0	20.0	0
MMA (calc.)	*71.4*	*28.6*	*0*

SEM-pictures showed that the plasma process caused an increase in pore diameter and a decrease in membrane thickness compared to an original PC-membrane. As before, FTIR- and NMR-measurements did not provide any interesting data. Combining the findings from all analytical measurements with the fact that spiropyran is known to more likely hinder than promote polymerization processes, leads to the conclusion that the developed photochromic coatings were thinner than 10 nm.

Solid state UV-Vis measurements

To obtain qualitative information about the stability of the different photochromic coatings, the absorptions of photochromic membranes was measured after different timespans under UV-irradiation. Additionally, ring-closing kinetics under dark conditions was measured for the different coatings. A slow ring-closing kinetics allows using a pulsed instead of a permanent UV-irradiation to keep spiro-compounds in their MC-state. Using a pulsed UV-irradiation would lower the overall irradiation dose that reaches the membrane which leads to less fading of the photochromic substance. Therefore, less UV-irradiation would extend the operating time of the membranes.

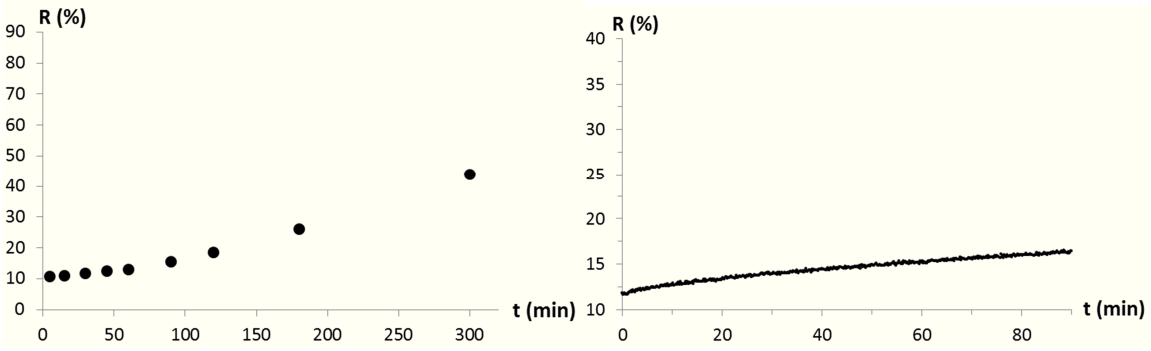

Figure 3.21 Fading-rate measurement (left) and ring-closing reaction kinetics measurement under dark conditions (right) of a postmodified, HEA/**SP12-**coated PC-membrane. Reflection (R in %) of the membrane at λ_{max} (see Table 3.15) was measured over time.

As shown in Figures 3.21 and 3.22, the postmodified membranes were more stable and showed slower ring-closing kinetics compared to the copolymerized membranes. Comparing the shapes of the stability measurements curves showed a fundamental difference from postmodified to copolymerized membranes. Whereas the postmodified sample showed a slow fading rate at the beginning and an increase over time (Figure 3.21), the copolymerized sample showed a higher, constant fading rate at the beginning with a decrease towards the end of the measurement (Figure 3.22).

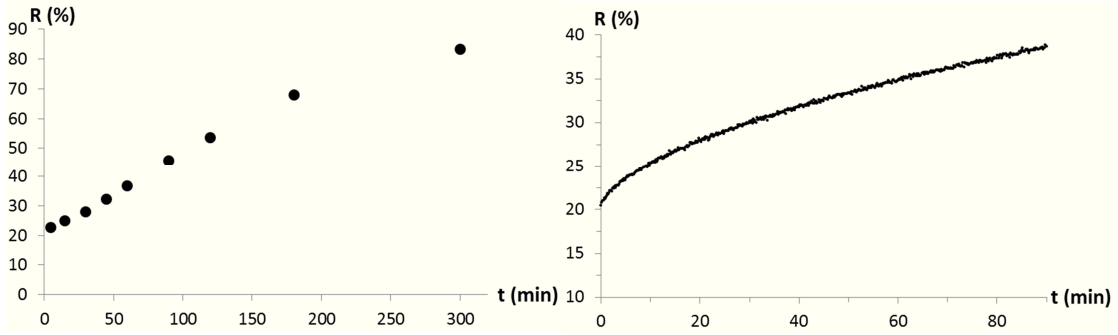

Figure 3.22 Fading-rate measurement (left) and ring-closing reaction kinetics measurement under dark conditions (right) of a copolymerized, HEA-**SP16**-coated PC-membrane. Reflection (R in %) of the membrane at λ_{max} (see Table 3.15) was measured over time.

Since fading and ring closing reaction do not follow a known reaction mechanism and measured curves are different for each sample, it was not possible to apply an appropriate model to exactly quantify the processes. To qualitatively compare the different membranes, a linear fit was applied assuming zero-order kinetics as a rough approximation. For fading rates, the measurements of the first 60 minutes were considered. The slopes of all linear fits are summarized in Table 3.15. High fading rates indicates fast decomposition of the spiro-compound on the membrane. Large slopes for ring-closing-kinetics indicate membranes where spiro-compounds undergo fast ring-closing reaction.

Table 3.15 Kinetics of ring closure reaction, stability of SP/SO under UV irradiation and λ_{max} for plasma-coated photochromic membranes. All copolymerized membranes were produced with 25.0 mM SP in the reaction mixture.

Membrane	Fading rate (ΔR%/min)	Ring closing kinetics (ΔR%/min)	λ_{max} (nm)
PM HEMA; **SP12**	0.13	0.02	552
PM HEA; **SP12**	0.14	0.05	545
PM AEMA; **SP12**	0.14	0.01	543
CP HEMA; **SP7**	0.26	0.14	595
CP HEMA; **SP14**	0.24	0.10	590
CP HEA; **SP9**	0.23	0.16	591
CP HEA; **SP16**	0.27	0.19	591
CP AEMA; **SP7**	0.53	0.10	570
CP MMA; **SP7**	0.19	0.10	579
CP HEMA; **SO39**	0.19	0.21	590

There were no evident differences in fading rates between the two different linker lengths (**SP7/9** and **SP14/16**) and between HEMA- and HEA-coating comparing the copolymerized samples. Considering postmodified membranes, the HEA-coated sample showed a faster ring-closing kinetics than the HEMA-coated membrane. **SO39** had – compared to **SP7** – a slightly higher stability and a faster ring-closing-kinetics (Table 3.15). Stability measurements showed clearly that the method of production had a higher impact on the stability of the photochromic membranes than substituting spiropyrans by spirooxazines.

3.4. CONCLUSIONS AND OUTLOOK

The importance of the control of surface hydrophilicity in membranes was demonstrated. It could be shown that the hydrophilicity of the membranes is determining the permeability rate of aqueous caffeine solutions. Thus, the pore wetting plays a key role for this kind of drug delivery systems.
Plasma induced graft surface modification in solution was shown to be a reliable method to tune the hydrophilicity and the permeability resistance of PC-membranes. Furthermore, it was shown that it is possible to further functionalize AEMA-coated PC-membranes, which in the example of the postmodification with octanoic acid resulted in an essential decrease of the hydrophilicity. This modification allows the fast and long-term stable functionalization of surfaces with a broad variety of molecules to tune the permeability resistances of membranes or to achieve other surface effects.
It was possible to transform nonresponsive coatings in a postmodification step into photochromic coatings by linking spiropyran to functional side-chains. Switching spiropyran from one into its other state influenced the caffeine permeability rate due to changed wettability properties of the pores. The photochromic coatings did no longer match the relation of permeability resistance and contact angle that was found for nonresponsive coatings. This indicated that – depending on the coating – the material properties inside the pores differed from the material properties on the membrane surface.
Photochromic coatings were also directly applied to polycarbonate membranes in a copolymerization process. Comparing the different coatings showed that copolymerizing HEMA with **SP7** resulted in the biggest change in permeability resistance switch if the membranes were stored under dry conditions. If the membranes were stored at ambient conditions, HEA with **SP9** showed the biggest switching potential.
Comparing postmodified and copolymerized membranes showed that postmodified membranes had a larger switching potential concerning caffeine permeability. Postmodified membranes showed also lower fading rates. The slow ring-closing kinetics of postmodified membranes would allow using a pulsed UV-irradiation. This increases the operating time of the membranes. Summing it up, postmodified HEA and HEMA coated membranes showed promising results. These membranes have the potential to be used as a key unit in a transdermal caffeine delivery setup.

3.5. REFERENCES

1. R. Barbey, L. Lavanant, D. Paripovic, N. Schüwer, C. Sugnaux, S. Tugulu and H.-A. Klok, *Chemical Reviews*, 2009, **109**, 5437-5527.
2. B. N. Chapman, *Glow Discharge Processes: Sputtering and Plasma Etching*, John Wiley & Sons, Inc., United States of America, 1980.
3. V. E. Golant, A. P. Zhilinskii and I. E. Sakharov, *Fundamentals of plasma physics* Wiley New York, 1980.
4. E. Nasser, *Fundamentals of gaseous ionization and plasma electronics*, Wiley-Interscience New York, 1971.
5. J. L. Vossen and W. Kern, *Thin film processes II*, Academia Press Inc, San Diego, 1991.
6. H. V. Boenig, *Fundamentals of plasma chemistry and technology*, Technomic Publishing Co., Lancaster, 1988.
7. R. d'Agostino, *Basic Approaches to Plasma Production and Control*, Wiley-VCH Verlag GmbH & Co. KGaA, 2008.
8. E. M. Liston, L. Martinu and M. R. Wertheimer, *Journal of Adhesion Science and Technology*, 1993, **7**, 1091-1127.
9. K. S. Siow, L. Britcher, S. Kumar and H. J. Griesser, *Plasma Processes and Polymers*, 2006, **3**, 392-418.
10. D. P. Lymberopoulos and D. J. Economou, *Journal of Vacuum Science & Technology A: Vacuum, Surfaces, and Films*, 1994, **12**, 1229-1236.
11. S. K. Øiseth, A. Krozer, B. Kasemo and J. Lausmaa, *Applied Surface Science*, 2002, **202**, 92-103.
12. D. Hegemann, H. Brunner and C. Oehr, *Nuclear Instruments and Methods in Physics Research Section B: Beam Interactions with Materials and Atoms*, 2003, **208**, 281-286.
13. W.-K. Choi, S.-K. Koh and H.-J. Jung, *Journal of Vacuum Science & Technology A: Vacuum, Surfaces, and Films*, 1996, **14**, 2366-2371.
14. S. Kitova, M. Minchev and G. Danev, *J. Optoelectron. Adv. Mater.*, 2005, **7**, 2607 – 2612.
15. M. M. Hossain, D. Hegemann, A. S. Herrmann and P. Chabrecek, *Journal of Applied Polymer Science*, 2006, **102**, 1452-1458.
16. S. Guimond, B. Hanselmann, M. Amberg and D. Hegemann, *Pure Appl. Chem.*, 2010, **82**, 1239-1245.
17. T. Hirotsu and S. Nakajima, *Journal of Applied Polymer Science*, 1988, **36**, 177-189.
18. J. Choi, P. Schattling, F. D. Jochum, J. Pyun, K. Char and P. Theato, *Journal of Polymer Science Part A: Polymer Chemistry*, 2012, **50**, 4010-4018.
19. C. T. Burns, S. Y. Choi, M. L. Dietz and M. A. Firestone, *Separation Science and Technology*, 2008, **43**, 2503-2519.
20. D. J. Chung, Y. Ito and Y. Imanishi, *Journal of Applied Polymer Science*, 1994, **51**, 2027-2033.
21. H. Kakwere and S. Perrier, *Polymer Chemistry*, 2011, **2**, 270-288.
22. J. Brandrup, E. H. Immergut, E. A. Grulke, A. Abe and D. R. Bloch, John Wiley & Sons.
23. C. B. Walsh and E. I. Franses, *Thin Solid Films*, 2003, **429**, 71-76.
24. J. F. Friedrich, R. Mix, R. D. Schulze, A. Meyer-Plath, R. Joshi and S. Wettmarshausen, *Plasma Processes and Polymers*, 2008, **5**, 407-423.
25. R. W. Paynter, *Surface and Interface Analysis*, 2002, **33**, 14-22.
26. R. Xie, L.-Y. Chu, W.-M. Chen, W. Xiao, H.-D. Wang and J.-B. Qu, *Journal of Membrane Science*, 2005, **258**, 157-166.
27. J. S. Kim, T. G. Kim, W. H. Kong, T. G. Park and Y. S. Nam, *Chemical Communications*, 2012.
28. R. Helmy, Y. Kazakevich, C. Ni and A. Y. Fadeev, *Journal of the American Chemical Society*, 2005, **127**, 12446-12447.
29. C. D. Eisenbach, *Berichte der Bunsengesellschaft für physikalische Chemie*, 1980, **84**, 680-690.
30. K. Horie, M. Tsukamoto and I. Mita, *European Polymer Journal*, 1985, **21**, 805-810.

4. SURFACE INDUCED ATRP ON POROUS POLYESTER MEMBRANES

4.1. INTRODUCTION

Atom transfer radical polymerization (ATRP) is known to reliably polymerize either 2-hydroxyethyl methacrylate (HEMA) or 2-hydroxyethyl acrylate (HEA).[1] Surface induced ATRP of HEMA was reported to allow to polymerize coating with thicknesses up to 700 nm in a controlled living process.[2] This would increase the coating thickness almost of a factor 100 compared to the plasma coating.
There is a chance to get steric instead of electrostatic control over caffeine permeability. Additionally, creating thicker coatings is expected to make analysis easier.
ATRP catalyst systems consist of a transition-metal species (e.g. Cu(I)) which can increase its state of oxidation and expand its coordination-sphere, a ligand (e.g. bipy), and a counterion (e.g. Br^-) which can form a bond with the metal. The metal complex facilitates the homolytic cleavage of an alkyl halogen bond (e.g. R-Br) to form an organic radical ($R^{\cdot}$) (k_{act}). The formed radical $R^{\cdot}$ can propagate with a monomer (M) (k_{pol}), terminate by either coupling or disproportionation (k_t), or be reversibly deactivated (k_{deact}) to form a halide-capped dormant polymer chain. Usually, the ATRP-equilibrium is strongly shifted towards the dormant species.[3] Addition of a reducing species to the reaction mixture (e.g. ascorbic acid) allows the regeneration of activators by electron transfer (ARGET ATRP) (Scheme 4.1).[4]

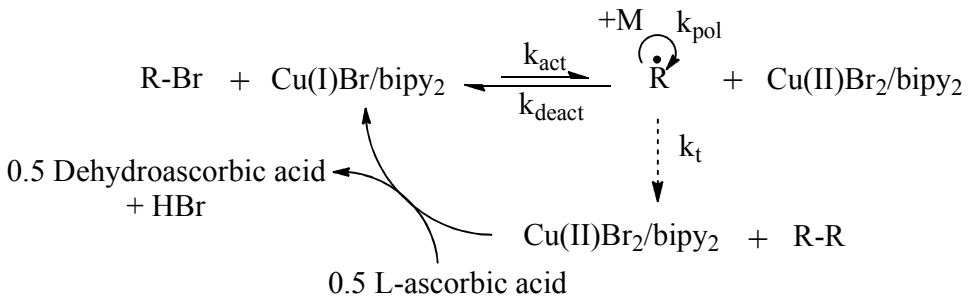

Scheme 4.1 Activators Regenerated by Electron Transfer (ARGET) ATRP mechanism with ascorbic acid.

An advantage of ATRP is that the rate of recombination of two radicals is significantly lowered due to the lowered concentration of free radicals. This leads to a low polydispersity index. A further advantage of living polymerizations is the easy control of polymer chain length, which dictates the coating-thickness by changing the polymerization time.[5]
Polymerization of 2-hydroxyethyl acrylate using ATRP was first reported to work in bulk and in solution by Coca *et al.*[6] One year later, the same group reported the successful polymerization of HEMA using ATRP.[7]
Addition of water to the reaction mixture was shown to increase the reaction kinetics without losing the living character of the reaction.[8-10] However, polymerization of HEMA in a pure aqueous media was shown to promote crosslinking reactions due to trans-esterification.[9] Therefore, solvent mixtures of water and organic alcohols are commonly used for ATRP of HEMA and HEA.

ATRP is known to be a good approach to perform polymerization of HEMA on surfaces. This surface polymerization was shown to work on different substrates as e.g. gold[2] or alumina[11] and under different conditions. In some approaches, CuX_2 was added additionally to the Cu(I) species.[7, 12] Halids association reduces the concentration of *tetra*-coordinated Cu(I) species with an open position for atom transfer. This shifts the ATRP-equilibrium more to the dormant species.[13] The polymerization slows down, and better control over the polymerization process can be gained. Lower polydispersities are reported for such systems due to the lowered concentration of free radicals.[2, 14-16]

Some other approaches report on the addition of reducing agents (ARGET ATRP).[17, 18] This allows to work at ambient conditions since all Cu(II) that is eventually formed due to a reaction of the catalyst with oxygen is reduced back into its Cu(I) state (Scheme 4.1). It is also possible to perform polymerization by only adding Cu(II) and reducing agent to the reaction mixture to create the Cu(I) species *in situ*.

There is remarkably less information available on the ATRP-surface polymerization of HEA than of HEMA. In general, it is known that acrylic radicals are less stable than methacrylic radicals and that acrylates polymerize faster due to a reduced steric hindrance. Therefore, it cannot be assumed that identical polymerization conditions of HEMA result in a similar polymerization behavior of HEA.[7]

ATRP processes are also known to be suitable for surface induced processes starting from porous media. There are for example reports on modified porous alumina[11] or porous PET[19] as ATRP-initiating surfaces.

Similar to Chapter 3, there are two approaches to produce membranes with a photochromic coating. One approach includes the creation of a pure pHE(M)A coating followed by postmodification via esterification of that coating to covalently link spiropyran to the side-chain of the polymeric coating.[20] The second approach includes the copolymerization of HE(M)A with monomeric spiropyran in a single ATRP approach. Advantage of postmodification is that the known ATRP process of pure HE(M)A can be used. Disadvantage is the additional reaction step that is needed to be performed. For the copolymerization, the reaction can be influenced by spiropyran. Therefore, similar reaction conditions as for pure HE(M)A may not be suitable. Especially, since spiropyran is known to interact with metals[21, 22], it is expected that the addition of spiropyran to the ATRP mixture has a major impact on the polymerization mechanism. ATRP processes including spiropyrans are known from literature.[21, 23, 24] No report on interactions of spiropyran with the catalyst has been found. But within these publications, no direct comparison of polymerization with and without spiropyran was reported.

PC-membranes used in Chapter 3 were decomposed upon the addition of CuBr to the reaction mixture. Therefore, track-etched polyester membranes (PES) were chosen as matrix. PES-membranes showed excellent chemical stability during grafting processes.

To introduce amine-functionalities on the PES-surface, a plasma-coating reported in literature was applied.[25, 26] These amines served as anchor sides for the ATRP-initiator.

Surface-induced ATRP of HE(M)A and spiropyran on porous polyester-membranes has never been reported before. Neither have any reports been found about the preformation of HE(M)A on PES-membranes with subsequent spiropyran postmodification.

4.2. EXPERIMENTAL

Materials and general methods

Track etched polyester (PES) Membranes, 0.2 μm pore diameter, 25 mm membrane diameter, were purchased from SterliTech Corporation. Caffeine (reagent plus) was delivered by Fluka. Anhydrous dichloromethane (DCM, 99.8%, dried over molecular sieve) was delivered by Acros. N,N-Dicyclohexylcarbodiimide (DCC, 99%), dimethyl aminopyridine (DMAP, 99%), copper(II) bromide ($CuBr_2$, 99%), copper(I) bromide (CuBr, 98%), copper(I) chloride (CuCl, 97%), L-ascorbic acid (AscA, reagent grade), 2,2'-bipyridine (bipy, puriss), methanol (MeOH, HPLC-grade), 2-hydroxyethyl methacrylate (HEMA, 97%) and 2-hydroxyethyl acrylate (HEA, 96%) were obtained from Sigma Aldrich. HEA and HEMA were dissolved in water and washed with hexane (Hx, 99%). Subsequently, the aqueous phase was saturated with sodium chloride, and extracted with Et_2O. The combined organic layers were dried over $MgSO_4$. After removing the solvent *in vacuo*, the monomer was distilled under reduced pressure. Distilled monomer was stored in the freezer for no more than one month. CuBr and CuCl were purified as described in literature.[27] Spiropyrans were synthesized and named according to Chapter 2. The relevant structures for this chapter can be seen in Figure 4.1.

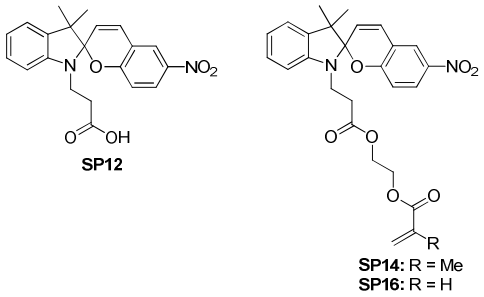

Figure 4.1 Used photochromic spiropyran structures for the different coatings.

All other chemicals, unless stated otherwise, were used as delivered. Distilled water from the in-house supply was used unless stated otherwise. UV-Vis measurements of all liquid samples were performed on a Varian 50Bio/50MPR. For weighing, a Mettler Toledo AB204-S and a Mettler ME30 were used if not stated otherwise. IR measurements were performed on a BioRad FTS 6000 equipped with an ATR Golden Gate. Scanning electron Microscopy (SEM) pictures were recorded on a Hitachi S4800. All samples were coated with a gold layer of about 3 nm. X-ray photoelectron spectroscopy (XPS) was performed on a PHI 5600 spectrometer under an angle of 45°.

Plasma Coating

Untreated PES-membranes were dunked in a gently stirred DCM bath for 3 hours at room temperature to remove possible coatings that were not denoted by the manufacturer. After drying the membranes, they were coated in a plasma deposition/polymerization process. 270 sccm ethylene, 250 sccm ammonium and 25 sccm argon were activated by 635 W at 0.1 mbar pressure in a coil coating-plasma chamber (BABE).[25, 26] Each side of the membrane was treated for 30 min under such plasma condition. The membranes were stored in a desiccator over molecular sieves.

Initiator Binding

A round-bottom flask was equipped with a stirring bar and a metal grid to protect the membrane from being damaged by the stirring bar. After charging the flask with 12 mL DCM and 1 mL NEt_3, a plasma-treated membrane was added. α-Bromoisobutyrylbromide (1.5 mL, 12 mmol) was added drop-wise via syringe. The whole mixture was stirred for 3 hours at room temperature. The membrane was then removed and subsequently washed with DCM, methanol and water in an ultrasonic-bath and dried in a desiccator over molecular sieves.

Surface Polymerization

The weight of all samples was measured before and after the polymerization. Relative weight gain was calculated by dividing the weight of the coated membrane by the weight of the uncoated membrane. All reactions were performed with an overall volume of 12 mL.

Without ascorbic acid: A two neck round-bottom flask was equipped with a stirrer and a protecting grid, sealed with a rubber septum and evacuated/flooded with argon for three times. Monomer, 2,2'-bipyridine (bipy) and $CuBr_2$ were dissolved in water and methanol (50:50 vol.%) and added to the flask. The monomer solution was degassed in three freeze-thaw cycles. After degasing and reaching the temperature for the polymerization, the Cu(I) species and the membrane were added at once under a gentle argon flow. After the polymerization time, the membrane was removed from the reaction mixture, washed with DCM, methanol and water and dried in a desiccator over molecular sieves.

With ascorbic acid: A round-bottom flask was equipped with a stirrer, a protecting grid and a membrane, sealed with a rubber septum and subsequently evacuated and flooded with argon for three times. This reaction flask was then heated to the polymerization temperature. In a second flask, the monomers, 2,2'-bipyridine and ascorbic acid were dissolved in water and methanol (50:50 vol.%). The monomer solutions were degased by bubbling argon through the solution for 1 hour. After degasing, the Cu(I)-species was added in one portion. This solution was added via syringe to the reaction flask. After the polymerization time, the membrane was removed from the reaction mixture, washed with DCM, methanol and water and dried in a desiccator over molecular sieves.

Post-Modification

A round-bottom flask was equipped with a stirrer and a protecting grid. The flask was dried under reduced pressure with a heat gun and flooded with argon. **SP12** (100 mg, 0.27 mmol), DCC (55 mg, 0.27 mmol), DMAP (33 mg, 0.27 mmol) and 12 mL DCM were added to the flask. The coated membrane was added und the whole mixture was gently stirred at room temperature for 12 hours.

Permeability

All measurements were performed in a Franz diffusion-cell purchased from SES Analyse Systeme with a receptor volume of 12.0 mL and an orifice area of 1.77 cm^2. Mass transfer rates of caffeine were measured under UV irradiation (366 nm, 15 W/m^2) and at daylight. After filling the receptor chamber with water (12.0 mL), the membrane was fixed in the diffusion cell. The donor chamber was charged with a caffeine solution (20 mM; 3.0 mL). Samples (200 μL) were collected from the receptor part of the cell after 1, 10, 20, 30, 45, and 60 minutes. The caffeine concentrations of these samples were assigned by measuring its UV absorption at 293 nm.

Resistance R (in s/cm) of a membrane was calculated according to Fick's law using the formula

$$R = \frac{\Delta c}{F} \quad (1)$$

where Δc represents the difference of caffeine concentration comparing the donor compartment with the receptor part of the used Franz cell. Δc was assumed to be constant over the time frame of the measurement. F was the molecular flux in number of molecules per time per area. Permeability measurements for all treated membranes were performed directly after the production. All membranes were dried *in vacuo* before the permeability measurements.

Contact Angle

All measurements were performed on a Krüss G10A. The membrane, fixed with a standard tape if necessary, was positioned on a metal O-ring. A drop of nanopure water (3.3 µL) was positioned on the part of the membrane surface, which was not in contact with the O-ring. For measuring the impact of switching SP on the surface tension of the membrane, the CA was measured first at day light. Then the membrane was illuminated with UV-light (366 nm, 80 W/m^2) for 1 minute and the contact angle was measured again. Subsequently, the membrane was illuminated with white-light until no more coloration was visible and contact angle was measured again. This circle was repeated at least three times.

Solid state UV-Vis measurements

All measurements were performed on a Lambda 9 in the reflection mode. UV illumination was always at 366 nm with an intensity of 80 W/m^2. The membrane itself, stored at daylight, was used for the base line measurements. After illuminating the membrane for 1 minute with UV light, the spectrum of that membrane was measured and the maximal absorbance was detected. The membrane was then illuminated with UV-light for five more minutes. Afterwards, the absorption at the assigned maximum wavelength was measured over a time span of 90 minutes to get information about the ring-closing kinetics of the spiro-compounds under dark conditions at room temperature. Subsequently, the membrane was illuminated for 5 hours with UV-light. After 15, 30, 45, 60, 90, 120, 180 and 300 minutes, the absorption at the assigned maximum was measured to obtain information about the speed of decomposition of the spiro-compounds under UV-irradiation. Since fading and ring closing reaction do not follow a known reaction mechanism and measured curves are different for each sample, it was not possible to apply an appropriate model to quantify the processes. To qualitatively compare the different membranes, a linear fit was applied. For fading rates, the measurements of the first 60 minutes were considered. For ring closing rates, all measurements between minute 20 and 40 were considered for the linear fit.

Polymerization-Kinetics

Five membranes with initiator on their surface where cut into four similar pieces each. The pieces where weighted and always four pieces from four different membranes were placed into one reaction flask. Polymerization was performed as described above. The first polymerization was stopped after 30 min, the second one after 60 min, the third after 90 min, and the fourth after 120

min. The last reaction mixture was stopped after 18 hours. The weight of all pieces was measured and the weight gains of the four pieces in the same reaction mixture were averaged.

Amount of spiropyran on the membrane

For the copolymerization approach, the coated polyester membrane was dunked in a 1 M NaOH-solution. It was stirred vigorously until the membrane was decomposed. The absorption of the resulting solution containing 2-hydroxy-5-nitrobenzaldehyde (decomposition product of spiropyran) was measured at 389 nm (ε = 10700 $M^{-1}cm^{-1}$).[28] It was assumed that spiropyran is quantitatively decomposed. For the postmodification approach, the weight gain during the esterification step was measured.

4.3. RESULTS AND DISCUSSION

Activation of Polyester Surface

Washing the original polyester (PES) membrane with DCM removed a small amount of unknown material. It was assumed that this was a coating to improve the wettability of the PES-membrane as reported for PC-membranes in Chapter 3. No changes in elemental composition or IR-spectrum were induced by the DCM-treatment. To enable ATRP on PES-surfaces, plasma coating introducing amines on the surface was applied (PES-NH_2). Subsequent reaction of these amines with the acid bromide of an ATRP-initiator yielded an activated surface for ATRP (PES-Init.) (Scheme 4.2).

Table 4.1 Resistance towards caffeine, contact angles, and XPS-measurements of PES-membranes. All XPS-results shown in At.-%.

Membrane	R (s/cm)	CA (°)	C 1s	O 1s	N 1s	Br 3p
PES orig.	11'300 ± 500	45	75.7	24.3	0	0
PES-NH_2	15'500 ± 430	30	84.4	3.9	11.7	0
PES-Init.	13'300 ± 560	75	90.6	6.9	1.4	1.2

As found by XPS-measurements, during the plasma process, 11.7% nitrogen was introduced at the membrane surface (Table 4.1). Additionally, the pore size was reduced from about 200 nm (Figure 4.2 a)) to 80 nm (Figure 4.2 b)).

XPS-measurements revealed that during the coupling of the initiator molecule, the amount of nitrogen was lowered to 1.4% (Table 4.1) and the pore size increased to 160 nm (Figure 4.2 c)). This indicates that part of the coating is removed during that coupling step. Nevertheless, enough coating was still present to couple the initiator-molecule to the surface. XPS-measurements clearly detected the Br 3p signal indicating the presence of the initiator (Table 4.1).

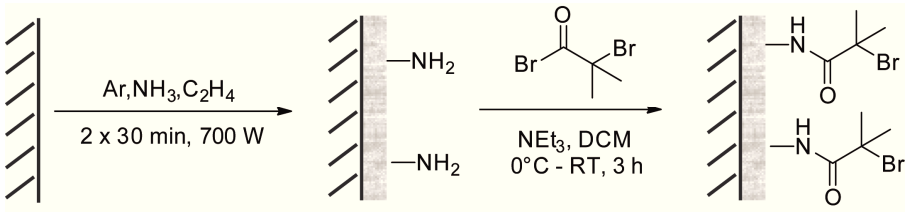

Scheme 4.2 Plasma-coating introduced amines on the PES-surface. Modification with the acid bromide of an ATRP-initiator led to an activated PES-surface. The ruled area represents PES. The grey area indicates the plasma-coating.

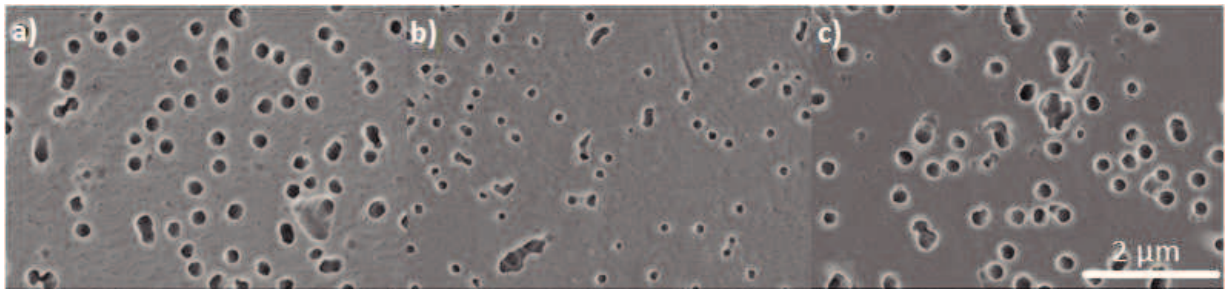

Figure 4.2 SEM-picture of a PES-membrane: **a)** DCM washed; **b)** NH_2-plasma coated; **c)** initiator coated.

IR-measurement of the original membrane showed no noteworthy signals above 1800 cm^{-1}. This indicates the absence of any C-H, N-H and O-H containing species (Figure 4.3). Especially the absence of C-H is surprising for polyester but facilitates the detection of coatings by IR-measurements.

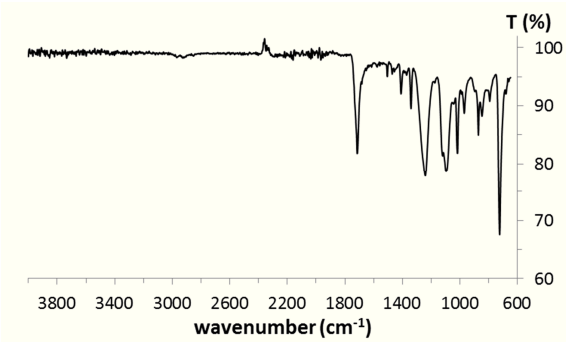

Figure 4.3 IR-spectrum of an untreated PES-membrane. No signal above 1800 cm^{-1} was detected.

Surface Polymerization

All relevant polymerization parameters for the different membranes are represented in tables. Membranes are named corresponding to the table numeration, e.g. preparation of membrane 4.3.2 can be found in table 4.3 as second entry.

First, different conditions for pure HEA were tested to find an appropriate system to perform surface induced ATRP on porous polyester. All reactions were conducted in a methanol-water mixture. Within both approaches Cu(I) bromide and chloride were tested as catalyst. Two different approaches reported in literature were compared. Approach one was to use ascorbic acid to avoid oxidation of the copper species during the reaction (Table 4.2).[4]

Table 4.2 Synthetic details for surface-induced ATRP with ascorbic acid (AscA) in methanol/water mixture. Weight gain and contact angle for the coated membranes were measured after 18 h.

	HEA (mol/L)	CuX (mmol/L)	Bipy (mmol/L)	AscA (mmol/L)	T (°C)	wt.%	CA (°)
1)	4800	CuBr 1.7	3.4	25	RT	12	60
2)	4800	CuBr 1.7	3.4	25	60	65	55
3)	4800	CuCl 1.7	3.4	25	60	33	60

Approach two was the addition of Cu(II) to the reaction mixture without addition of ascorbic acid to lower the reaction speed and thus to gain better control over the reaction (Table 4.3).[7]

Table 4.3 Synthetic details for surface-induced ATRP with $CuBr_2$ in methanol/water mixture. Weight gain for all treated membranes was measured after 18 h.

	HEA (mmol/L)	CuX (mmol/L)	Bipy (mmol/L)	$CuBr_2$(mmol/L)	T (°C)	wt.%
1)	4800	CuBr 1.7	3.4	0.2	RT	0
2)	4800	CuBr 1.7	3.4	0.2	60	0
3)	4800	CuCl 1.7	3.4	0.2	60	0

Only approaches with ascorbic acid were successful and resulted in a measurable weight gain for the treated membranes. Addition of $CuBr_2$ inhibited the polymerization reaction in the present case to such an extent that even after 18 hours no weight gain was measurable. The reaction mixture with ascorbic acid and CuBr at 60°C resulted in the highest weight gain. Therefore, this catalytic system was chosen for further investigations (Scheme 4.3).

Measuring the surface-polymerization kinetics of HEA on porous polyester resulted in a bent curve approaching a plateau after a steep increase at the beginning. This indicates that the main part of the polymerization takes place very quickly after the initiation. Most coating is built during the first hour of polymerization. The process constantly slows down during the following hours. This indicates that polymerization mechanism is not corresponding to a living polymerization (Fig. 4.4).

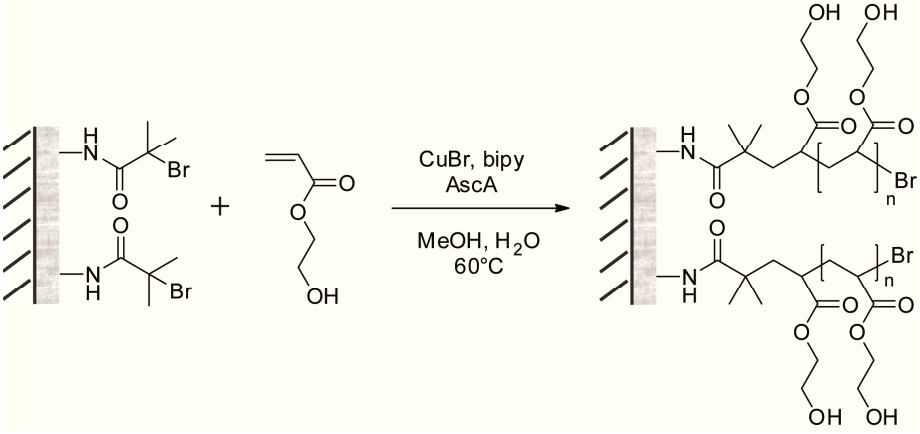

Scheme 4.3 Successful surface-induced polymerization of HEA was achieved when CuBr and ascorbic acid were used for polymerizations at 60°C. The ruled area represents the polyester. The grey area indicates the amine-containing plasma-coating that was described above.

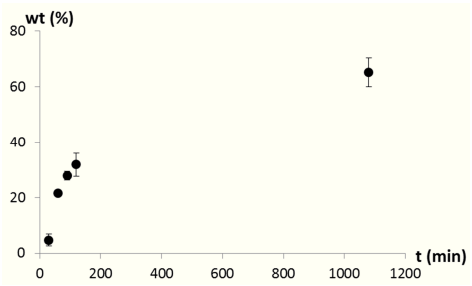

Figure 4.4 Surface-induced polymerization kinetics of HEA on PES (membrane 4.4.2).

For further optimization of the surface polymerization process, the concentration of HEA was varied (Table 4.4). The monomer concentration was found to have a disproportionately high impact on the amount of polymer that was grafted onto the surface. The amount of polymer on the surface is a critical factor concerning the porosity and the surface morphology of the membrane (Figure 4.5). If the amount of grafted polymer was too high, it was not possible to measure a caffeine flux through the membrane (e.g. for membrane 4.4.3). Additionally, determination of the surface contact angle was impossible since the membrane became bumpy.

Table 4.4 Different concentration of HEA for surface-induced ATRP with ascorbic acid. All reactions were conducted at 60°C and quenched after 18 h. Weight gain, contact angle and permeability resistance for caffeine were measured.

	HEA (mmol/L)	CuBr (mmol/L)	Bipy (mmol/L)	AscA (mmol/L)	wt.%	CA (°)	R (s/cm)
1)	3400	1.7	3.4	25	2	55	11'900 ± 340
2)	4800	1.7	3.4	25	65	55	18'700 ± 930
3)	6200	1.7	3.4	25	133	-	-

SEM-pictures of the membranes coated with three different monomer concentrations showed a clear change in morphology. Whereas the membrane coated with the lowest concentration is still porous (Figure 4.5 a)) the other two membranes showed no pores anymore at the surface. On membrane 4.4.2, a morphology starts to appear on the surface (Figure 4.5 b)) and membrane 4.4.3 is entirely coated with this structure (Figure 4.5 c)). IR-spectroscopy showed a broad peak around 3400 cm^{-1}. This peak indicates the presence of OH-groups on the membrane surface. Since this peak was never observed for uncoated membranes, this is a strong indication for the presence of a HEA coating (Figure 4.6).

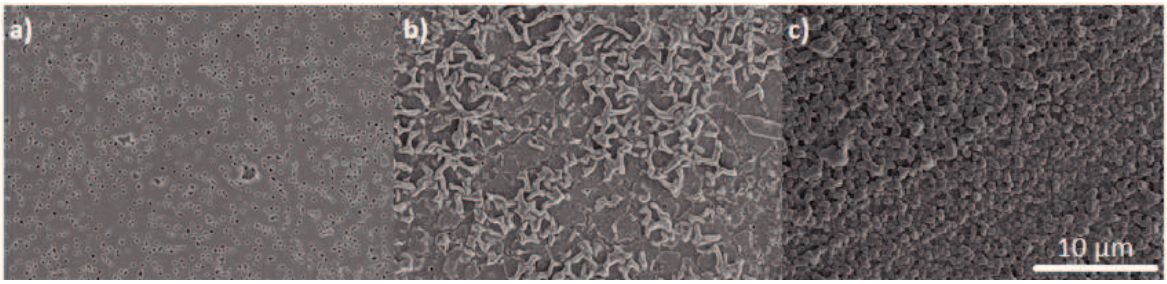

Figure 4.5 SEM-pictures of pHEA-coated PES-membranes: **a)** membrane 4.4.1; **b)** membrane 4.4.2; **c)** membrane 4.4.3.

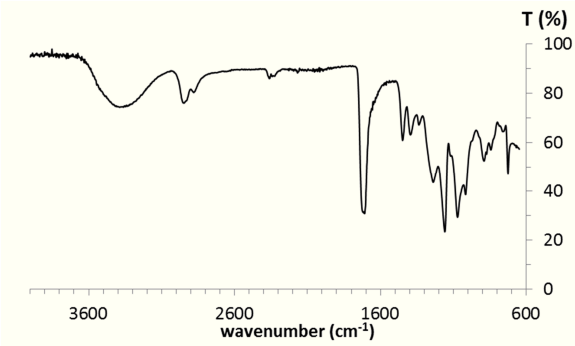

Figure 4.6 IR-spectrum of a pHEA-coated PES-membrane (membrane 4.4.3).

The same investigation on the concentration dependency of the amount of grafted polymer was performed with HEMA. Similar findings support the results from the HEA-grafting experiments. The amount of grafted polymer was again disproportionally high depending on the monomer concentration (Table 4.5). If the amount of grafted polymer was too high, the membrane became bumpy and brittle (e.g. membrane 4.5.3). Therefore it was impossible to fix these membranes in a Franz cell to measure its permeability resistance. Determination of the contact angle was meaningless since the surface was not smooth.

Table 4.5 Experimental details for surface ATRP with ascorbic acid using different HEMA-concentrations. All reactions were conducted at 60°C and quenched after 18h. Weight gain, contact angle and permeability resistance for caffeine were measured.

	HEMA (mmol/L)	CuBr (mmol/L)	Bipy (mmol/L)	AscA (mmol/L)	wt.%	CA (°)	R (s/cm)
1)	3400	1.7	3.4	25	1	60	12'100 ± 620
2)	4800	1.7	3.4	25	49	60	15'300 ± 920
3)	6200	1.7	3.4	25	189	-	-

Measuring the surface polymerization kinetics of HEMA on porous polyester resulted in a straight line. This indicates that the polymerization progresses at constant speed within the first 18 hours as a living polymerization process. Therefore, stopping the polymerization after a certain time allows dictating the amount of coating on a membrane (Figure 4.7).

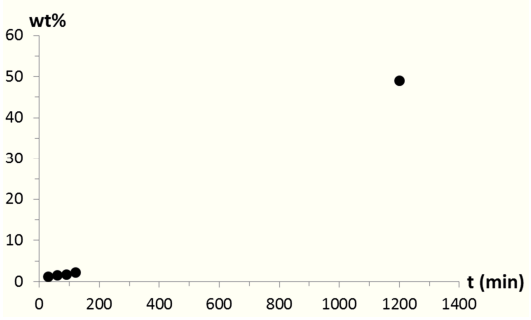

Figure 4.7 Surface polymerization kinetics of HEMA on PES (membrane 4.5.2)

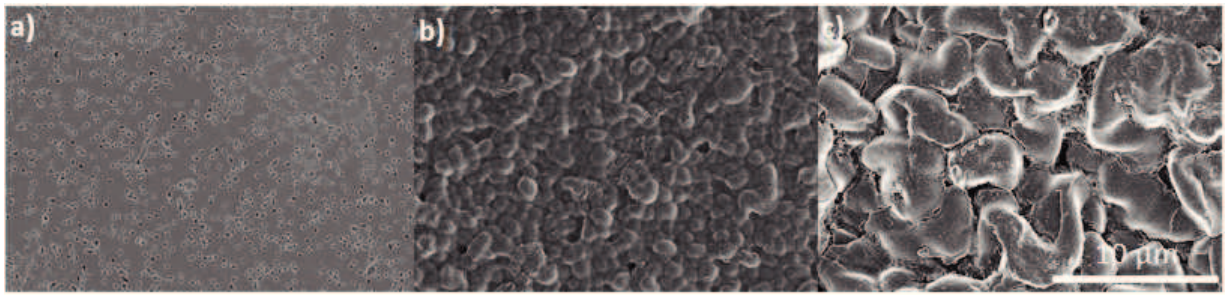

Figure 4.8 SEM-pictures of pHEMA-coated PES-membranes: **a)** membrane 4.5.1; **b)** membrane 4.5.2; **c)** membrane 4.5.3.

Comparing SEM-pictures of membranes 4.5.1, 4.5.2 and 4.5.3 shows a change in surface morphology that is connected to the monomer concentration that was used during the coating process. Membrane 4.5.1 is still porous with a flat surface (Figure 4.8 a)). Membrane 4.5.2 is entirely coated with polymer and therefore turns up to be nonporous. The polymer creates a pattern on the surface inducing a changed morphology compared to the porous membrane (Figure 4.8 b)). Membrane 4.5.3 with the most polymer coating on the surface shows again a different surface morphology. The pattern looks similar to membrane 4.5.2 but the size of the structure was increased (Figure 4.8 c)).
A side-view of membrane 4.5.2 shows that the porous membrane was still present below the coating. To measure the coating thickness in such a picture is rather impossible since it is not clear, where the coating ends and where the PES-membrane starts. Nevertheless, a rough estimation indicated that the coating was between 1 and 5 μm (Figure 4.9).

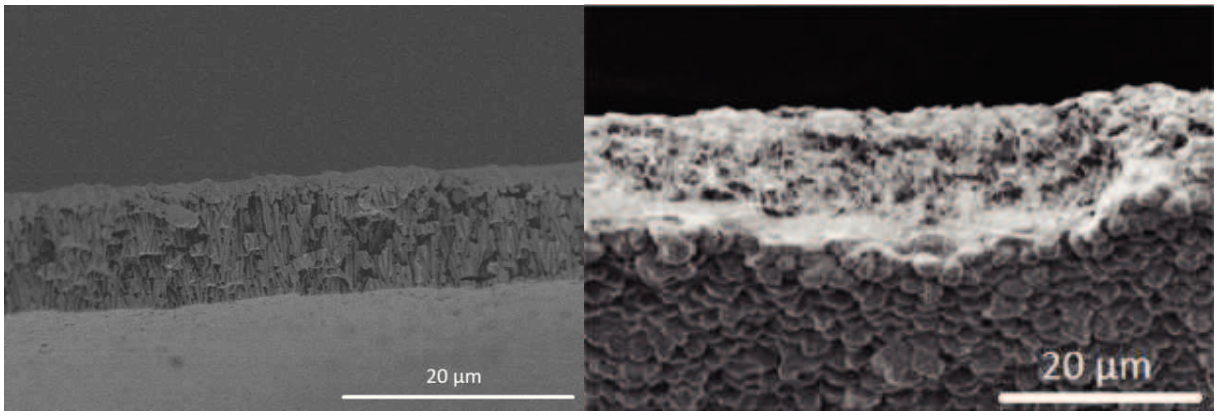

Figure 4.9 SEM side-view of membrane 4.5.2 before (left) and after (right) surface-induced ATRP.

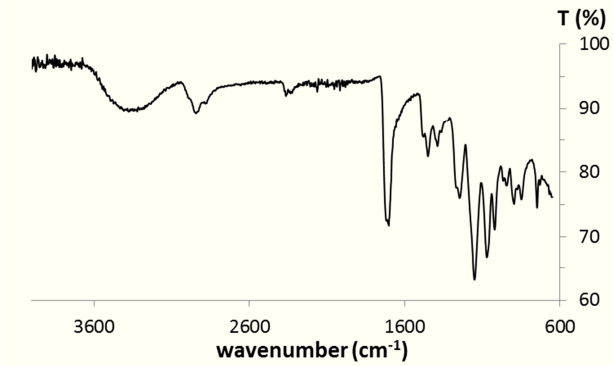

Figure 4.10 IR-spectrum of a pHEMA-coated PES-membrane (membrane 4.5.2).

IR-measurement of pHEMA coated membranes showed again a broad peak at 3400 cm^{-1} for membranes 4.5.2 and 4.5.3, indicating the presence of OH-groups (Figure 4.10). Membrane 4.5.1 showed no signal in that region. Either there was no coating or the coating was too thin to be detected.

XPS-measurements of the coated membranes showed a clear trend for the different concentrations. For the highest concentration, the same elemental composition was measured as for pure pHE(M)A. For the lowest monomer concentration, the elemental composition was similar to the one measured for the membrane with only initiator. For the intermediate monomer concentration, not the same elemental composition as for pure pHE(M)A was detected (Table 4.6). This is a surprising result, since SEM-pictures indicated a homogenous coating with a thickness beyond the measuring depth of XPS (Figure 4.8 + 4.9).

Table 4.6 XPS-measurements of differently coated PES-membranes. All results shown in At.-%.

Membrane	C 1s	O 1s	N 1s	Br 3p
PES-Init	90.6	6.9	1.4	1.2
Mem 4.4.1	87.4	10.5	2.1	0.0
Mem 4.4.2	70.2	29.0	0.8	0.0
Mem 4.4.3	64.7	35.3	0.0	0.0
HEA calc.	*62.5*	*37.5*	*0.0*	*0.0*
Mem 4.5.1	83.5	13.0	3.5	0.0
Mem 4.5.2	74.3	24.3	1.4	0.0
Mem 4.5.3	66.6	33.4	0.0	0.0
HEMA calc.	*66.7*	*33.3*	*0.0*	*0.0*

The fact that membranes produced with the highest concentration of monomer showed similar atomic composition as pure pHEA and pHEMA respectively, reveal that the formed polymer chains did not undergo side-reactions during polymerization (compare to Chapter 3, AEMA-coating).

Postmodification of HE(M)A-Coated Membranes

Only for membranes 4.4.1, 4.4.2, 4.5.1 and 4.5.2, a flux of caffeine was detected. Therefore, only these four coatings were postmodified with spiropyran to create photochromic coatings. The coated membranes were esterified in a **SP12** containing DCM-solution (Scheme 4.4).

After the postmodification process, photochromic membranes were obtained. UV-irradiation resulted in a purple coloration of the membrane. Illumination with visible light allowed discoloring the photochromic membrane (Figure 4.11).

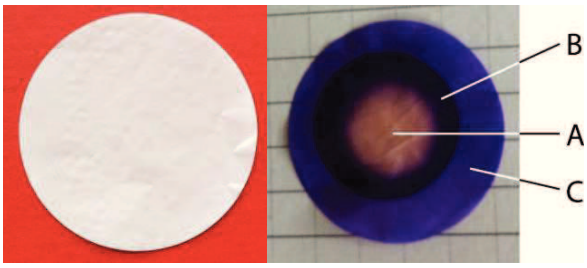

Figure 4.11 Membrane before (left) and after (right) permeability measurement: inner white circle (A) induced by visible light after the measurement; dark purple ring (B) induces by UV-irradiation during the measurement; outer purple ring (C) partially covered area during the measurement, therefore less intense colored.

Measuring the caffeine permeability for these membranes at daylight and under UV-irradiation showed the highest permeability switch for membrane 4.5.2-**SP12**, followed by membrane 4.4.2-**SP12**. It looks like an intermediate amount of coating is beneficial concerning the switch of permeability resistance (Table 4.7). If the amount of coating was too small, no or only small changes in permeability resistance was detected. If the amount of coating was too high, the membranes were no longer permeable for caffeine. For the membranes with a high amount of coating, a high amount of incorporated spiropyran was detected. A modest correlation of permeability resistance with contact angle was detected. High contact angles resulted in a high permeability resistance. However, the correlation was not clear enough to reliably predict the permeability resistance from contact angle measurements (Table 4.7).

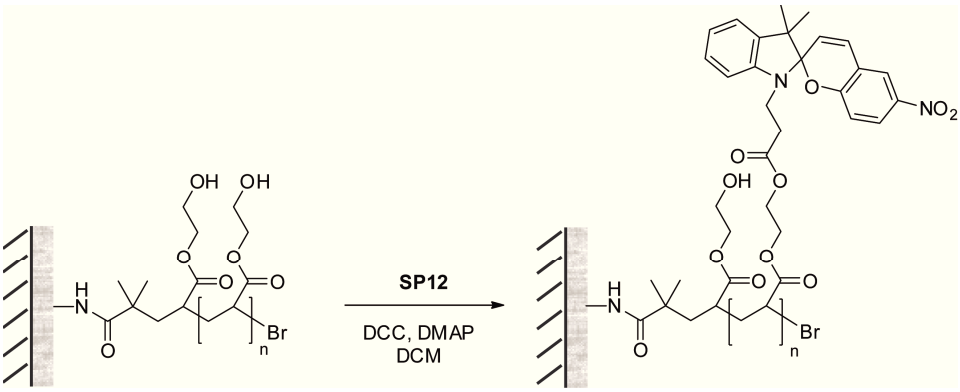

Scheme 4.4 Postmodification of pHEA-coated PES-membranes with **SP12.** The ruled area represents the polyester. The grey area indicates the amine-containing plasma-coating that was described above.

Table 4.7 Permeability resistances, contact angles, spiropyran content and λ_{max} of different postmodified PES-membranes.

Membrane	R_{DL} (s/cm)	R_{UV} (s/cm)	CA_{DL} (°)	CA_{UV} (°)	SP on Mem (wt.%)	λ_{max} (nm)
Mem 4.4.1-**SP12**	23'100 ± 750	15'400 ± 450	65	55	4.9	564
Mem 4.4.2-**SP12**	31'000 ± 3400	11'100 ± 610	85	55	12.8	543
Mem 4.5.1-**SP12**	12'000 ± 240	11'600 ± 560	60	55	0.4	590
Mem 4.5.2-**SP12**	39'000 ± 3200	13'600 ± 840	75	55	10.0	588

Contact angle measurements showed that the surface tension can be influenced by switching spiropyran from one into its other state. Under UV-irradiation the surface tension was significantly lowered compared to measurements at daylight (Table 4.7). Switching the surface tension was repeated for at least three entire cycles with recovering the initial values for all photochromic coatings (Figure 4.12).

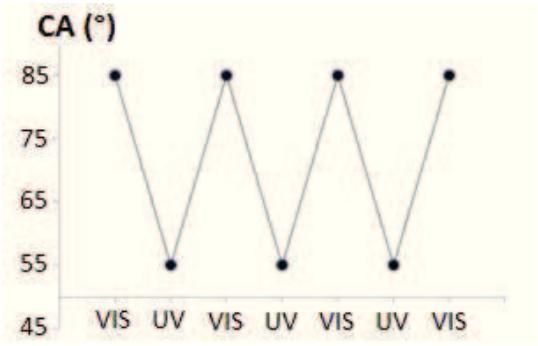

Figure 4.12 Contact angle measurements of a postmodified, pHEA-coated PES-membrane (membrane 4.4.2-**SP12**) under UV-irradiation and at daylight.

Copolymerization of HE(M)A and Spiropyran on Membranes Including Comparison with Postmodified Membranes

A one-step copolymerization-approach was successfully developed. Instead of a polymerization process followed by an esterification step, a monomeric derivative of spiropyran was added to the polymerization process (Scheme 4.5). **SP14** was used for copolymerization with HEMA whereas HEA was copolymerized with **SP16**.

For the polymerization process, the same conditions as for pure HE(M)A were applied. A monomer concentration of 4.8 M was chosen, since this concentration gave the most promising results for postmodification as showed above. Weight gain was found to be 77% for HEA-SP copolymerization where as a weight gain of 45% was found for HEMA-SP copolymerization. These values are slightly lower than the values found for the surface-induced polymerization of HE(M)A alone, used in the postmodification approach (Table 4.8). Since spiropyran is a steric demanding monomer that can also interact with radicals, it is not surprising that the degree of polymerization is somewhat lower for the copolymerization than for homopolymerization of HEA and HEMA, respectively.

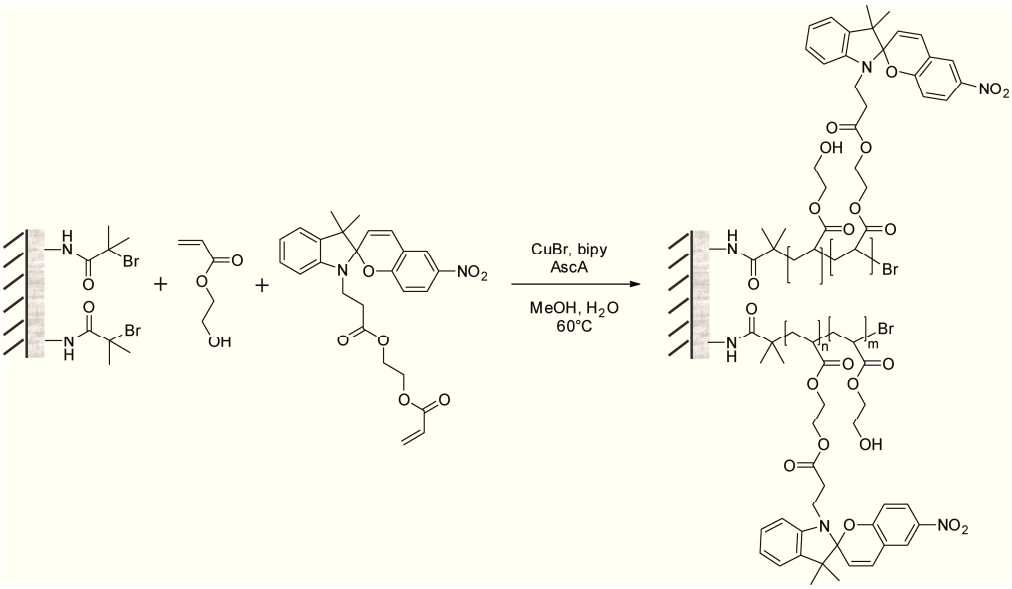

Scheme 4.5 Surface-induced ATRP of HEA and **SP16** on a polyester surface. The ruled area represents the polyester. The grey layer represents the amine-containing plasma-coating that was described above.

Table 4.8 Comparison of photochromic membranes produced in a postmodification (**1** + **3**) or in a copolymerization (**2** + **4**) process. All reactions were conducted at 60°C and quenched after 18 h. Weight-gains were calculated after postmodification. Reaction conditions are only shown for the polymerization process. Postmodification was performed as described above.

	HE(M)A (mmol/L)	CuBr (mmol/L)	Bipy (mmol/L)	AscA (mmol/L)	SP (mmol/L)	wt.%
1)	HEA; 4800	1.7	3.4	25	0	89
2)	HEA; 4800	1.7	3.4	25	8.5 (**SP16**)	77
3)	HEMA; 4800	1.7	3.4	25	0	54
4)	HEMA; 4800	1.7	3.4	25	8.5 (**SP14**)	45

Other than the homopolymerization of HEA, the polymerization kinetics of HEA mixed with **SP16** was linear and had thus a living character. This indicated a constant speed of polymerization at least for the first 18 hours. **SP16** slows down the polymerization process during the first hours compared to neat HEA-polymerization but keeps polymerization speed constant during the later state of the process (Figure 4.13 compared to Figure 4.4).

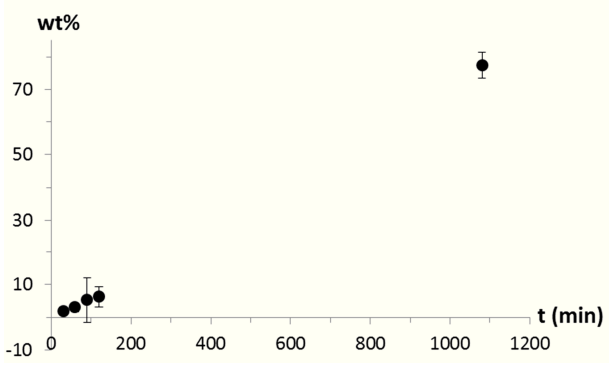

Figure 4.13 Surface polymerization kinetics of HEA with **SP14** on PES (membrane 4.8.2).

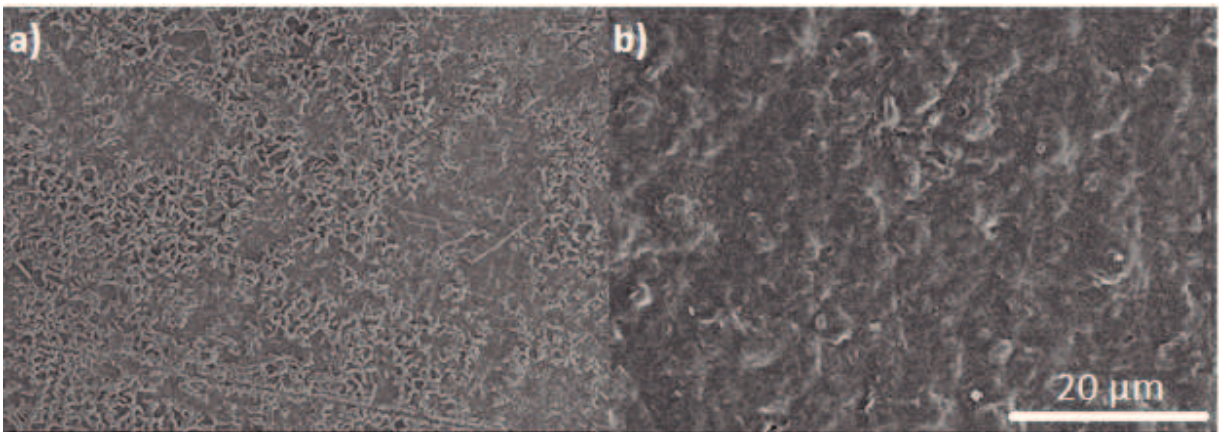

Figure 4.14 SEM picture of pHEA-coated PES: **a)** after homopolymerization (membrane 4.4.2); **b)** after copolymerization with **SP14** (membrane 4.8.2).

Comparing SEM pictures of a postmodified and a copolymerized HEA-coated PES-membrane showed a significant change of surface topography in both cases compared to the original PES-membrane. The structured surface observed for the polymerization of pure HEA was not observed when HEA was copolymerized with **SP16** on a porous PES-surface (Figure 4.14). In both cases, the pores of the membrane were covered by the formed coating.
Comparison of the permeability measurements of postmodified and copolymerized membranes showed that postmodification leads to a more pronounced switching of the permeability resistance. Copolymerization of HEA and **SP16** resulted in no switch at all, whereas copolymerization of HEMA and **SP14** resulted in a minimal switch of the permeability resistance. Also the changes concerning the contact angle were significantly lower for copolymerized membranes than for postmodified ones. Additionally, less spiropyran was incorporated during the copolymerization process than during the postmodification (Table 4.9).

Table 4.9 Comparison of permeability resistances, contact angles, spiropyran content and λ_{max} of postmodified and copolymerized PES-membranes.

	R_{DL} (s/cm)	R_{UV} (s/cm)	CA_{DL} (°)	CA_{UV} (°)	SP on Mem (wt.%)	λ_{max} (nm)
Mem 4.8.1 (PM)	31'000 ± 3400	11'100 ± 610	85	55	12.8	543
Mem 4.8.2 (CP)	14'600 ± 690	14'900 ± 300	65	50	5.5	557
Mem 4.8.3 (PM)	39'000 ± 3200	13'600 ± 840	75	55	10.0	588
Mem. 4.8.4 (CP)	18'400 ± 670	16'700 ± 400	45	40	4.2	580

The fact that for membranes with entirely covered pores, the permeability resistance was reduced under UV-irradiation revealed that the caffeine transport took place through the swollen pHEA-SP, respectively pHEMA-SP matrix.

Solid state UV-Vis measurements

For the final application of the membrane, it is important to have a product that can be used for several switching cycles. Therefore, the stability towards UV-irradiation of the produced membranes was measured.

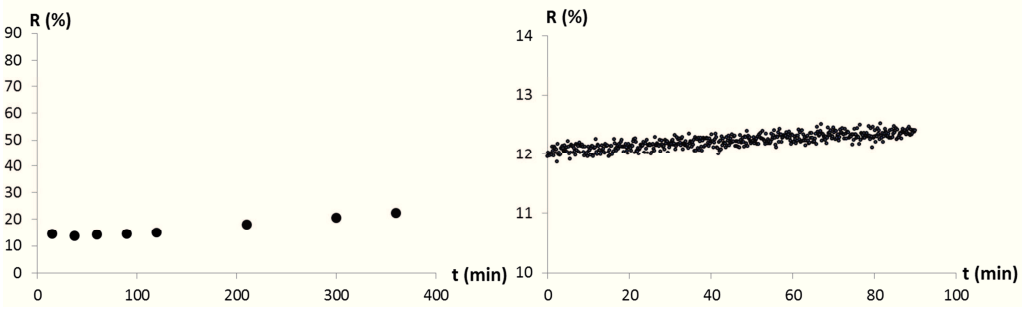

Figure 4.15 Fading-rate measurement (left) and ring-closing reaction kinetics measurement under dark conditions (right) of postmodified pHEA/**SP12**-coated PES (membrane 4.4.2-**SP12**). Reflection (R in %) of the membrane at λ_{max} (see Table 4.10) was measured over time for both measurements.

It would be a possibility to prolong the membrane's lifespan by illuminating the membrane with pulsed UV-light. The longer the timespan between two UV-pulses can be chosen, the longer the membrane will survive. Long periods between the pulses are only reasonable when the ring-closing reaction of the concerning spiropyran is slow, however. Therefore, the ring-closing kinetics was measured under dark conditions.

Postmodified membranes showed a minimal fading with a linear fading rate over 6 hours and constant ring closing kinetics over 90 minutes (Figure 4.15). In contrast, the copolymerized membranes showed a high fading rate approaching a plateau already after 3 hours. Ring-closing kinetics was also found to be much faster for copolymerized coatings. (Figure 4.16). The higher stability towards UV-irradiation of postmodified membranes corroborated the theory, that the way the spiropyran was incorporated into the polymer matrix, is crucial.

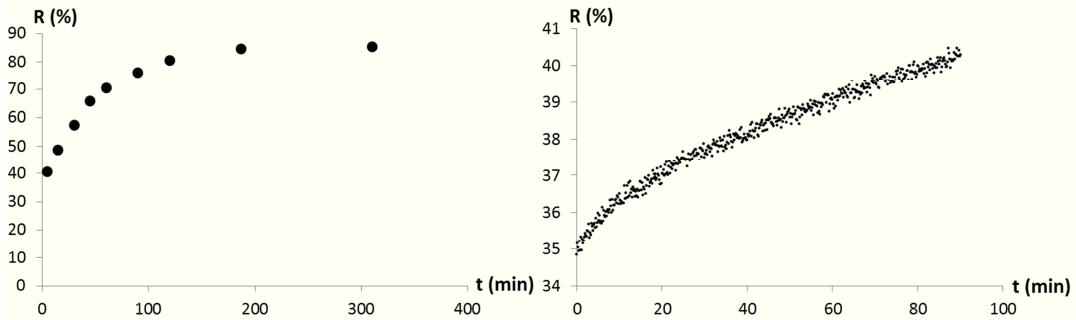

Figure 4.16 Fading-rate measurement (left) and ring-closing reaction kinetics measurement under dark conditions (right) of copolymerized pHEA/**SP14**-coated PES (membrane 4.8.2). Reflection (R in %) of the membrane at λ_{max} (see Table 4.10) was measured over time for both measurements.

In general, pHEMA coatings showed lower fading rates compared to similarly produced pHEA-coatings. Lowest fading rate combined with slowest ring closing kinetics was found for pHEMA-coated, postmodified membrane 4.7.4. Very similar results were found for pHEA-coated, postmodified membrane 4.7.2 (Table 4.10).

The fading rates and the ring-closing kinetics of postmodified samples strongly depended on the amount of coating. The more coating there was on a membrane, the lower fading rates and the slower kinetics were found. Therefore, it can be concluded that there is an interaction of the polymer with spiropyran in such a manner, that the molecular switch was stabilized in its MC-state and towards UV-irradiation. The nature of the involved interactions is unclear at the moment. More and probably more complex experiments have to be performed to find solid explanations for the observed phenomena.

Table 4.10 Ring-closing reaction kinetics, fading rate under UV-irradiation and λ_{max} of the different photochromic PES-membranes.

Sample	Fading rate (ΔR%/min)	Ring closing kinetics (ΔR%/min)	λ_{max} (nm)
Mem 4.4.1-**SP12** (PM, HEA)	1.56	0.09	564
Mem 4.4.2-**SP12** (PM, HEA)	0.03	0.01	543
Mem 4.5.1-**SP12** (PM, HEMA)	0.72	0.04	590
Mem 4.5.2-**SP12** (PM, HEMA)	0.03	0.01	588
Mem 4.8.2 (CP, HEA)	0.62	0.05	557
Mem 4.8.4 (CP, HEMA)	0.45	0.15	580

4.4. CONCLUSION AND OUTLOOK

Development of surface induced polymerization on track-etched polyester membranes was successfully achieved for HEA and HEMA as monomer by using an ARGET ATRP process. Other ATRP-approaches with the addition of Cu(II) and without reducing species were not suitable for this system. The monomer concentration had a high impact on the amount of grafted coating. Esterification of the polymeric side chains with spiropyran resulted in photochromic coatings. Copolymerization of monomeric spiropyran with either HEA or HEMA, applying identical conditions as for pure HE(M)A resulted as well in photochromic membranes. However, the additional spiropyran monomer had an influence on the polymerization kinetics. For the HEA-polymerization, the addition of the spiropyran acrylate improved the living character of the polymerization.

The formed photochromic membranes changed their caffeine permeability resistances triggered by light. Postmodified membranes showed higher switching combined with lower fading rates and slower ring-closing reaction. Additionally, postmodification eases the analysis of the coating. A homopolymer was created during the first reaction step. Introduction of the photochromic molecular switch followed in a second step. This allowed determination of the incorporated amounts by weighing the samples after each step. Usually, pHEMA coated membranes showed better results regarding switching potential than pHEA coated membranes.

Generally, it was found that an intermediate amount of coating is beneficial for a well operating membrane. If the coating became too thick, no permeability was anymore measurable. On the other hand, if the coating was too thin, no change in permeability was detected. Since the grafted polymer-coating entirely covered the pores in the best switching membranes, it was assumed that non-porous membranes were created, with a similar diffusion transport mechanism as the membranes discussed in the following chapter. A good control over the amount of grafted polymer revealed to be essential. Therefore, a living character of the polymerization is necessary, which for the homopolymerization was observed with HEMA as monomer. In contrast, HEA did not show a real living polymerization character. Up to now, only three different monomer concentrations have been compared. Since it was found that monomer concentration has a big impact on the amount of coating that was grafted to the membrane, a detailed optimization of the polymerization process regarding monomer concentration still has to be done. It would be interesting to see if it is possible to tune the polymer length such that when stretched out, they would just close the pores, while when contracted, the pores would open. This change could be triggered by changing from the polar merocyanine state to the less polar spiropyran state. In such a case, a reversed permeability change would be expected.

4.5. REFERENCES

1. H. Kakwere and S. Perrier, *Polymer Chemistry*, 2011, **2**, 270-288.
2. W. Huang, J.-B. Kim, M. L. Bruening and G. L. Baker, *Macromolecules*, 2002, **35**, 1175-1179.
3. W. A. Braunecker and K. Matyjaszewski, *Progress in Polymer Science*, 2007, **32**, 93-146.
4. S. M. Paterson, D. H. Brown, T. V. Chirila, I. Keen, A. K. Whittaker and M. V. Baker, *Journal of Polymer Science Part A: Polymer Chemistry*, 2010, **48**, 4084-4092.
5. K. Matyjaszewski, *Progress in Polymer Science*, 2005, **30**, 858-875.
6. S. Coca, C. B. Jasieczek, K. L. Beers and K. Matyjaszewski, *Journal of Polymer Science Part A: Polymer Chemistry*, 1998, **36**, 1417-1424.
7. K. L. Beers, S. Boo, S. G. Gaynor and K. Matyjaszewski, *Macromolecules*, 1999, **32**, 5772-5776.
8. X. S. Wang and S. P. Armes, *Macromolecules*, 2000, **33**, 6640-6647.
9. K. L. Robinson, M. A. Khan, M. V. de Paz Báñez, X. S. Wang and S. P. Armes, *Macromolecules*, 2001, **34**, 3155-3158.
10. X. S. Wang, S. F. Lascelles, R. A. Jackson and S. P. Armes, *Chemical Communications*, 1999, **0**, 1817-1818.
11. A. M. Balachandra, G. L. Baker and M. L. Bruening, *Journal of Membrane Science*, 2003, **227**, 1-14.
12. E. L. Brantley and G. K. Jennings, *Macromolecules*, 2004, **37**, 1476-1483.
13. K. Matyjaszewski, *Macromolecules*, 2012, **45**, 4015-4039.
14. C. R. Becer, R. Hoogenboom, D. Fournier and U. S. Schubert, *Macromolecular Rapid Communications*, 2007, **28**, 1161-1166.
15. H. Zhang, B. Klumperman, W. Ming, H. Fischer and R. van der Linde, *Macromolecules*, 2001, **34**, 6169-6173.
16. W. Tang, N. V. Tsarevsky and K. Matyjaszewski, *Journal of the American Chemical Society*, 2006, **128**, 1598-1604.
17. J. K. Oh, H. Dong, R. Zhang, K. Matyjaszewski and H. Schlaad, *Journal of Polymer Science Part A: Polymer Chemistry*, 2007, **45**, 4764-4772.
18. K. Min, S. Yu, H.-i. Lee, L. Mueller, S. S. Sheiko and K. Matyjaszewski, *Macromolecules*, 2007, **40**, 6557-6563.
19. A. Friebe and M. Ulbricht, *Langmuir*, 2007, **23**, 10316-10322.
20. R. Adelmann, P. Mela, M. O. Gallyamov, H. Keul and M. Möller, *Journal of Polymer Science Part A: Polymer Chemistry*, 2009, **47**, 1274-1283.
21. K. H. Fries, J. D. Driskell, S. Samanta and J. Locklin, *Analytical Chemistry*, 2010, **82**, 3306-3314.
22. N. Shao, J. Y. Jin, S. M. Cheung, R. H. Yang, W. H. Chan and T. Mo, *Angewandte Chemie*, 2006, **118**, 5066-5070.
23. C. Ventura, R. Byrne, F. Audouin and A. Heise, *Journal of Polymer Science Part A: Polymer Chemistry*, 2011, **49**, 3455-3463.
24. Q. Jin, G. Liu and J. Ji, *Journal of Polymer Science Part A: Polymer Chemistry*, 2010, **48**, 2855-2861.
25. S. Guimond, U. Schütz, B. Hanselmann, E. Körner and D. Hegemann, *Surface and Coatings Technology*, 2011, **205, Supplement 2**, S447-S450.
26. D. Hegemann, E. Körner, N. Blanchard, M. Drabik and S. Guimond, *Applied Pysics Ltters*, 2012, **101**, 211603.
27. R. K. Dieter, L. A. Silks, J. A. Fishpaugh and M. E. Kastner, *Journal of the American Chemical Society*, 1985, **107**, 4679-4692.
28. J. H. Ramm, in *Mathematisch-Naturwissenschafltiches Fakultät*, University of Zurich, Zürich, 210.

5. NONPOROUS PHOTOCHROMIC MEMBRANES CONSISTING OF AMPHIPHILIC CONETWORKS

5.1 INTRODUCTION

Working with porous substrate membranes and coatings allowed only limited adaption of the basic permeability resistance. Therefore, developing nonporous membranes with adjustable basic permeability resistances was the aim of the following investigation. The permeability resistance of amphiphilic conetworks was expected to be tunable by changing the thickness and/or the composition of the membrane.[1]

Amphiphilic conetworks are defined as two-component networks of covalently interconnected hydrophilic and hydrophobic phases of co-continuous morphology (Scheme 5.1); as such they swell both in water and hydrocarbons, and respond to changes in the surrounding by morphological isomerization.[2-4]

To get a functional amphiphilic conetwork, it is important that hydrophilic as well as hydrophobic components are in continuous phases. If one component is dispersed in the other one, swelling capability of the dispersed phase would strongly be lowered or totally vanished. If for example the hydrophobic phase would not be continuous, no or only little swelling in hexane would be detectable since the hydrophobic part would be isolated from the solvent by the continuous, hydrophilic domains.[2]

There are three main routes to prepare amphiphilic conetworks[2, 4]: (a) random free radical copolymerization of monomers with bitelechelic macromolecules [1, 5] (Scheme 5.2 1)); (b) Ionic sequential living polymerization[6, 7] (Scheme 5.2 2)); (c) chemical combination of hydrophilic and hydrophobic prepolymers (Scheme 5.2 3)).[8, 9]

To avoid phase separation of the incompatible hydrophilic and hydrophobic precursors before crosslinking of the material, several strategies are possible. Using an amphiphilic solvent (e.g. THF) is one possibility. It allows the easy mixing of the precursors to achieve a homogeneous mixture. Another strategy that was applied sometimes is to start with a protected monomer. [2, 10] If the protecting group alters the hydrophilicity of the monomer to such an extent that it can be mixed with the second monomer, no further mixing-strategy is needed.

Scheme 5.1 Schematic representation of an amphiphilic conetwork. bright: hydrophobic phase; dark: hydrophilic phase. Both phases are continuous and connected to the surface.[2]

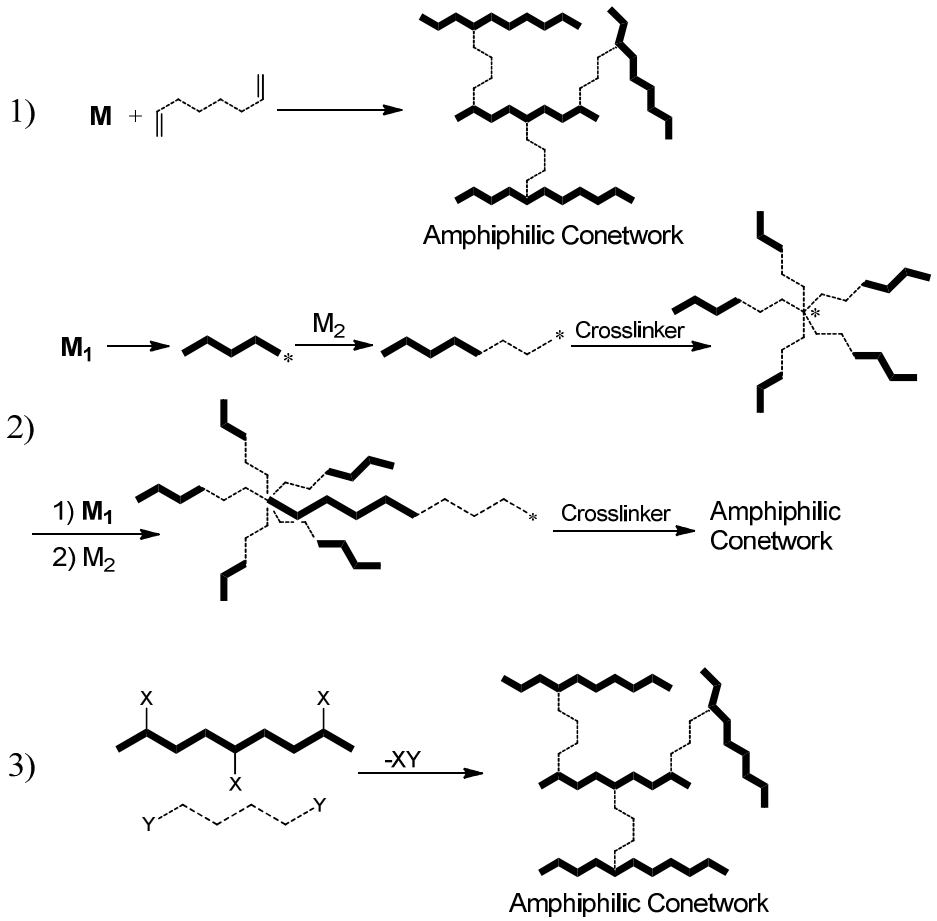

Scheme 5.2 Main routes for the production of amphiphilic conetworks: **1)** random free radical copolymerization; **2)** ionic sequential living polymerization; **3)** chemical combination of prepolymers.

2-((trimethylsilyl)oxy)ethyl acrylate (TMS-HEA) is known to be miscible with bitelechelic poly(dimethylsiloxane) (PDMS*). The protection-group lowers the hydrophilicity of HEA such that it becomes well miscible with PDMS*. Since TMS-HEA as well as PDMS* are liquid at room temperature, no additional solvent is needed. After the polymerization and crosslinking process, the TMS-group can easily and quantitatively be removed to obtain an amphiphilic conetwork.[1]

Amphiphilic conetworks based on HEA and the macro-monomer PDMS* are a promising class of materials for sensors, phase transition reactions or nano-reactors.[1, 10-13]

Nevertheless, only a few groups have published on such materials up to now. We report for the first time on the incorporation of light-responsive molecules into HEA/PDMS* based amphiphilic conetworks to create photochromic membranes. As discussed in the previous two chapters, we compared a copolymerization and a postmodification process. Preforming of a non-photochromic amphiphilic conetwork allows an additional postmodification step due to the reactive free alcohol groups. Copolymerization of all components in a single step involves the potential risk that spiropyran disturbs or inhibits the polymerization process.

5.2 EXPERIMENTAL

Materials and general methods

Microscope glass slides from Thermo Scientific were used as support and cover for the membrane production. Self-adhesive tape (Tesafilm universal, transparent) was used as spacer unit between the two glass slides. 2-((trimethylsilyl))oxy)ethyl acrylate (TMS-HEA, 97%) and polydimethyl siloxane – methacryloxy propyl terminated (PDMS*, 48 to 75 monomer units) were purchased from ABCR. TMS-HEA was distilled under reduced pressure before usage and stored in the freezer for no more than one month. Irgacure 651® and Irgacure 819® were provided by *BASF*. N,N-Dicyclohexylcarbodiimide (DCC, 99%), dimethyl aminopyridine (DMAP, 99%), *tert*-butylmethylether (TBME, 98%) and 2-butanone (MEK, 99%) were obtained from Sigma Aldrich. Tetrahydrofuran (THF, analytical grade) was purchased from Fisher Chemicals. Hexane (Hx, 99%) was obtained from Biosolve. Caffeine (reagent plus) and N,N-dimethylformamid (DMF, purum) were purchased from Fluka. Spiropyrans were synthesized and named according to Chapter 2. The relevant structures for this chapter can be seen in Figure 5.1.

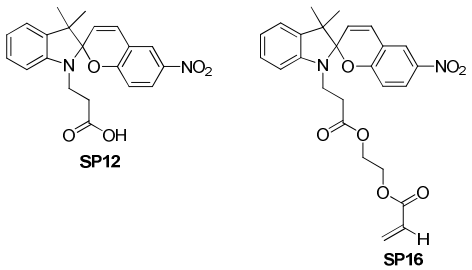

Figure 5.1 Used photochromic spiropyrans for the different amphiphilic conetworks.

All chemicals, unless stated otherwise, were used as delivered without further purification. Distilled water from the in-house supply was used unless stated otherwise. UV-Vis measurements of all liquid samples were performed on a Varian 50Bio/50MPR. For weighing, a Mettler Toledo AB204-S and a Mettler ME30 were used. IR measurements were performed on a Bruker ALPHA FT-IR spectrometer. Scanning electron Microscopy (SEM) pictures were recorded on a Hitachi S4800. All SEM-samples were coated with a gold layer of about 3 nm. X-ray photoelectron spectroscopy (XPS) was performed on a PHI 5600 spectrometer. Profilometric measurements were performed on a Detak 150 from *Vecco*.

Preparation of amphiphilic conetwork

Mold: The thickness of the membrane was adjusted by the number of tesa film stripes which were stuck on each other as spacers (Scheme 5.3). Each stripe is about 50 μm thick. Since the spacer was built up of four layers of tape, membranes with a thickness of 200 μm were formed.

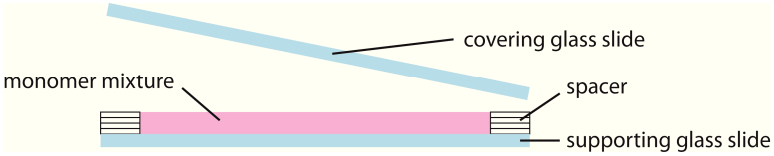

Scheme 5.3 Mold for the preparation of membranes made of amphiphilic conetworks.

Network without SP: After premixing TMS-HEA with Irgacure 651, PDMS* was added and the mixture was vortexed for 5 minutes. The prepared supporting glass slide was generously soused with monomer solution. Then the system was covered with a second glass. Illumination with UV-light (366 nm, 80 W/m^2) initiated the polymerization process. The membrane was illuminated three times for one minute from both sides. After that, the slides were dunked into a mixture of 100 mL THF and 100 mL water, slightly acidified with 25 μL aqueous HCl. After 12 hours the membrane was removed from the bath and stored in pure water. Two different ratios of TMS-HEA to PDMS* were produced as can be seen in Table 5.1.

Table 5.1: Ratio of HEA, PDMS* and photo-initiator for postmodification (PM) approaches.

Network HEA/PDMS (wt.%)	TMS-HEA (g/mmol)	PDMS* (g/mmol)	Irgacure 651 (mmol)
70/30	3.41 / 36.3	1.46 / 0.3	0.09
50/50	2.41 / 25.6	2.41 / 0.5	0.09

Network with SP: TMS-HEA was premixed with **SP16**. Afterwards, PDMS* was added and shaken vigorously for one minute. Under red light, Irgacure 819 was added and the mixture was again shaken vigorously for 5 minutes. The prepared supporting glass slide was generously soused with monomer solution. Then the system was covered with a second glass. After that, white light (500 W bulb) was turned on and after irradiating the membrane for 20 minutes from each side, the slides were dunked into a mixture of THF and water (50/50 vol%). After 12 hours, the membrane were removed from the glass slides and stored in water. Three different ratios of TMS-HEA to PDMS* were used to produce such membranes (Table 5.2).

Table 5.2: Ratio of HEA, PDMS* and photo-initiator for copolymerization (CP) approaches.

Network HEA/PDMS (wt.%)	TMS-HEA (g/mmol)	PDMS* (g/mmol)	Irgacure 819 (mmol)	**SP16** (mmol)
70/30	3.41 / 36.3	1.46 / 0.3	0.09	0.21
60/40	2.91 / 30.9	1.94 / 0.4	0.09	0.21
50/50	2.41 / 25.6	2.41 / 0.5	0.09	0.21

Post-Modification

A round-bottom flask was equipped with a stirrer and a protecting grid. The flask was dried under reduced pressure with a heat gun and flooded with argon. **SP12** (100 mg, 0.27 mmol) DCC (55 mg, 0.27 mmol), DMAP (16 mg, 0.14 mmol) and 40 mL DMF were added to the flask. A membrane

without SP that had been stored in DMF for at least 4 hours was added and the whole mixture was gently stirred at room temperature for 12 hours.

Permeability

All measurements were performed in a Franz diffusion-cell purchased from SES Analyse Systeme with a receptor volume of 12.0 mL and an orifice area of 1.77 cm^2. Mass transfer rates of caffeine were measured under UV irradiation (366 nm, 15 W/m^2) and at daylight. After filling the receptor chamber with water (12.0 mL), the membrane was fixed in the diffusion cell. The donor chamber was charged with a caffeine solution (280 mM; 3.0 mL). Samples (200 μL) were collected from the receptor part of the cell after 1, 2, 3, 4, 5, 6, 7 8, 9, 10, 11, 12 and 13 hours. The caffeine concentrations of these samples were assigned by measuring its UV absorption at 293 nm. Resistance R (in s/cm) of a membrane was calculated according to Fick's law using the formula

$$R = \frac{\Delta c}{F} \quad (1)$$

where Δc represents the difference of caffeine concentration comparing the donor compartment with the receptor part of the used franz cell. Δc was assumed to be constant over the time frame of the measurement. F was the molecular flux in amount per time per area. Permeability measurements for all treated membranes were performed directly after the production. All membranes were stored in water to precondition the membranes for the permeability measurements.

Contact angle

All measurements were performed on a Krüss G10A. The membrane – fixed with a standard tape if necessary – was positioned on a metal O-ring. A drop of nanopure water (3.3 µL) was positioned on that part of the membrane surface, which was not in contact with the O-ring. To measure the impact of switching spiropyran on the surface tension of the membrane, the CA was measured first at day light. Then the membrane was illuminated with UV-light (366 nm, 80W/m^2) for 1 minute and the contact angle was measured again.

Swelling of membranes

All dimensions were callipered with an *Antichoc 05.10008* from *Tesa*. A membrane was dried for one day in the desiccator over molecular sieves. Afterwards, its volume (V_0) was determined by measuring the side lengths and the thickness. Then the membrane was placed into water or hexane for 1 h and the volume (V_1) was measured again. For measuring the impact of the MC state on the swelling behavior, a membrane was illuminated with UV-light (366 nm, 80 W/m^2) for 1 minute before swelling in water. Each measurement was repeated three times. The volumetric degree of swelling S was calculated by using the following formula:

$$S = \frac{V_1}{V_0} \quad (2)$$

IR measurements

First, the surface of the membrane was measured by standard measuring procedure. Then the membrane was frozen with liquid nitrogen and pestled to a powder. This powder was measured again to obtain information about the inner face of the membrane.

AFM measurements

The measurements were performed on a Veeco Enviroscope with a Vistaprobes tip (FMR-25, 3 N/m, 56 kHZ). All measurements were performed in tapping mode.

Solid state UV-Vis measurements

All measurements were performed on a Lambda 9 in the transition mode. UV illumination was always at 366 nm with an intensity of 80 W/m^2. The membrane itself, stored at daylight, was used for the base line measurements. After illuminating the membrane for 1 minute with UV light (80 W/m^2, 366 nm), the spectrum of the membrane was measured and the maximal absorbance was detected. The membrane was then illuminated with UV-light for five more minutes. Afterwards, the absorption at the assigned maximum was measured over a time span of 90 minutes to obtain information about ring-closing kinetics of the spiro-compounds under dark conditions at room temperature. Subsequently, the membrane was illuminated for 5 hours with UV-light. After 15, 30, 45, 60, 90, 120, 180 and 300 minutes, the absorption at the assigned maximum was measured to obtain information about the speed of decomposition of the spiro-compounds under UV-irradiation. Since fading and ring closing reaction did not follow a simple reaction mechanism, a linear fit was applied as a rough approximation. For fading rates, two linear fits for the two domains were applied. For ring closing rates, all measurements between minute 20 and 40 were considered for the estimation of the reaction speed.

Amount spiropyran on the membrane

When **SP16** was copolymerized with the network, the amount of leaking spiropyran was analyzed. Therefore, the THF/water bath, in which the membrane was stored after production, was collected and the solvent was removed. The residual material was analyzed using ^{1}H NMR spectroscopy. When **SP12** was introduced in a postmodification step, the weight of the dried membrane was measured before and after the modification. Additionally, the amount of spiropyran was estimated for both approaches by dunking a membrane in a 1 M NaOH-solution. It was stirred for 48 hours and the absorption of the resulting solution containing 2-hydroxy-5-nitrobenzaldehyde (decomposition product of spiropyran) was measured at 389 nm (ε = 10700 M^{-1}cm^{-1}).[14]

5.3 RESULTS AND DISCUSSION

Changing the thickness of the amphiphilic conetwork was only possible in a very limited range. If the membrane was too thin, the mechanical stability became very low and the handling of the membrane was extremely difficult. If membrane thickness was chosen to high, phase separation occurred.[1]

Creating photochromic membranes consisting of an amphiphilic conetwork was achieved with a postmodification as well as a copolymerization process.

For the postmodification approach, an amphiphilic conetwork was created according to literature.[1] In a postmodification step, the free alcohols of HEA side-chains were esterified with the carboxylic acid functionality of **SP12** (Scheme 5.4).

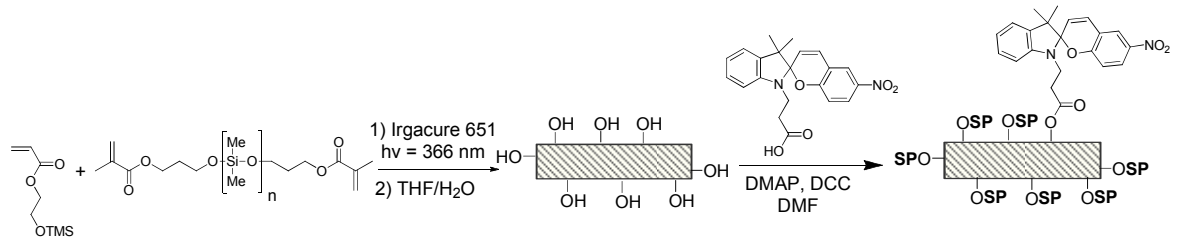

Scheme 5.4 Creation of an amphiphilic network followed by postmodification with **SP12** via esterification. The ruled area represents the amphiphilic conetwork.

The second approach was the copolymerization of spiropyran into the amphiphilic conetwork. Therefore, monomeric **SP16** was mixed with HEA and PDMS* before polymerization was initiated. The molecule (Irgacure 651) used in the previous approach to initiate the polymerization process, absorbs in the same UV-region as **SP12**. Thus, when **SP12** was in the monomer mixture, polymerization did not properly proceed. Subsequently, initiation of the polymerization process had to be promoted by Irgacure 819 (Scheme 5.5). Irgacure 819 creates radicals when irradiated with blue light. Therefore, preparation of the samples had to be performed under red light.

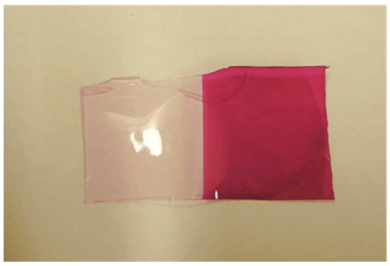

Figure 5.2 Color change of a postmodified amphiphilic network after illumination with white light (left) and after UV-irradiation (right).

The postmodified membranes were light-red at daylight. Illumination with white light led to decoloration. Irradiation with UV-light led to a strongly red-colored membrane (Figure 5.2). Copolymerized membranes were redder at daylight but showed similar behavior under white-light and UV-irradiation as the postmodified membranes.

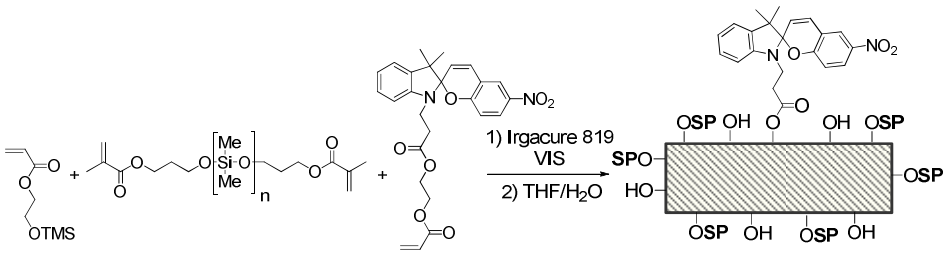

Scheme 5.5 Copolymerization of TMS-HEA, PDMS* and **SP16** led to a photochromic amphiphilic conetwork. The ruled area represents the amphiphilic conetwork.

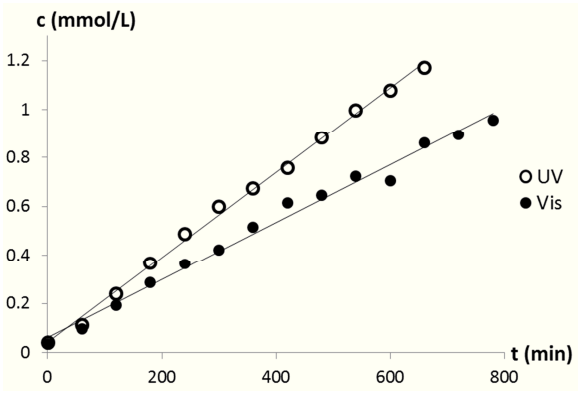

Figure 5.3 Caffeine permeability measured in a Franz cell at daylight and under UV-irradiation (membrane CP 60/40).

Measuring the contact angles of these photochromic membranes was not meaningful since the membranes started to swell when in contact to water droplets. The contact angle changed therefore over time. Nevertheless, a rough estimation of the contact angle showed no or only very little change of surface tension comparing the membrane at daylight and under UV-irradiation. However, a clear trend was observed for water on membranes of different composition. Increasing amount of PDMS* in a membrane resulted in an increased surface tension.

Measuring the caffeine permeability resistance of the membranes showed a dependency not only on the composition and the preparation of the membranes but also on the used wavelength to illuminate them. Under UV-irradiation, caffeine permeability resistance was found to be lower than at daylight (Figure 5.3).

In general, it was found that the more pHEA the network contained, the lower the permeability resistance of the membrane was (Table 5.3).

For the copolymerization process, a relation between the composition of the membrane and the permeability switch was found. More hydrophobic membranes showed more pronounced permeability resistance switches. If a network contained too much HEA, the impact of switching spiropyran into its more hydrophilic merocyanine state seemed to have a negligible influence on the overall hydrophilicity of a membrane and thus on the permeability resistance.

In contrast to the copolymerized membranes, the postmodified membranes only showed a switch of the permeability resistance when a high content of pHEA was present. For the postmodified 70/30 (HEA/PDMS) membrane, the permeability resistance under UV-irradiation was slightly decreased compared to permeability measurements at daylight. The postmodified 50/50 membrane showed no significant switch of permeability resistance. A possible explanation is that spiropyrans predominantly reacted at the surface during the postmodification process of the preformed membrane. The more HEA was used for the production, the more pHEA was on the surface. As a consequence, more **SP12** was bound to the surface of that membrane (Table 5.3).

Overall, the highest permeability switch was found for the copolymerized 50/50-amphiphilic conetwork. The amount of incorporated spiropyran was similar for all copolymerized membranes.

Table 5.3 Permeability resistances, switching potential and spiropyran content of all amphiphilic conetworks.

Membrane	R_{DL} (s/cm)	R_{UV} (s/cm)	Switch (%)	SP (wt.%)
50/50 neat	1'100'000 ± 100'000	-	-	-
70/30 neat	210'000 ± 20'000	-	-	-
PM 50/50	1'200'000 ± 250'000	1'100'000 ± 160'000	8	0.7
PM 70/30	310'000 ± 17'000	225'000 ± 8700	27	1.0
CP 50/50	2`600`000 ± 270`000	1`490`000 ± 74`000	43	1.0
CP 60/40	660`000 ± 28`000	469`000 ± 8`600	29	1.2
CP 70/30	390`000 ± 10`000	365`000 ± 8`600	6	1.1

Measuring the swelling behavior of the amphiphilic membranes was performed in water to swell the hydrophilic parts and in hexane to swell the hydrophobic components of the networks. For non-photochromic membranes, no significant change in swelling behavior was measured when swelling the membrane at daylight or under UV-irradiation. Membranes with more pHEA swelled more in water than membranes with less pHEA. As expected, an opposite trend was observed in hexane (Table 5.4). After postmodification, swelling behavior of the same membranes was investigated again at daylight and under UV-irradiation. Almost identical values were observed as for the non-photochromic membranes. No changed swelling behavior under UV-irradiation and at daylight was observed. Since the amount of spiropyran in the membrane was rather small, possible changes in swelling were too small to be detected.

Similar results were obtained for copolymerized membranes. No significant change in swelling was found comparing the measurements at daylight and under UV-irradiation.

Comparing membranes of the same composition (e.g. 50/50), it becomes obvious that neat conetworks and postmodified membranes show very similar swelling behavior. Therefore, it can be concluded that the introduction of spiropyran in a postmodification process did not change the structure of the amphiphilic conetwork. Swelling behavior of copolymerized membranes was found to be different. Copolymerization of spiropyran seems to have an essential influence on the structure of the amphiphilic conetwork.

Table 5.4 Swelling behavior of amphiphilic conetworks before and after postmodification (PM) and of copolymerized (CP) amphiphilic conetworks.

Sample	**S_{H2O}**		**S_{Hx}**	
	Vis	UV	Vis	UV
50/50 neat	1.22 ± 0.03	1.24 ± 0.04	1.29 ± 0.04	1.25 ± 0.02
70/30 neat	1.48 ± 0.04	1.44 ± 0.07	1.14 ± 0.04	1.05 ± 0.07
PM 50/50, **SP12**	1.21 ± 0.05	1.27 ± 0.08	1.28 ± 0.02	1.21 ± 0.05
PM 70/30, **SP12**	1.45 ± 0.04	1.50 ± 0.07	1.13 ± 0.02	1.15 ± 0.03
CP 50/50, **SP16**	1.24 ± 0.02	1.18 ± 0.03	1.32 ± 0.05	1.36 ± 0.03
CP 60/40, **SP16**	1.51 ± 0.01	1.51 ± 0.01	1.22 ± 0.03	1.19 ± 0.03
CP 70/30, **SP16**	1.68 ± 0.01	1.70 ± 0.03	1.21 ± 0.04	1.17 ± 0.06

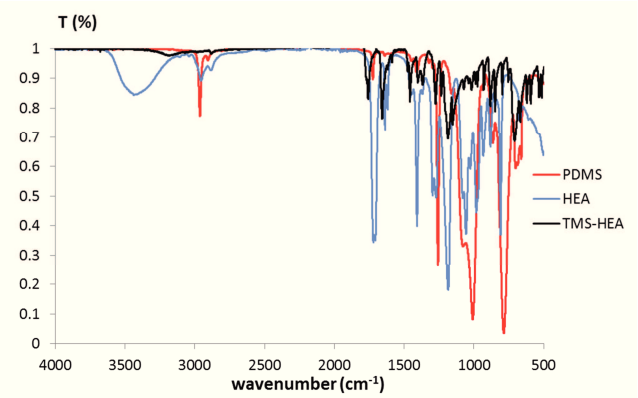

Figure 5.4 IR spectra of the single components of amphiphilic conetworks.

IR-measurements of the single compounds of the networks showed characteristic peaks that were also assigned in the final product. PDMS had a sharp signal at around 2900 cm^{-1} and unprotected HEA had a broad signal at around 3400 cm^{-1} (Figure 5.4). The signal at 3400 cm^{-1} was used to follow the deprotection of TMS-HEA.

The composition of the membrane is not only interesting at its surface but also at its inner face. Therefore, the IR-spectrum of the surface was first measured (Figure 5.5, black) and the membrane was then frozen in liquid nitrogen and pestled to a powder to measure the inner face of the membrane (Figure 5.5, red). In all measured spectra a broad peak at 3400 cm^{-1} was present, indicating that the deprotection of TMS-pHEA was successful. Postmodified as well as copolymerized membranes showed similar spectra for the surface and the inner phase. Therefore it can be concluded that pHEA as well as PDMS were not only present at the surface but also at the inner phase of the membranes (Figure 5.5).

XPS-measurements showed a Si-signal for all membranes. This indicates the presence of PDMS on the surface. For the copolymerization approach, all measured Si-concentrations were below the calculated concentration for pure PDMS. This indicates the coexistence of pHEA and PDMS on the surface. Since there is no correlation of the amount of PDMS used for the production of a membrane and the measured Si-concentration on the surface of that membrane, it has to be concluded that the structure of the amphiphilic conetwork was constitutionally changed depending on the HEA/PDMS-ratio (Table 5.5).

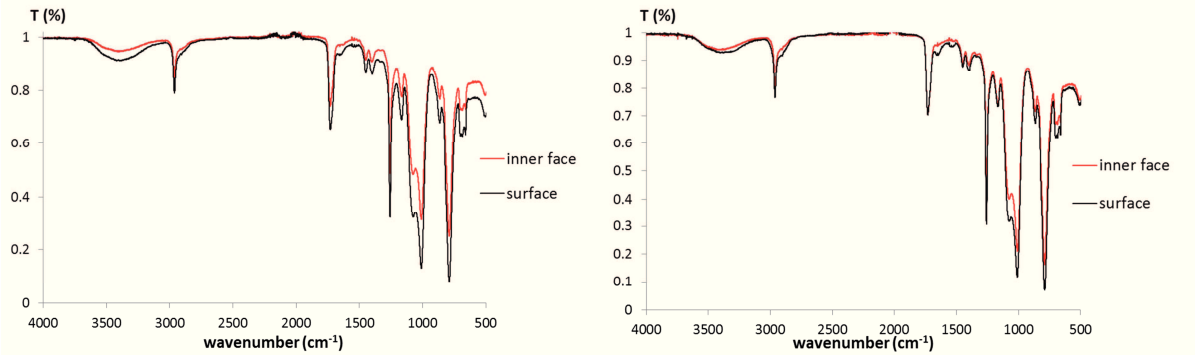

Figure 5.5 IR-spectra of a postmodified (left) and a copolymerized (right) amphiphilic conetwork (both 50/50 wt.% HEA/PDMS). The inner face was compared with the surface of the membranes.

XPS-measurements of the postmodified 70/30-membrane showed similar values as for pure PDMS. Nevertheless, the membrane swelled in water and caffeine was able to pass through the membrane. This indicates the presence of a continuous pHEA-network, but most probably with only minimal connections to the surface. If pHEA would only be dispersed in a PDMS-matrix, no swelling would be observed because water would not be able to reach any pHEA trough the isolating PDMS-layer on the surface.

Table 5.5 XPS-measurements of all photochromic amphiphilic conetworks. All results shown in At.-%.

Membrane	C 1s	O 1s	Si 2p
50/50 neat	61.1	22.9	16.0
70/30 neat	50.6	24.6	24.8
PM 50/50	59.9	25.7	14.4
PM 70/30	49.0	24.9	26.1
CP 50/50	54.7	26.8	18.6
CP 60/40	53.6	24.9	21.6
CP 70/30	63.2	24.7	12.1
HEA calc.	*62.5*	*37.5*	*0*
PDMS calc.	*50.0*	*25.0*	*25.0*

SEM-pictures showed that the surfaces of all membranes were smooth and without any pores or cracks within the visualizable range. Focusing on the surface was not easy due to the absence of any surface structure. Therefore positions with small pieces of dust had to be measured to enssure an accurate focus on the surface of the sample (Figure 5.6).
AFM phase pictures showed two phases. The bright phase was assumed to be pHEA whereas the dark phase was assumed to correlate with PDMS.[1] For the copolymerized 70/30-membrane, some big bright structures were found, indicating the presence of large pHEA structures (Figure 5.7, left). For the copolymerized 50/50-membrane, the big structures were dark, indicating the presence of more PDMS on the surface compared to the 70/30-membrane (Figure 5.7, right).

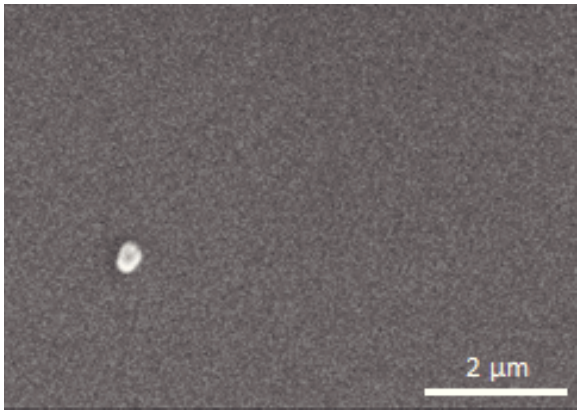

Figure 5.6 SEM-picture of an amphiphilic conetwork (PM50/50) with a dust particle (bright) that allowed focusing on the surface.

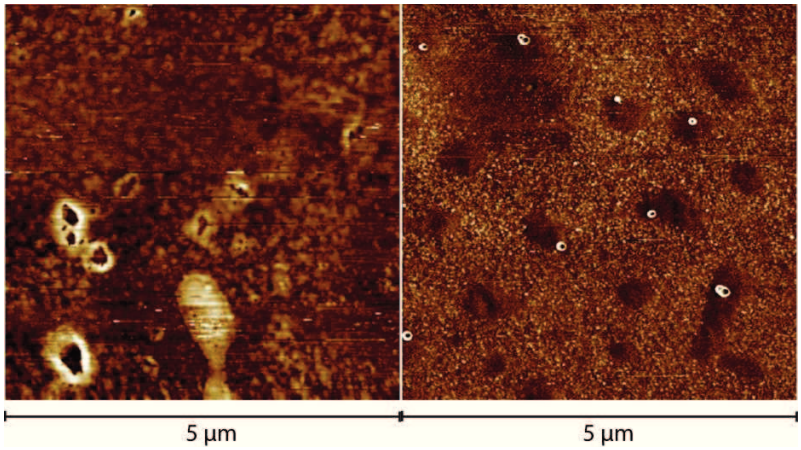

Figure 5.7 AFM-phase-pictures of CP70/30 (left) and CP50/50 (right). Bright areas correspond to pHEA, dark areas correspond to PDMS.

Comparing AFM phase pictures of postmodified and copolymerized 70/30-membranes showed as well some fundamental differences. The postmodified membrane showed almost no pHEA on the surface (Figure 5.8). This finding supports the XPS-measurements reported above.
Taking a closer look at the copolymerized 50/50-membrane showed some interesting structures (Figure 5.9). Donut-shaped structures were present in high concentration. Basically all pHEA present at the surface showed this structure. Besides the obviously bigger structure at the bottom left of Figure 5.9, all "donuts" had about the same diameter. Changing the cantilever had no influence on the image. A cantilever-artifact can therefore be excluded. Driving force behind the creation of this structure is unclear at the moment. It is also unclear whether this structure is only present at the surface or whether there are similar structures at the inner face. More AFM-measurements are needed (e.g. measurements of membrane cross sections) to get more information about the observed structures.

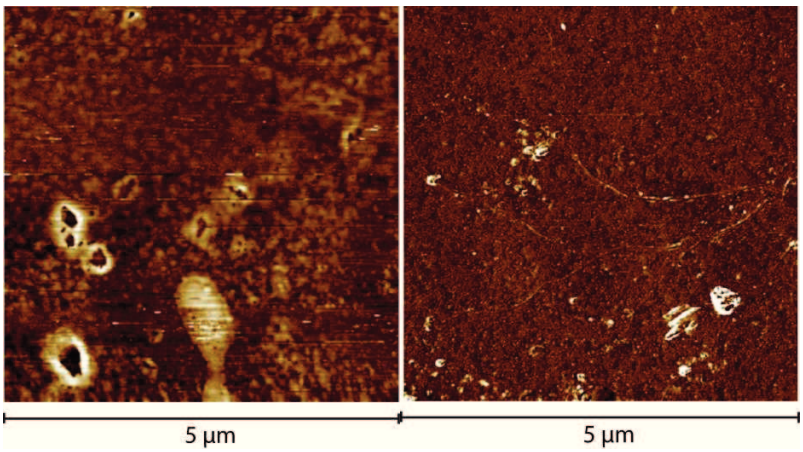

Figure 5.8 AFM-phase-pictures of CP70/30 (left) and PM70/30 (right). Bright areas correspond to pHEA, dark areas correspond to PDMS.

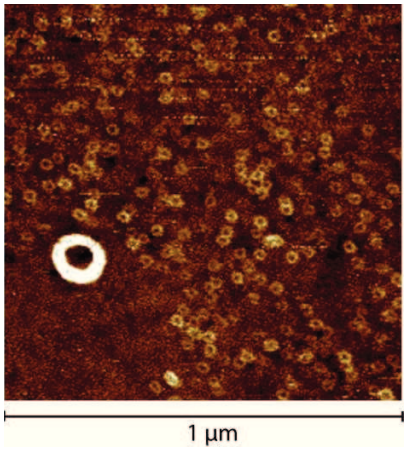

Figure 5.9 AFM-phase-picture of CP5050. Bright areas correspond to pHEA, dark areas correspond to PDMS.

Solid state UV-Vis measurement

Stability measurements of postmodified and copolymerized membranes showed fundamental differences between the two approaches. Measuring the fading rate of postmodified membranes resulted in a curve with two domains. During the first hour under UV-irradiation, the membrane seemed to be very stable with almost no change in transmission. After one hour, bleaching was accelerated significantly. Also the ring-closing reaction was found to be slow at the beginning with a constant acceleration of the reaction rate over time (Figure 5.10).

The fading rate of copolymerized amphiphilic conetworks resulted to be linear with minor deceleration, detectable towards the end of the measurement. Fading can therefore be assumed to be at a constant rate under permanent UV-irradiation. Ring-closing kinetics under dark condition was found to be linear (Figure 5.11).

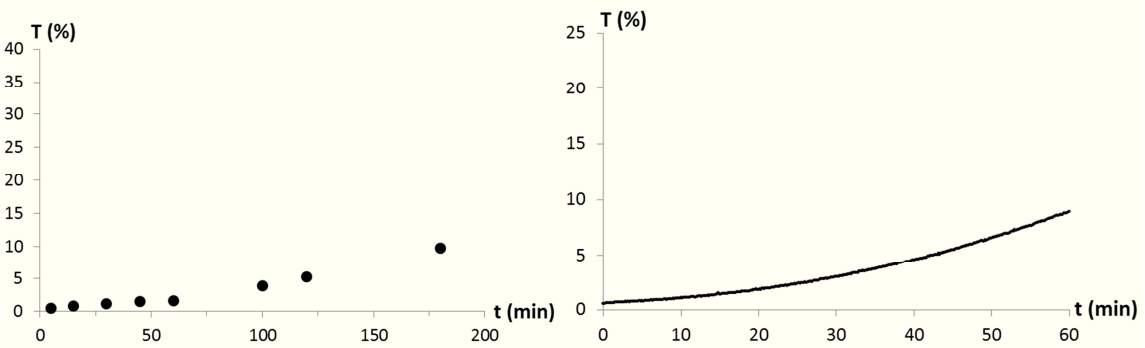

Figure 5.10 Fading rate measurement (left) and ring-closing reaction kinetics measurement under dark conditions (right) of PM 50/50. Transmission (T in %) of the membrane at λ_{max} was measured over time for both measurements.

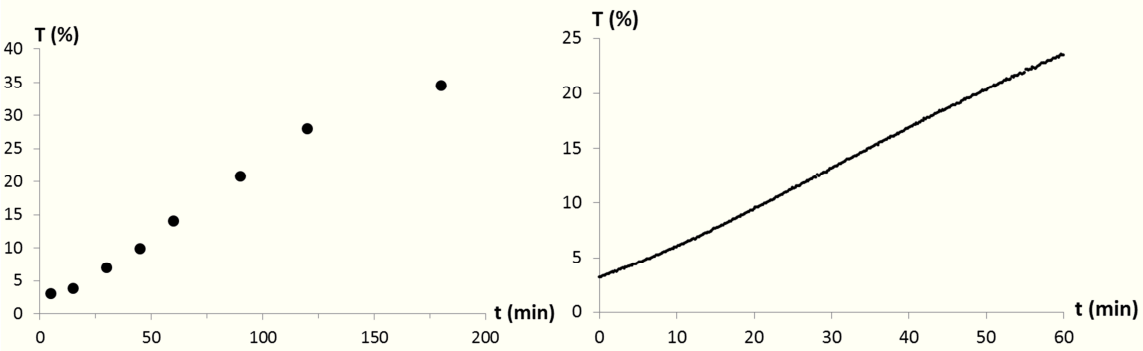

Figure 5.11 Fading rate measurement (left) and ring-closing reaction kinetics measurement under dark conditions (right) of CP 50/50. Transmission (T in %) of the membrane at λ_{max} was measured over time for both measurements.

Postmodified membranes turned out to be more stable than copolymerized ones. Especially during the first hour the postmodified membranes appear to be extremely fading resistant. But also after the first hour, the fading rate of postmodified membranes was considerably lower than fading rates of copolymerized membranes (Table 5.6).

Table 5.6 Stability measurement, ring-closing kinetics and λ_{max} of all photochromic amphiphilic membranes.

Membrane	Fading rate (ΔT%/min)	Ring-closing kinetics (ΔT%/min)	λ_{max} (nm)
PM 50/50	0.02 / 0.01	0.14	544
PM 70/30	0.02 / 0.01	0.10	548
CP 50/50	0.23	0.37	540
CP 60/40	0.72	0.27	534
CP 70/30	0.24	0.35	544

Additionally, ring-closing kinetics was found to be much slower for postmodified membranes (Table 5.6). Slow kinetics allows the use of a pulsed UV-irradiation. This can increase the lifetime of a photochromic membrane remarkably.

5.4 CONCLUSION AND OUTLOOK

Postmodification of amphiphilic conetworks as well as copolymerization of spiropyran with HEA/PDMS resulted in photochromic membranes. To regulate the basic resistance of a membrane, it was easier to change the composition of the membrane than changing the thickness of the membrane. Addition of more PDMS to the monomer mixture resulted in membranes with higher permeability resistances. Changing the thickness of the membranes had a big influence on the mechanical stability and on phase separation processes. An intermediate thickness of 200 μm turned out to be suitable for the production of amphiphilic membranes. When the basic permeability resistance of a membrane is adjusted by changing the composition of a membrane, it has to be considered, that the switching potential of a membrane is influenced as well. If a membrane was too hydrophilic, no switching was observed. Best switching potential was observed for copolymerized membranes with a composition of 50 wt.% HEA and 50 wt.% PDMS. The amount of spiropyran that was incorporated into membranes was found to be independent from the membrane composition for copolymerization processes. For postmodified membranes it was found that more spiropyran was incorporated in a membrane, if there was more pHEA in the membrane. The best stability was observed for postmodified membranes. The composition of these membranes had only little influence on the fading rate of the membrane under UV-irradiation. However, postmodified membranes did only insufficiently change the caffeine permeability resistance under UV-irradiation.

5.5 REFERENCES

1. N. Bruns, J. Scherble, L. Hartmann, R. Thomann, B. Iván, R. Mülhaupt and J. C. Tiller, *Macromolecules*, 2005, **38**, 2431-2438.
2. G. Erdodi and J. P. Kennedy, *Progress in Polymer Science*, 2006, **31**, 1-18.
3. A. Domján, G. Erdödi, M. Wilhelm, M. Neidhöfer, K. Landfester, B. Iván and H. W. Spiess, *Macromolecules*, 2003, **36**, 9107-9114.
4. C. S. Patrickios and T. K. Georgiou, *Current Opinion in Colloid & Interface Science*, 2003, **8**, 76-85.
5. E. J. Goethals, M. F. Dubreuil and L. Tanghe, *Macromolecular Symposia*, 2000, **161**, 135-140.
6. A. I. Triftaridou, S. C. Hadjiyannakou, M. Vamvakaki and C. S. Patrickios, *Macromolecules*, 2002, **35**, 2506-2513.
7. T. K. Georgiou, M. Vamvakaki and C. S. Patrickios, *Polymer*, 2004, **45**, 7341-7355.
8. M. Delerba, J. R. Ebdon and S. Rimmer, *Macromolecular Rapid Communications*, 1997, **18**, 723-728.
9. S. Yamashita, K. Kodama, Y. Ikeda and S. Kohjiya, *Journal of Polymer Science Part A: Polymer Chemistry*, 1993, **31**, 2437-2444.
10. N. Bruns, M. Hanko, S. Dech, R. Ladisch, J. Tobis and J. C. Tiller, *Macromolecular Symposia*, 2010, **291**, 293-301.
11. M. Hanko, N. Bruns, S. Rentmeister, J. C. Tiller and J. Heinze, *Analytical Chemistry*, 2006, **78**, 6376-6383.
12. J. C. Tiller, C. Sprich and L. Hartmann, *Journal of Controlled Release*, 2005, **103**, 355-367.
13. N. Bruns and J. C. Tiller, *Nano Letters*, 2004, **5**, 45-48.
14. J. H. Ramm, in *Mathematisch-Naturwissenschafltiches Fakultät*, University of Zurich, Zürich, 210.

6. GRAFTING THROUGH A MODIFIED POLYESTER SURFACE

6.1. INTRODUCTION

To improve the mechanical stability of amphiphilic conetwork systems discussed in Chapter 5, it is a known process to covalently coat more stable substrates with amphiphilic materials.[1] Coating appropriate substrates allows creating thin amphiphilic conetworks. It is no longer necessary to take care of the mechanical stability of the conetworks because the mechanical stability of the sample is ensured by the substrate. To affix the amphiphilic conetwork to the supporting surface, a grafting-through process is usually chosen.[1, 2] To enable grafting through processes, it is essential to allocate monomeric units at the surface of the substrate as anchor places. These monomeric units are then incorporated into the conetwork structure during the grafting through polymerization process. Therefore, the conetwork will become covalently linked to the supporting surface.[1]

Grafting a PDMS/HEA based amphiphilic conetwork through a surface is a known process to obtain thin coatings on glass substrates.[1, 3] Up to now, no process has ever been reported for grafting such conetworks through the surface of porous polymeric membranes. In this study, we combined the plasma-surface-modification reported in Chapter 4 to incorporate monomeric units on the membrane-surface with the light-responsive behavior of spiropyran-containing HEA/PDMS based amphiphilic conetworks reported in Chapter 5.

Influencing the caffeine transfer rates of the supported amphiphilic conetworks by switching spiropyran from one into its other state can either be achieved by changing the hydrophilicity of the domains in the conetwork or by opening and closing the pores based on changed swelling behavior of the amphiphilic conetwork. Since solutions pass much easier through pores (free diffusion) than through coatings (hindered diffusion), changes of hydrophilic and hydrophobic domains in the coating are only relevant in the case of entirely coated membranes. If there are uncoated pores from the matrix-membranes or if there are small cracks in the coating, this will be the main route for molecules through the membrane and a steric hindrance due to swelling of the coating is more likely to be observed.[4]

The aim of grafting an amphiphilic conetwork on a porous polyester membrane was not only to improve the mechanical stability of the network but also to compare its photochromic behavior to non-supported amphiphilic conetworks reported in Chapter 5.

6.2. EXPERIMENTAL

Materials and general methods

Track etched polyester membranes (PES) (0.2 μm pore diameter, 25 mm membrane diameter) were purchased from SterliTech Corporation. Caffeine (reagent plus) was delivered by Fluka. Acryloyl chloride (AcCl, 99%) was obtained from Sigma Aldrich. Dichloromethane (DCM, 99.8%, dried over molecular sieve) was delivered by Acros. Irgacure 819® was provided by BASF. 2-(acryloxyethoxy)trimethylsilane (TMS-HEA, 97%) and polydimethyl siloxane – methacryloxy propyl

terminated (PDMS*, 48 to 75 monomer units) were purchased from ABCR. TMS-HEA was freshly distilled under reduced pressure before usage. Spiropyran 16 (**SP16**) was synthesized according to Chapter 2. All other chemicals were used as delivered. Distilled water from the in-house supply was used unless stated otherwise. UV-Vis measurements were performed on a Varian 50Bio/50MPR for all liquid samples. For weighing, a Mettler Toledo AB204-S and a Mettler ME30 were used. IR-measurements were performed on a BioRad FTS 6000 equipped with an ATR Golden Gate. Scanning electron Microscopy (SEM) pictures were recorded on a Hitachi S4800. All samples were coated with a gold layer of about 3 nm. X-ray photoelectron spectroscopy (XPS) was performed on a PHI 5600 spectrometer under an angle of 45°. XPS-data were analyzed with the program CasaXPS. Profilometric measurements were performed on a Dektak 150 from Veeco.

Plasma coating

Untreated PES-membranes were dunked in a gently stirred DCM bath for 3 hours at room temperature, to remove possible coatings that were not denoted by the manufacturer. After drying the membranes, they were coated with nitrogen-enriched polyethylene in a plasma deposition/polymerization process. Therefore, 270 sccm ethylene, 250 sccm ammonium and 25 sccm argon were activated by 635 W at 0.1 mbar in a coil coating plasma chamber (BABE).[5, 6] Each side of the membrane was treated for 30 min in this plasma condition. The membranes were stored in a desiccator over molecular sieves.

Monomer binding

A round bottom flask was equipped with a stirring bar and a protecting grid. After charging the flask with 12 mL DCM and NEt_3 (1.0 mL, 7.2 mmol), a plasma-treated membrane was added. Acryloyl chloride (1.0 mL, 12.4 mmol), diluted in 3 mL DCM, was added drop-wise at room temperature via syringe. The whole mixture was stirred for 3 hours. The membrane was then removed and washed with DCM, MeOH and H_2O in an ultrasonic-bath and dried in a desiccator over molecular sieves.

Grafting through polymerization

TMS-HEA (2.4 g, 2.3 mL, 2.6 mmol) was premixed with **SP16** (100 mg, 0.21 mmol). Afterwards PDMS* (2.4 g, 2.5 mL, 0.5 mmol) was added and shacked vigorously for one minute. Under red light, Irgacure 819 (39 mg, 0.09 mmol) was added and the mixture was shacked vigorously for 5 minutes. A membrane coated with acrylates was dipped into the solution. The membrane was then illuminated with visible light (500 W bulb) for 1 hour from each side. Then, the membrane was ultrasonicated with DCM, methanol and water. The weight of the dry membrane was measured before and after the grafting through process, to know the amount of amphiphilic network that was grafted through the membrane.

Permeability

All measurements were performed in a Franz diffusion-cell purchased from SES Analyse Systeme with a receptor volume of 12.0 mL and an orifice area of 1.77 cm^2. Mass transfer rates of caffeine were measured under UV irradiation (366nm, 15 W/m^2) and at daylight. After filling the receptor chamber with water (12.0 mL), the membrane was fixed in the diffusion cell. The donor chamber was charged with a caffeine solution (280 mM; 3.0 mL). Samples (200 μL) were collected from the receptor part of the cell after 1, 30, 60, 90, 120, 180, 240 and 270 minutes. The caffeine

concentrations of these samples were assigned by measuring its UV absorption at 293 nm. Resistance R of a membrane was calculated according to Fick's law using the formula

$$R = \frac{\Delta c}{F} \quad (1)$$

where Δc represents the difference of caffeine concentration comparing the donor compartment with the receptor part of the used franz cell. Δc was assumed to be constant over the time frame of the measurement. F was the molecular flux in amount per time per area. Permeability measurements for all treated membranes were performed directly after the production. All membranes were stored in water to precondition the membranes.

Contact angle

All measurements were performed on a Krüss G10A. The membrane – fixed with a standard tape if necessary – was positioned on a metal O-ring. A drop of nanopure water (3.3 µL) was positioned on that part of the membrane surface, which was not in contact with the O-ring. For measuring the impact of switching SP on the surface tension of the membrane, the CA was measured first at day light. Then the membrane was illuminated with UV light (366 nm, 80 W/m^2) for 1 minute and the contact angle was measured again.

Swelling of membranes

The thickness of the membranes was measured with a profilometer. A membrane was dried *in vacuo* in a desiccator over molecular sieves for 24 hours. Afterwards, its thickness (d_0) was measured. Then the membrane was placed into water or hexane for 1 h and the thickness (d_1) was measured again. For measuring the impact of the MC state on the swelling behavior, a membrane was illuminated with UV-light (366 nm, 80W/m^2) for 1 minute before swelling in water. Each measurement was repeated three times. The linear degree of swelling was calculated with the following formula:

$$S = \frac{d_1}{d_0} \quad (2)$$

Solid state UV-Vis measurements

All measurements were performed on a Lambda 9 in the reflection mode. UV-irradiation was always at 366 nm with an intensity of 80 W/m^2. The membrane itself, stored at daylight, was used for the base line measurements. After illuminating the membrane for 1 minute with UV light, the spectrum of that membrane was measured and the maximum absorbance was detected. The membrane was then illuminated with UV-light for five more minutes. Afterwards, the absorption at the assigned maximum was measured over a time span of 90 minutes to obtain information about ring-closing kinetics of the spiro-compounds under dark conditions at room temperature. Subsequently, the membrane was illuminated for 5 hours with UV-light. After 15, 30, 45, 60, 90, 120, 180 and 300 minutes, the absorption at the assigned maximum was measured to determine the speed of decomposition of the spiro-compounds under UV-irradiation. Since fading and ring closing reaction do not follow a known reaction mechanism, it was not possible to apply an appropriate model to quantify the processes. To qualitatively compare the different membranes, a linear fit was

applied. For fading rates, the measurements of the first 60 minutes were considered. For ring closing rates, all measurements between 20 and 40 minutes were considered for the linear fit.

6.3. RESULTS AND DISCUSSION

Grafting an amphiphilic conetwork consisting of PDMS*, HEA and **SP16** through a polyester surface, resulted in a photochromic membrane (Figure 6.1). To enable a grafting process through the surface of a porous polyester membrane, an amine-containing polyethylene plasma-coating was first applied.[5, 6] The free amines at the surface where then allowed to react with acryloyl chloride yielding acrylic units covalently bound to the surface. This activated membrane was then dipped in a TMS-HEA/PDMS* solution. After removing the membrane from the solution, the polymerization process was initiated by irradiating the membrane with white light. By storing the membranes in THF and water for 12 hours, the TMS-groups were removed resulting in a photochromic membrane coated with an amphiphilic conetwork (Scheme 6.1).

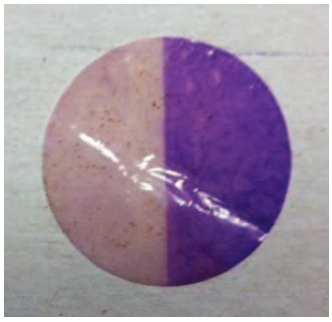

Figure 6.1 PES-membrane after grafting through process – left: irradiated with white light; right: irradiated with UV-light.

Weighing the sample before and after the grafting through process resulted in a weight gain of 1.44 mg (27%). For the determination of the amount of spiropyran on the membrane, it was assumed that the concentration of the spiropyran and the comonomers is the same in the monomer mixture as well as in the polymeric coating. This assumption is based on the measurements made for the determination of the amount of spiropyran in copolymerized amphiphilic conetworks presented in Chapter 5. With this assumption, a spiropyran content of 0.4 wt.% on the coated membrane was calculated.

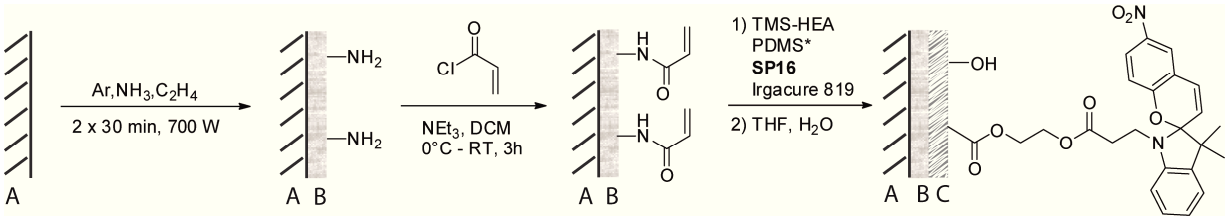

Scheme 6.1 Monomer binding to the surface of a porous polyester membrane followed by grafting an amphiphilic conetwork through the surface; **A:** polyester membrane; **B:** amine-containing plasma coating; **C: SP16**-containing amphiphilic conetwork.

Compared to the previous chapters, there was an inversed switch of permeability resistance towards caffeine detected. This means that the detected permeability resistance was high under UV-irradiation and was significantly reduced at daylight (Table 6.1 & Figure 6.2).

Table 6.1 Permeability resistances, contact angles, spiropyran content and λ_{max} of the PES-membrane after the grafting-through modification.

Coating	R_{DL} (s/cm)	R_{UV} (s/cm)	CA_{DL} (°)	CA_{UV} (°)	SP (wt.%)	λ_{max} (nm)
HEA-PDMS 50/50	126'000 ± 5500	1'110'000 ± 25'000	95	95	0.4	565

Contact angle measurements showed similar values for measurements at daylight and for measurements under UV-irradiation. Comparing this result with the previous chapters it can be concluded, that no significant amount of spiropyran is on the membrane surface. Since surface tension did not change under UV-irradiation, a surface tension effect on the permeability can be excluded. Additionally, the measured contact angle of 95° corresponds quite closely to the contact angle of pure PDMS (105°).[7] Thus it can be concluded, that predominantly PDMS is on the surface of the grafted amphiphilic conetwork and that spiropyran predominantly copolymerized in the hydrophilic pHEA phase of the conetwork.

Table 6.2 Swelling behaviour of the modified PES-membrane at daylight and under UV-irradiation.

Condition	Thickness (µm)	S (%)
dry	29.1 ± 0.6	-
wet DL	32.0 ± 0.4	9.8
wet UV	32.8 ± 0.4	12.0

The inverse switch can be explained with the swelling behavior of the membrane. At daylight, the membrane swelled around 10%, whereas it swelled 12% under UV-irradiation (Table 6.2). An increased membrane thickness in the vertical direction under UV-irradiation is most probably accompanied by an increased swelling of the coating in the lateral direction.

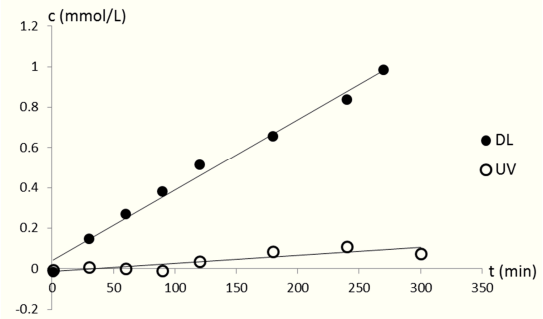

Figure 6.2 Caffeine permeability measurements in a Franz cell at daylight and under UV-irradiation.

This increased lateral swelling reduced the area of open pores accessible for permeation or even converted the membrane into a non-porous system. The reduced pore-area or the disappearance of open pores explains the increased permeability resistance under UV-irradiation.
XPS-measurements showed that there is almost only PDMS on the surface of the membrane (Table 6.3). Since the membrane swelled in water, the pHEA-phase had to be continuous and connected to the surface. If pHEA had been non-continuously dispersed in a PDMS-matrix, it would be isolated from water by a layer of PDMS and no swelling of the membrane in water would be expected. No nitrogen has been measured for the coated membrane. This supports the assumption made before from the observation of the contact angle measurements, that no or only very little spiropyran was polymerized on the surface of the amphiphilic conetwork.

Table 6.3 XPS-measurements of the membrane before and after the grafting through process. Calculated values for pHEA and PDMS are shown in italic. All results shown in At.-%.

Sample	C 1s	O 1s	N 1s	Si 2p
PES-Acrylate	90.6	6.9	2.6	0
PES-pHEA-PDMS	51.0	24.5	0	24.5
pHEA calc.	*62.5*	*37.5*	*0*	*0*
PDMS calc.	*50.0*	*25.0*	*0*	*25.0*

IR-measurements showed a sharp peak around 2900 cm^{-1} indicating the presence of PDMS on the surface. As expected – based on the XPS-measurements – no peak around 3400 cm^{-1} was detected (Figure 6.3). This supports the assumption made before from the observation of the contact angle and XPS-measurements that only very little pHEA was situated on the surface of the coated membrane.

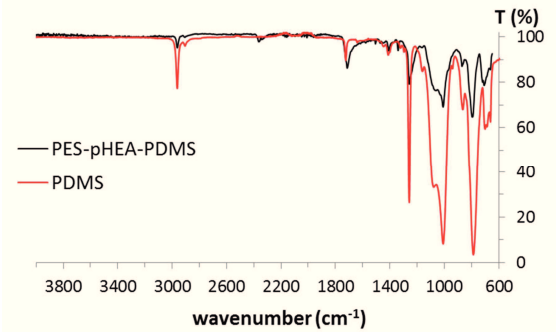

Figure 6.3 IR-measurement of the coated membrane (black) and of pure PDMS (red).

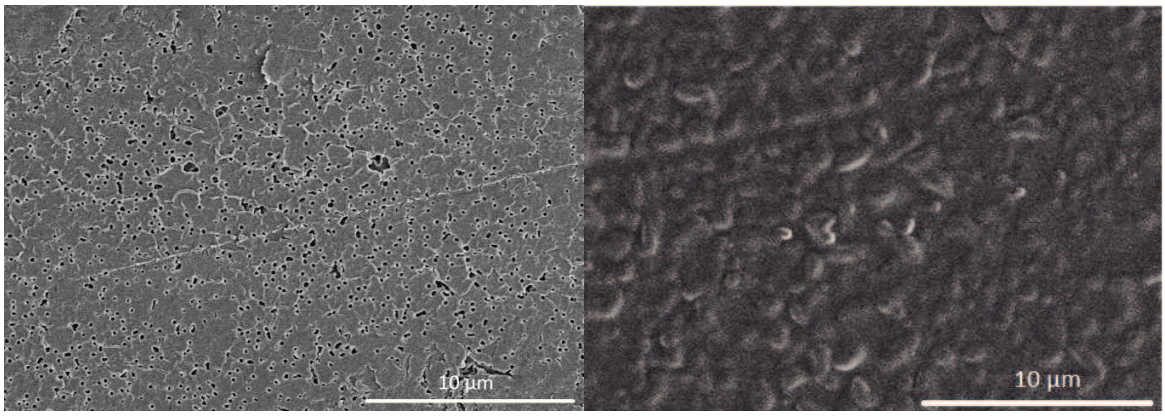

Figure 6.4 SEM-picture of the PES-membrane before and after the grafting through process.

It was expected that aqueous caffeine solution passed only through the pHEA domain of an amphiphilic network. The finding that there was almost only PDMS on the surface, supports the conclusion that caffeine passes through small open pores in the membrane and that these pores are narrowed under UV-irradiation due to the swelling of the coating.

SEM-pictures showed a changed topography on the surface due to the coating (Figure 6.4). No pores or cracks in the coating were detected even at high magnifications (Figure 6.4, right). This is contradictory to the conclusions made before. But SEM-pictures do not allow visualizing pores and cracks in the nanometer-domain. Side views show that the pores are only entirely coated at the membrane's surface. At the inner face, the pores remained open (Figure 6.5).

AFM-measurements showed the presence of two different phases at the surface of the modified PES-membrane (Figure 6.6). The size of these domains was significantly larger than the domains found in amphiphilic conetworks without a supporting membrane (see Chapter 5).

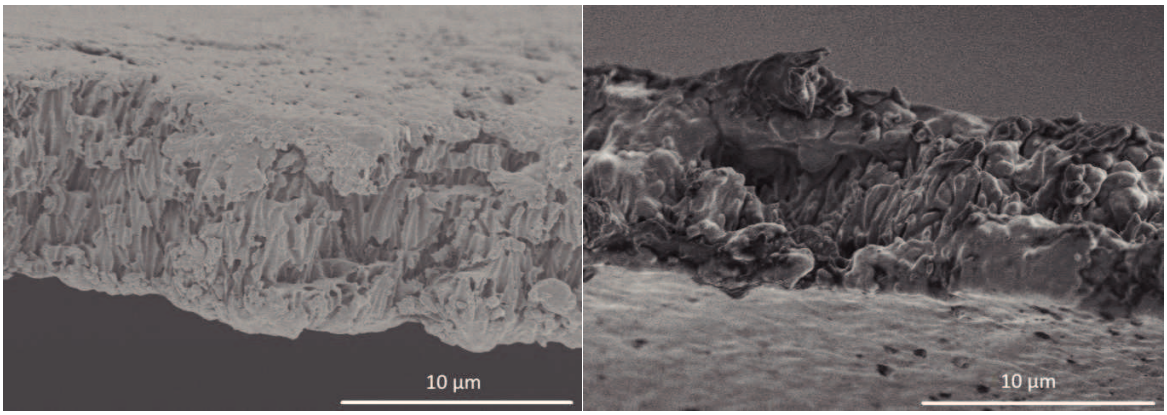

Figure 6.5 Side-view of a PES-membrane before (left) and after (right) the grafting-through process.

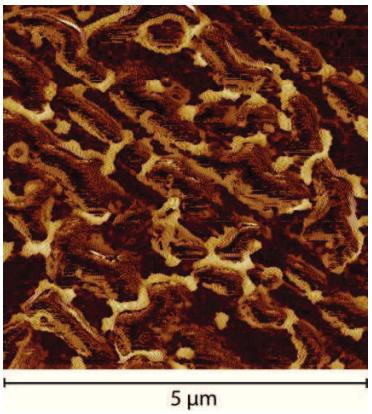

Figure 6.6 AFM-phase picture of the membrane. Bright areas correspond to pHEA, dark areas correspond to PDMS.

The presence of two different phases at the surface is supported by the findings of the swelling measurements that indicated the presence of a continuous pHEA-phase that is connected to the surface. But the presence of pHEA at the surface is contradictory to the IR- and XPS-measurements that showed only PDMS on the surface of the membrane. More experiments are needed to reliably assert whether there is pHEA at the surface or not.

Solid state UV-Vis measurements

Stability measurements showed a fading rate of 0.13% per minute for the first hour. After that time, a plateau was reached after 80% color disappearance (Figure 6.7, left). The fact that not 100% was reached, was explained by a slight brownish color of the membrane after the stability measurements, which might have occurred due to a side reaction taking place during UV-irradiation. Kinetic-measurement of the ring closing reaction resulted in an absorption-change of about 0.046% per minute (Figure 6.7, right). Values for fading rate and ring-closing kinetics have to be handled with great carefulness since the involved reaction mechanisms are not known and linear models are applied (see experimental section).

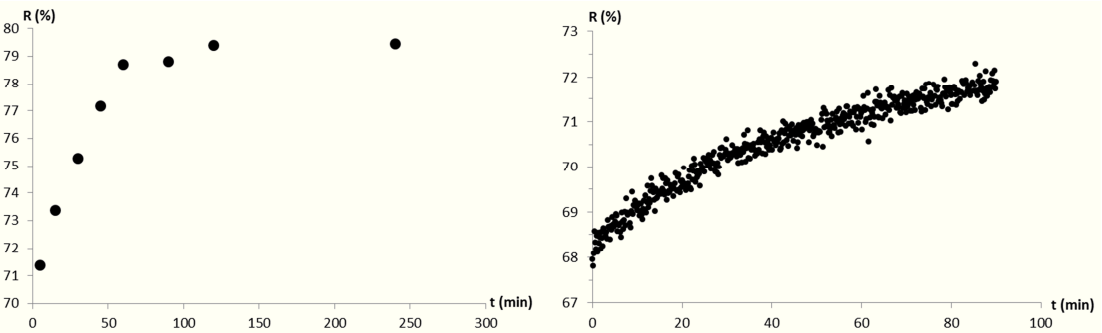

Figure 6.7 Fading-rate measurement (left) and ring-closing reaction kinetics measurement under dark conditions (right) of the modified PES-membrane. Reflection (R in %) of the membrane at λ_{max} was measured over time for both measurements.

6.4. CONCLUSION AND OUTLOOK

Grafting an amphiphilic network through an acrylate functionalized surface of a porous polyester membrane, allowed to achieve a steric control over the caffeine permeability of the membrane. The caffeine permeability resistance is – in contrast to previous chapters – low at daylight and much higher under UV-irradiation. It was shown that the amphiphilic network swelled more under UV-irradiation, than at daylight. Caffeine permeability resistance changed from 100'000 s/cm at daylight (typical value for open pore membranes, see Chapter 3) to 1'200'000 s/cm under UV-irradiation (typical value for closed pore amphiphilic membranes, see Chapter 4). XPS, CA and IR measurements showed that the membrane had almost only PDMS on its surface. But since the membrane swelled in water, there has to be a continuous pHEA-phase connected to the surface. Since PDMS is known to be impermeable for aqueous solutions, it is assumed that caffeine passes rather through small pores in the membrane than through the coating itself. Under UV-irradiation, the coating swelled and thus the pores were narrowed (or even completely closed). This closing of the pores was responsible for the increased permeability resistance.

To obtain more information about the mechanism of the pore blocking of the membranes, it would be necessary to produce more coatings with different compositions to see for example what would happen with the permeability resistance, when pHEA appears more prominently on the surface. Grafting coatings with 70/30 (HEA/PDMS wt.%) and 60/40 compositions through the surface of PES-membranes would be of great interest to compare these results with the according amphiphilic membranes reported in Chapter 5. It would also be interesting to compare the longtime stability of spiropyran in different coatings, to see if it behaves as in pure amphiphilic networks (Chapter 5) or if the supporting PES-membrane or the porous structure of the matrix have some impact on the stability of spiropyrans.

6.5. REFERENCES

1. N. Bruns, J. Scherble, L. Hartmann, R. Thomann, B. Iván, R. Mülhaupt and J. C. Tiller, *Macromolecules*, 2005, **38**, 2431-2438.
2. M. Balcı, A. Allı, B. Hazer, O. Güven, K. Cavicchi and M. Cakmak, *Polym. Bull.*, 2010, **64**, 691-705.
3. J. C. Tiller, C. Sprich and L. Hartmann, *Journal of Controlled Release*, 2005, **103**, 355-367.
4. E. L. Cussler, *Diffusion – Mass Transfer in Fluid Symstemy*, Cambridge University Press, Cambridge, 2009.
5. S. Guimond, U. Schütz, B. Hanselmann, E. Körner and D. Hegemann, *Surface and Coatings Technology*, 2011, **205**, Supplement 2, S447-S450.
6. D. Hegemann, E. Körner, N. Blanchard, M. Drabik and S. Guimond, *Applied Pysics Ltters*, 2012, **101**, 211603.
7. K. Haubert, T. Drier and D. Beebe, *Lab on a Chip*, 2006, **6**, 1548-1549.

7. CONCLUSION AND OUTLOOK

Synthesis of several spiropyrans and spirooxazines showing photochromic behavior at room temperature was achieved. Copolymerization of methacrylic and acrylic photochromic spiro-compounds with HEMA and HEA resulted in photochromic materials. Additionally, a spiropyran with carboxylic acid functionality was synthesized. This structure was linkable to the side chains of pHEMA, pHEA and pAEMA resulting in postmodified photochromic polymers.

A first approach to obtain membranes with switchable caffeine permeability resistances included the covalent linkage of photochromic coatings to the surface of porous polymeric membranes. Polymers were grown from the surface of porous membranes, either in an ATRP-process or after plasma-activation of the surface in a free radical polymerization process.
Surface-induced copolymerization of monomeric spiropyran with appropriate comonomers from plasma-activated porous membranes allowed the production of photochromic membranes with a single reaction step. Postmodification of a preformed membrane-coating with spiropyran included two reaction steps to obtain photochromic membranes, but the analysis of the coating was much easier (e.g. measuring the amount of SP by determining the weight gain). UV-irradiation of photochromic membranes induced not only a change in color but also a decrease of surface tension and thus a decrease in caffeine permeability resistance. Postmodified membranes showed usually higher changes in caffeine permeability resistance than copolymerized samples. The reason for the light-responsiveness of the permeability was the change in surface tension of the membrane surface, which led to an improved wetting of the track-etched pores.
It was discovered that hydrophilic copolymers with a low T_g increased the switching potential of a membrane, compared to membranes coated with a hydrophobic or rigid copolymer.
Plasma induced random free radical surface polymerization turned out to be an easy and fast way to produce photochromic membrane coatings, leading to switchable caffeine permeability resistances. But there was no control over the polymerization process. Therefore, adaption of the produced membranes in a predicted manner was impossible. Also, the analysis turned out to be demanding due to the fact that the achieved coating thicknesses were in the order of 10 nm or below and the membrane surface was not flat.
Surface-induced ATRP allowed changing the coating thickness either by changing the concentration of monomer or by changing the reaction time. Due to the obtained thicker coatings, the analysis of these membranes was much easier. The amount of coating for example was measured by weighing the samples. SEM-pictures showed that the coating was – at least for the samples with visualizable coatings – homogeneous.

A second approach to produce light-responsive membranes included the production of amphiphilic conetworks to achieve nonporous photochromic membranes with switchable caffeine permeability resistance. Basic permeability resistances of nonporous membranes were found to be much higher and easier adaptable than the permeability resistances of porous membranes. Changing the composition of the amphiphilic conetwork for example, resulted in a changed permeability resistance. Copolymerized amphiphilic conetworks showed higher changes in caffeine permeability

resistances than postmodified samples. For copolymerization of amphiphilic conetworks, it was found that the more PDMS was used in the production process the higher permeability switches of membranes were achieved.
In order to obtain mechanically more stable systems, the amphiphilic conetworks were grafted through a modified porous tack-etched membrane. The caffeine permeability resistance of the obtained membrane was found to be switchable but with an inversed adaption. A higher permeability resistance was detected at daylight than under UV-irradiation. The reason for that was the finding that not an alteration in surface tension was causing the change in the permeability resistance, but the sterically opening and closing of the pores due to the change of hydrophilicity of the material determined the caffeine permeability rate.

Membranes with highest switching potential concerning caffeine permeability resistance were achieved when porous membranes were coated with pHEMA using a plasma-induced random free polymerization process, followed by postmodification with spiropyran. This membrane lowered its caffeine permeability resistance from 590'000 cm/s to 15'700 cm/s (97%) upon UV-irradiation. Postmodified membranes, coated with pHEMA in an ATRP-process, followed by postmodification with spiropyran, resulted in a membrane that lowered its permeability resistance by about 65% (from 39'000 s/cm to 13'600 s/cm). Amphiphilic conetworks resulted in only 43% lower permeability resistances for copolymerized membranes and even smaller resistance switches for postmodified membranes. The inversed switch, provided from the grafted amphiphilic conetwork through a porous membrane, allowed increasing the permeability resistance for about a factor eight under UV-irradiation.

Since high stability towards fading while irradiating with UV-light is important when it comes to applications, the UV-stability of all membranes were studied. Stability measurements showed that spirooxazines were more stable than spiropyrans under UV-irradiation. Postmodified membranes provided usually lower fading rates than copolymerized samples. Therefore, postmodified spirooxazine containing membranes are expected to be most suitable for applications where long term stability of the material is essential.
Using postmodification processes resulted not only in better UV-stabilities of the membranes but also allowed a better control of the polymerization process and facilitated the analysis of the produced materials. Additionally, postmodification resulted in high switching potential regarding caffeine permeability resistance when porous membranes were used. Therefore, using postmodification processes is recommended for future investigations with porous membranes. Furthermore, using soft polymers that change their surface tension significantly from hydrophobic to hydrophilic upon switching spirooxazine from its SP to its MC-state is advisable.
But if an exact adjustment of the permeability resistance is important, the application of photochromic amphiphilic conetworks produced in a copolymerization process is recommended. It could also be a good approach to further investigate the grafting through approach, since it led to an inversed change of permeability resistance and combined the advantages of porous membranes (e.g. mechanical stability) with the advantages of amphiphilic conetworks (easy and reproducible processing).

Furthermore, it is important to investigate the biocompatibility of the different photochromic membranes since no data are available examining the biocompatibility of spiropyran/spirooxazine in a polymer matrix. Additionally, it is important to integrate the membranes into drug delivery setups to proof their functionality for caffeine delivery approaches. *In vitro* tests have to be performed for example with pig-ear skin as a model for the skin of preterm neonates. Initial experiments showed that preparing the pig-skin with a scalpel is not suitable due to low reproducibility of the preparation. Therefore, it is essential to work with a dermatome to prepare pig-skin for permeability measurements. Additionally, it would be interesting to see if the transepidermal water loss (TEWL) is correlated with the caffeine permeability of the skin. If there is a correlation, the prepared pig-skin samples could easily be analyzed with a TEWL-analyzer before performing time consuming permeability measurements. Finally, *in vivo* studies have to be performed to prove the suitable function of the caffeine delivery setup.

„Ich bin mit einem Chemiker zu vergleichen,
der die Stoffe kennt, und die Resultate abwartet.
Immer wieder überraschen mich meine Figuren damit,
dass sie Dinge tun, oder sagen, die ich nicht von ihnen erwartet hatte;
ja, sie können manchmal meinen ursprünglichen Plan völlig umkrempeln,
diese Teufel."

Henrik Ibsen, Interview, 1898